NTNU
Norwegian University of
Science and Technology

Dynamic Collapse of the Hull Girder in a Container Ship in Waves

Tjark Tilman Schwebe

Maritime Engineering
Submission date: June 2016
Supervisor: Jørgen Amdahl, IMT

Norwegian University of Science and Technology
Department of Marine Technology

NTNU
Norges teknisk-naturvitenskapelige universitet
Institutt for marin teknikk

MASTER THESIS 2016

for

Stud. Techn. Tjark Tilman Schwebe

Dynamic collapse of the hull girder in a container ship in waves
Dynamisk sammenbrudd av skrogbjelken til et containerskip i bølger

Recently the importance of whipping stresses on the extreme hull girder loadings has received much attention. Full scale measurements clearly show magnifications of the usual wave-induced bending moment by a factor of two due to the hull girder elasticity, see e.g. Andersen and Jensen (2014), in moderate sea states. The hull girder collapse of MOL Comfort in 2013 has also increased the focus on this matter.

The whipping induced stresses have a considerable higher frequency than the ordinary wave induced hull girder stresses. An important issue is whether the whipping induced stresses (on top of the wave induced stresses) can be allowed to exceed the static capacity of hull girder, which is typically governed by buckling of stiffened plates in compression. One reason is to the whipping stress component during buckling may be displacement controlled, so that the plate is not pushed far into the post-buckling range. Further, dynamic effects, such as inertia forces during buckling and/or strain rate effects may yield additional strength reserves for the stiffened plate. Change in hydrostatic hull loads due to "rigid body" rotation at the critical cross-section may also contribute positively.

In addition to checking of static and dynamic buckling, failure in the form of incremental plasticity or low-cycle fatigue during the repeated action of large waves must also be considered.

The project work is proposed carried out in the following steps:

1. Brief review of work related to investigation of the MOL Comfort accident. Review requirements issued by ship classification societies (e.g. DNV-GL) concerning the use of nonlinear finite element methods for assessment of hull girder capacity.

2. Establish relevant wave and whipping induced bending moment histories for the container vessel based on available full scale measurements. Discuss the frequency/temporal characteristics of the histories and the expected ship response to

these histories. Determine the lay-out and scantlings of a representative hull girder, based on drawings of similar vessels and software for ship design based on rule requirements (e.g. DNV-GL)

3. Establish a detailed finite element model of three holds in the midship area of a container vessels connected to a beam model of the forward and aft part of the ship. Include also the effect of water plane stiffness for "rigid body rotation" of the hull girder. Discuss various options for modelling of initial imperfections and explain why the selected strategy was chosen. Discuss the choice of boundary conditions for the finite element model. Apply relevant hull girder and local sea loads. Perform static analysis of hull girder resistance subjected to extreme hull bending moment. Identify when yielding and buckling starts in various strength members.

4. Perform time domain analysis of the resistance to regular wave induced hull girder loads, where the wave histories are increased proportionally, bringing the response of the most exposed members into the inelastic region. Compare the results with those from the static analysis.

5. Perform analysis of the hull girder response when it is subjected to whipping induced vibrations in addition to regular wave loads. It is especially interesting to see if stiffened panels loaded beyond their static capacity will buckle or develop permanent plastic shortening that may give rise to low cycle fatigue problems or incremental collapse. Do the bottom panels buckle in the "hungry horse" or the "asymmetric" mode? Can the bottom panels, which undergo plastic straining in compression be subjected to reversed cycling?

6. Establish the hysteresis loop for members/cross-section carried out into the nonlinear domain. Estimate the number of load cycles the ship can sustain before failure, depending upon the magnitude of the hull girder loads. Discuss the severity of whipping induced loads on regular wave loads. Discuss how whipping induced stresses could be accounted for in ship rules.

7. Conclusions and recommendations for further work

References:

Andersen, I.M.V., Jensen, J.J. (2012). On the Effect of Hull Girder Flexibility on the Vertical Wave Bending Moment for Ultra Large Container Vessels. *Proc. OMAE2012, paper no. 83043, Rio de Janeiro, Brazil, June 2012*

Andersen, I.M.V., Jensen, J.J. (2014). Measurements in a container ship of wave-induced hull girder stresses in excess of design values. *Accepted for publication Marine Structures*

Iijima, K., Fujikubo, M. and Xu, W. (2011), Hydroelasto-plasticity approach to predicting the post-ultimate strength behavior of a ship's hull girder in waves. *J Mar Science & Technology,* 16:379-389

Xu, W., Iijima, K. and Fujikubo, M. (2012). Investigation into dynamic collapse behavior of a bulk carrier under extreme loads. *Proc. Hydroelasticity in Marine Technology, Japan*

Xu, W., Iijima, K. and Fujikubo, M. (2012). Parametric dependencies of the post-ultimate strength behavior of a ship's hull girder in waves. *J Mar Science & Technology,* 17:203-215

Xia J, Wang, S. and Jensen, J.J. (1998), 'Non-linear Wave Loads and Ship Responses by Time-Domain Strip Theory', *Marine Structures*, 11(3):101-123.

Seng, S., Andersen, I.M.V., Jensen, J.J. (2012). *On the influence of hull girder flexibility on the wave induced bending moments. Proc. Hydroelasticity 2012, Tokyo, 2012*

Seng, S., Jensen, J.J. (2013). *An Application of a Free Surface CFD method in the Short-Term Extreme Response Analysis of Ships, Proceedings PRADS'2013*

The work scope may prove to be larger than initially anticipated. Subject to approval from the supervisors, topics may be deleted from the list above or reduced in extent.

In the thesis the candidate shall present her personal contribution to the resolution of problems within the scope of the thesis work.

Theories and conclusions should be based on mathematical derivations and/or logic reasoning identifying the various steps in the deduction.

The candidate should utilise the existing possibilities for obtaining relevant literature.

Thesis format
The thesis should be organised in a rational manner to give a clear exposition of results, assessments, and conclusions. The text should be brief and to the point, with a clear language. Telegraphic language should be avoided.

The thesis shall contain the following elements: A text defining the scope, preface, list of contents, summary, main body of thesis, conclusions with recommendations for further work, list of symbols and acronyms, references and (optional) appendices. All figures, tables and equations shall be numerated.

The supervisors may require that the candidate, in an early stage of the work, presents a written plan for the completion of the work. The plan should include a budget for the use of computer and laboratory resources which will be charged to the department. Overruns shall be reported to the supervisors.

The original contribution of the candidate and material taken from other sources shall be clearly defined. Work from other sources shall be properly referenced using an acknowledged referencing system.

The report shall be submitted in two copies:
- Signed by the candidate
- The text defining the scope included
- In bound volume(s)
- Drawings and/or computer prints which cannot be bound should be organised in a separate folder.

- The report shall also be submitted in pdf format along with essential input files for computer analysis, spreadsheets, MATLAB files etc. in digital format.

Ownership
NTNU has according to the present rules the ownership of the thesis. Any use of the thesis has to be approved by NTNU (or external partner when this applies). The department has the right to use the thesis as if the work was carried out by a NTNU employee, if nothing else has been agreed in advance.

Thesis supervisors
Prof. Jørgen Amdahl /Prof 2 Jørgen Juncher Jensen

Deadline: June 10 2016

Trondheim, January 25, 2016

Jørgen Amdahl

Abstract

The interest on the influence of dynamic effects on the hull girder loading has increased in the last years. Research shows a high influence of whipping and springing on the fatigue loading. The influence on the extreme loading and the resulting dynamic collapse is currently not estimated. The ultimate capacity is described by a static estimation neglecting dynamic influences. Recent research has proven a high contribution of whipping and springing on the hull girder strains. In this thesis methods are discussed and a first approach on the estimation of the dynamic collapse is performed. A broad literature review is performed to base the work on solid research.

Calculations are performed in the non-linear finite element program ANSYS. The influence of several parameters on the buckling behaviour is checked and the method validated against analytical results. A model of the midship section is build and is verified by a check of the ultimate capacity against an incremental method. The effect of inertia and rigid body motion of the ship is accounted for. A measured strain series is applied on the hull girder as a quasi-static load set and a full load set including whipping. The results are critical discussed and a plan for future research is provided. The project means to give a first investigation in this topic and shows the pitfalls encountered during the work.

Preface

This report is a result of the master thesis conducted by Stud. Techn. Tjark Tilman Schwebe. The thesis is carried out as a cooperation between DTU and NTNU in terms of the Nordic Master in Maritime Engineering. The work is performed at the Department of Marine Technology at NTNU in spring of 2016 and build up on the previous project thesis.

Trondheim, 2016-06-27

Tjark Tilman Schwebe

Acknowledgments

The work has been carried out under the supervision of Professor Jørgen Amdahl (NTNU) and Professor Jørgen Juncher Jensen (DTU). I would like to thank both for the good supervision and the inspirations through out the thesis. Jørgen Amdahl has helped me a lot with the set up of the finite element analysis and Jørgen Juncher Jensen brought insides into the dynamic effects.
Additionally I would like to thank Dr. Ingrid Marie Andersen her helping thoughts and for providing me with the measured strain data and the program to assess them. As well I would like to thank Dr. Henry Piehl for his help with the theoretical background of the non-linear finite element method and their application.
Especially I would like to thank the Lloyd Werft Bremerhaven AG for supporting my master studies and in person Benedikt Dreymann and Grzegorz Drozd for the help with the design of the midship section.
Last but not least I would like to thank every body else involved in interesting discussions about the topic and proofreading this thesis.

Summary

In recent events, the container vessels *MSC Napoli* and *MOL Comfort* broke into two parts. In both cases, whipping loads are assumed to contribute to the failure of the ships structure. However the dynamic collapse of ships is insufficiently studied so far. Currently the ultimate capacity of a container vessel is defined through a static calculation, thus dynamic effects like springing and whipping are not directly included. Research has shown a high influence of dynamic effects on the fatigue loading but there has been no adaptions for the ultimate strength.

The topic is of high relevance because the classification societies are forced to implement whipping loads in their class rules from 1. July 2016. The developed rules of the different classification societies are presented in the thesis. Main objective of this thesis is to apply measured strain data of a container ship on a finite element model. The ANSYS 15.0 code is used to calculate the structural effects. A container ship similar to the *MOL Comfort* is designed according to the Germanischer Lloyd SE (GL) design rules in POSEIDON. The method has been verified on a simple plate and compared with analytical solutions. The midship section is modeled as a non-linear finite element model. The ultimate capacity is calculated and compared with an incremental method. A procedure to include the effect of inertia and rigid body motions is reviewed and applied.

In a next step, quasi-static loads and full wave loads including whipping are applied on the structure. The results are discussed. The thesis is meant to lay a foundation for future research. Especially the difficulties which have arisen during the work and the evaluation of the results are discussed in depth. Thoughts are given for the continuation of this topic.

Contents

Acronyms

ABS American Bureau of Shipping Inc.

BV Bureau Veritas SA

CFD Computational Fluid Dynamic

ClassNK Nippon Kaiji Kyokai

COV Coefficient of Variation

CS Cowper-Symonds

CSE College of Shipbuilding Engineering

DNV Det Norske Vertitas AS

DNVGL DNVGL AS

DoF Degree of Freedom

DTU Danish Technical University

EPP Elastic Perfectly Plastic

FEA Finite Element Analysis

FEM Finite Element Method

FEU Fourty foot equivalent unit

FFT Fast Fourier Transformation

GL Germanischer Lloyd SE

HF High Frequency

HPC High performance cluster

IACS International Association of Classification Societies LTD.

ISUM Idealized structural unit method

LF Low Frequency

LR Lloyds Register Ltd.

MPC Multi Point Constraint

NAPA Naval Architecture Package

NTNU Norwegian University of Technology

SLS Serviceability limit state

TEU Twenty foot equivalent unit

TULCS Tools for Ultra Large Container Ships

ULCC Ultra large container carrier

ULS Ulitmate limit state

VBM Vertical Bending Moment

VFLS Very large floating structures

Latin Symbols

Symbol	Unit	Description
$\underline{\underline{a_i}}$	–	Connectivity matrix
$A_{waterplane}$	m^2	Water plane area of the section
B	m	Breadth
b	m	Width of the plate
$\underline{\underline{B}}$	–	Strain-displacement matrix
b_e	m	Effective width of the plate
B_x	–	Moulded Breadth at the Waterline at the considered cross section
C_x	–	Coefficient
C	–	Strain rate material coefficient
c_0	–	Wave coefficient
$\underline{\underline{C}}$	–	Global damping matrix
C_B	–	Block coefficient
C_{f_T}	–	Service Area reduction factor
c_L	–	Distribution factor
C_M	–	Distribution factor
c_S	–	Distribution factor

C_{T1}	–	Distribution factor
C_{T2}	–	Distribution factor
C_W	–	Wave coefficient
D	m	Draft
$\underline{\underline{D}}$	–	Stiffness
∇	m^3	Displacement at scantling draft
D_{plate}	–	Plate stiffness
E	Pa	Youngs' Modulus
f_h	–	Coefficient
f_m	–	Distribution factor
f_{nl}	–	Coefficient for non-linear effects
f_{nl-s}	–	Non-linear effects for sagging coefficient
f_{nl-vh}	–	Non-linear effects for hogging coefficient
f_{nl-vs}	–	Non-linear effects for sagging coefficient
f_p	–	Coefficient
f_{ps}	–	Coefficient for strength assessement
f_{SW}	–	Ship length distribution factor
f_T	–	Reduction factor related to service restriction
f_{yB}	–	Ratio between Y-coordinate and the load point
f_{yz}	–	Girth coefficient
g	m/s^2	Gravitational acceleration
I	m^4	Moment of Inertia
$\underline{\underline{I}}$	–	Unit matrix (Identity matrix)
K	–	Power Law coefficient

k	–	Linear Buckling coefficient
$\overline{k}$	–	Modal stiffness
$\underline{\underline{K}}$	–	Global stiffness Matrix
$\underline{\underline{k}}$	–	Local stiffness matrix in global coordinates
$\underline{\underline{\overline{k}}}$	–	Local stiffness matrix in local coordinates
$\underline{\underline{K_0}}$	–	Small displacement global stiffness Matrix
$\underline{\underline{K_G}}$	–	Geometric global stiffness Matrix
k_a	–	Amplitude coefficient in the longitudinal direction
k_p	–	Phase coefficient
k_{spring}	N/m	Spring stiffness
L_0	m	Design Length
$\underline{\underline{L}}$	–	Lower triangular matrix
$\underline{\underline{L}}^{\mathsf{T}}$	–	Upper triangular matrix
L_{ao}	m	Length over all
L_{PP}	m	Length between perpendicular
L_{Rule}	m	Rule Length of the Ship
L_{WL}	m	Length of waterline
$\overline{m}$	–	Modal mass
$\underline{\underline{M}}$	–	Global mass matrix
M_S	Nm	Permissible still water bending moment
M_{ST}	Nm	Static torsional moment
M_{SW}	Nm	Vertical still water bending moment
$M_{SW-h-min}$	Nm	DNVGL vertical still water bending moment hogging
$M_{SW-s-min}$	Nm	DNVGL vertical still water bending moment sagging

M_T	Nm	Total vertical bending moment
M_U	Nm	Hull girder ultimate bending moment capacity
M_W	Nm	Vertical wave bending moment
M_{WV}	Nm	Vertical wave bending moment
$M_{WV-h-mid}$	Nm	DNVGL vertical wave bending moment hogging
$M_{WV-s-mid}$	Nm	DNVGL vertical wave bending moment sagging
n	–	Power Law coefficient
$\underline{N}$	–	Vector of shape functions
$n_{modified}$	–	Modified Power Law coefficient
N_x	N/m	Membrane stress resultant in x direction
N_{xy}	N/m	Membrane shear stress resultant
N_y	N/m	Membrane stress resultant in y direction
p	–	Strain rate material coefficient
P_{ex}	N/m^2	Total external pressure
P_{HS}	N/m^2	Hydrodynamic pressures for headseas
P_S	N/m^2	Hydrostatic pressure
P_W	N/m^2	Wave pressure
$P_{W,WL}$	N/m^2	Wave pressure at the waterline
q	N/m	Line Load
Q_{SW}	N	Vertical still water shear force
Q_T	N	Total vertical shear shear force
Q_{WV}	N	Vertical wave shear force
$\underline{r}$	–	Global displacement vector
$\underline{\underline{R}}$	–	Global total nodal load vector

T	m	Depth
t	m	Thickness of the plate
T_{LC}	m/s^2	Draft at midship
US	Nm	Ultimate state
V	kn	Ship velocity
w	–	Interpolation polynominal
W_{bot}	m^3	Section Moduli Bottom
W_{top}	m^3	Section Moduli Top
$\underline{x}$	–	Eigenvector

Greek Symbols

Symbol	Unit	Description
α_1	–	Rayleigh mass damping parameter
α_2	–	Rayleigh stiffness damping parameter
β	-	Plate slenderness parameter
Δ	-	Laplace Operator
δ	–	Imperfection scaling factor
δ_{plate}	m	Maximum Imperfection of a plate
$\delta_{stiffener,ip}$	m	Maximum Imperfection of a stiffener in plane
$\delta_{stiffener,op}$	m	Maximum Imperfection of a stiffener out of plane
δ_{unit}	m	Unit displacement
μ	-	Location parameter
ϵ	m	Elongation
$\dot{\epsilon}$	m	Uniaxial strain rate
ϵ_{eng}	N/m^2	Engineering strain
$\epsilon_{fracture}$	m	Fracture strain
$\epsilon_{necking}$	m	Necking strain
$\epsilon_{plateau}$	m	Plateau strain
ϵ_{true}	m	True strain

γ_{DB}	-	Partial safety factor for the bending moment capacity
γ_{dU}	-	Partial safety factor reducing effectivness of whipping
γ_M	-	Partial safety factor for the ultimate capacity
γ_R	-	Partial safety factor for the ultimate bending capacity
γ_S	-	Partial safety factor for the still water bending moment
γ_W	-	Partial safety factor for the wave bending moment
γ_{WH}	-	Partial safety factor for add. whipping contribution
γ_{Wh}	-	Min. partial safety factor wave bending + whipping
γ_{WHmin}	-	Min. partial safety factor for add. whipping contr.
λ	m	Wave length
$\bar{\lambda}$	-	Slenderness parameter
λ_i	–	Eigenvalue
∇	-	Nabla Operator
ν	–	Poisson ration
ω	–	Circular frequency
ω_0	rad/s	Eigenfrequency
ϕ	-	Johnson-Ostenfeld parameter
$\underline{\phi}$	–	Mode Shape
ρ	kg/m^3	Density
σ	-	Scale parameter
σ_{cr}	N/m^2	Johnson-Ostenfeld stress
$\sigma_{dynamic}$	N/m^2	Yield stress accounting for strain rate effects
σ_E	N/m^2	Euler Buckling Stress
σ_{eng}	N/m^2	Engineering stress

σ_{static}	N/m^2	Static yield stress
σ_{true}	N/m^2	True stress
σ_{UTS}	N/m^2	Tensile stress
σ_{xm}	N/m^2	Effective width stress
σ_y	N/m^2	Yield stress
ξ_i	–	Damping ratio

1. Introduction

The dynamic collapse of the hull girder is insufficiently studied so far. Ultimate limit state calculations are typically performed in a static manner. The collapse behaviour of a container vessel in a realistic load environment is not estimated. Measured strain data reveal a high influence of dynamic loads caused by hull girder vibrations. The fatigue loading increases up to 73 % due to springing and whipping. Their influence on the extreme loading is not fully studied so far.

In this thesis the non-linear Finite Element Method (FEM) program ANSYS 15.0 is used. A simple plate is considered to verify the finite element method against analytical models and semi analytical program PULS 2.0.6. Further is the influence of several parameters on the collapse behaviour checked.

A midship section of a container vessel with main dimensions similar the evaluated load data is designed according to the GL design rules in POSEIDON 16.0. The design is modelled in ANSYS. The ultimate capacity of the hull girder is estimated and compared with an incremental method. The structure is extended to represent realistic inertias and eigenfrequencies of a ship in a marine environment.

Further a transient analyses with measured strain data of a 9,400 Twenty foot equivalent unit (TEU) container vessel is applied on the structure as a bending moment. Aim is develop a method to estimate the effect of the dynamic loads on the collapse. The focus of this thesis is the validation of the model and the results, as it should serve as the foundation for further research. The pre- and post-processing is performed in MATLAB R2016a.

1.1. Background

The influence of dynamic collapse is a current topic of research. On January 2007 the container vessel *MSC Napoli* encountered severe damage of the hull girder it then beached and later broke into two (Marine Accident Investigation Branch, 2008).
More recently the container vessel *MOL Comfort* split in June 2013 in the arabic ocean into two (Sumi et al., 2013). Both parts sunk after a short time. In both cases an influence of dynamic effects on the collapse is likely and might have contributed to the loss of both vessels. Intensive investigations have been undertaken in both cases to estimate causes of the loss. Additionally intensive research is going on in the field of the estimation of whipping loads and the effect on the hull girder. Whipping loads were not considered in classification rules until June 2015 when the International Association of Classification Societies LTD. (IACS) announced its new (IACS UR-S, 2016, Unified Requirements for Large Container Ships) rules. After short time, in October 2015, DNVGL AS (DNVGL) published its new merged rules. Therein a safety factor for whipping loads is defined which needs to be considered for container ships.

1.2. Objective

The objectives are taken from the previous problem description and are defined as:

1) Brief review of work related to investigation of the MOL Comfort accident. Review requirements issued by ship classification societies (e.g. DNV-GL) concerning the use of non-linear finite element methods for assessment of hull girder capacity.

2) Establish relevant wave and whipping induced bending moment histories for the container vessel based on available full scale measurements. Discuss the frequency/temporal characteristics of the histories and the expected ship response to these histories. Determine the lay-out and scantlings of a representative hull girder, based on drawings of similar vessels and software for ship design based on rule requirements (e.g. DNV-GL)

3) Establish a detailed finite element model of three holds in the midship area of a container vessels connected to a beam model of the forward and aft part of the ship. Include also the effect of water plane stiffness for "rigid body rotation" of the hull girder. Discuss various options for modelling of initial imperfections and explain why the selected strategy was chosen. Discuss the choice of boundary conditions for the finite element model. Apply relevant hull girder and local sea loads. Perform static analysis of hull girder resistance subjected to extreme hull bending moment. Identify when yielding and buckling starts in various strength members.

4) Perform time domain analysis of the resistance to regular wave induced hull girder loads, where the wave histories are increased proportionally, bringing the response of the most exposed members into the inelastic region. Compare the results with those from the static analysis.

5) Perform analysis of the hull girder response when it is subjected to whipping induced vibrations in addition to regular wave loads. It is especially interesting to see if stiffened panels loaded beyond their static capacity will buckle or develop permanent plastic shortening that may give rise to low cycle fatigue problems or incremental collapse. Do the bottom panels buckle in the "hungry horse" or the "asymmetric" mode? Can the bottom panels, which undergo plastic straining in compression be subjected to reversed cycling?

6) Establish the hysteresis loop for members/cross-section carried out into the non-linear domain. Estimate the number of load cycles the ship can sustain before failure, depending upon the magnitude of the hull girder loads. Discuss the severity of whipping induced loads on regular wave loads. Discuss how whipping induced stresses could be accounted for in ship rules.

7) Conclusions and recommendations for further work

1.3. Limitation

The main factor of limitation is the required calculation time. Non-linear analysis have a high time consumption because several iteration steps are necessary. The calculations have been performed on a Mac Book Pro (Retina, 13", End 2012) using Parallels Desktop 11.1.3 as a virtual machine for Windows 7. On the personal computer ANSYS Mechanical 15.0 is used. For the final calculations, the High performance cluster (HPC) VILJE with the following specification has been used:

Number of Nodes	1404 Intel Xeon E5-2670
Cores per Node	16 (dual eight-core)
Processor Speed	2.6 GHz
Memory per Node	32 GB DDR3

Norwegian University of Technology (NTNU) has licenses available for 16 nodes. A submitted will be queued up to four days until a suitable spot is available. This limits the use of the HPC to only a few nodes with a relatively long queuing time. This restricts the number of calculations during the limited time of the thesis.

2. Literature Survey

The topic is in a field of several recent research projects. To be able to put this project into perspective it is necessary to mention previous work. The following chapter will give an introduction into topic of the dynamic influence of wave loads, the applied finite element method, the two recent accident and the newly developed classification rules.

2.1. Composition of Wave Loads

Vessels are exposed to a frequently changing environment. Several external loads are causing stresses on the hull girder. Static loads are static water pressure and those loads resulting from different loading conditions of the ship. Main interest in this thesis is the composition and superposition of the vertical bending moment on the midship section of a container vessel. The considered contributions are:

- Still water bending moment
- Quasi-static wave bending moment
- Whipping bending moment
- Springing bending moment

The still water bending moment is results from the difference between load distribution and buoyancy distribution over the ship length. The typical large bow and stern flares of modern container vessels increase this effect. Therefore the mass of the ship and loading higher at the ends compared to the buoyancy. Vice versa the buoyancy is higher than the mass of the

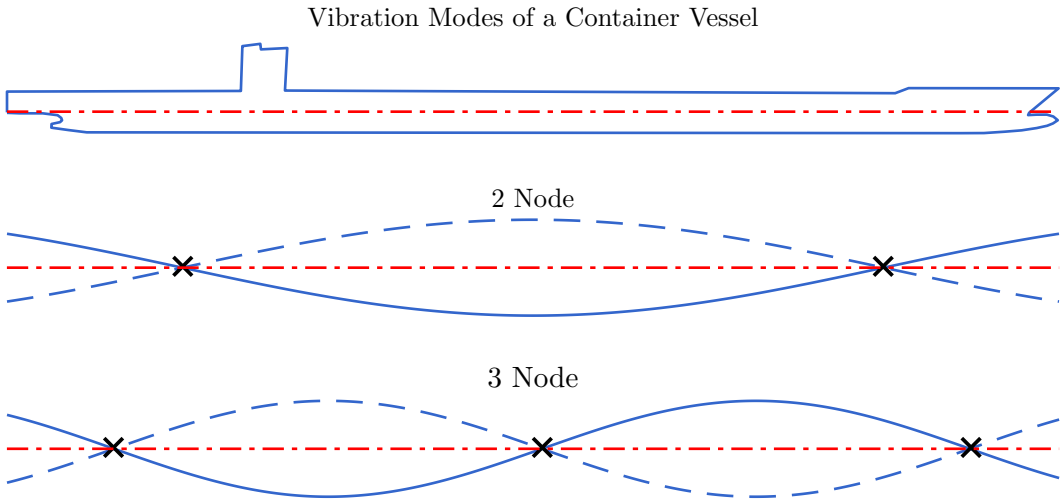

Figure 2.1.: Two- and three-noded vertical vibration mode of a ship. (Jensen, 2001, Fig.: 6.1).

ship at midship to satisfy equilibrium. This results in a hogging still water bending moment. The quasi static wave bending moment is caused by wave passing the ship. The severest case occur when the wave length is equal to the ship length. The ship can either bend in hogging or sagging. First condition is reached if a wave crest is located at midship and wave troughs are located at bow and stern. Latter if a trough is at midship and crests at bow and stern. The change of loading, from hogging to sagging condition appears with the wave frequency. The frequency of load change is equal to the wave encounter frequency. For a wave with length equal ship length the frequency is roughly ten seconds. The change of load is comparably slow, thus mass and inertia effects can be neglected. The loading is thereafter called quasi static.

Whipping loads are caused for instance by slamming loads resulting in transient elastic vibration of the hull girder (Faltinsen, 1990). In the last years container vessels have rapidly grown in size and slenderness. This makes the considered ships more flexible and unfavourable for vibrations. Additionally, the requirement to carry more cargo has caused changes in hull design. Large bow and stern flare is common, leading to greater risk of high impact loading due to slamming. A ship hull can vibrate in several modes. The most severe are the two-, three- and sometimes even the four-node vibration mode. The vibration pattern is shown in Figure 2.1. Container ships possess a high damping ratio caused by the interaction of the cargo, thus vibrations are dying out after certain time. In a nutshell, a slamming im-

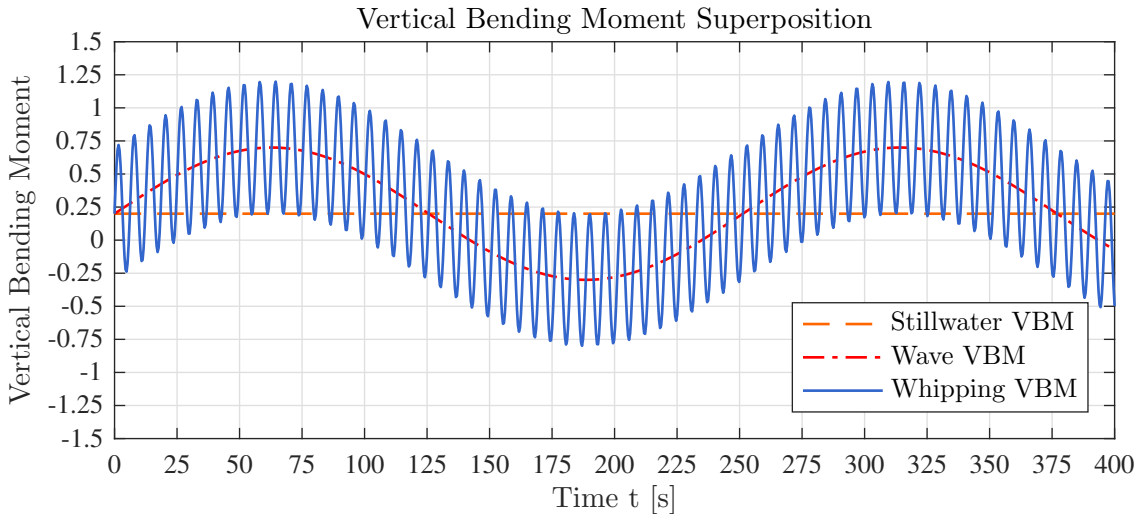

Figure 2.2.: Load superpostion in time domain. Consisting of the three considered load parts: still water, wave, and whipping moment. The moment is non-dimensionalised by the maximum capacity of the midship section. Sumi et al. (2014, Fig.: A13-1).

pact caused by a wave in bow or stern area will excite the ship to vibrate. The magnitude of the vibration will slowly decay after the impact due to damping of the ship hull.

Springing is a steady state elastic vibration of the vessel, resulting from linear and non-linear effects of wave loading. It only occurs when the wave frequency is similar to the ship eigen-frequency. Typical frequencies are a half and one second. Using the dispersion relation the wave length will be much shorter than the ship length (Faltinsen, 1990). Summing up, in an extreme load case springing will not occur, since the frequencies are too different. Anyway Whipping and Springing have an influence on the fatigue loading of a ship. Whereas only whipping loads need to be considered for extreme loading DNVGL-CG-0153 (2015).

The total vertical bending moment applied on the midship section is a superposition of still water bending moment, wave bending moment and dynamic effects. In Figure 2.2 the superposition between the three effects is shown. Outlining the static still water bending moment, the quasi static wave bending moment with a frequency between 0.05 and 0.2 Hz and the whipping moment, where the two node mode is between 0.4 and 1 Hz DNVGL-CG-0153 (2015).

2.2. Influence of Dynamic Loads

Several studies have been performed to estimate the influence of dynamic effects. The first published study has been performed by Moe et al. (2005) including strain measurements on the fatigue loading of a 4,000 TEU container carrier. The finding was a considerable contribution by wave induced vibrations to the total fatigue damage.

Drummen (2008) has investigated a 4,440 TEU container ship. Model tests of an elastic ship model with spring connections were performed at MARINTEK, Norway. The model contained four rigid parts connected by springs. As a core statement the fatigue damage caused by vibrations was estimated to be approximately 40 % for this ships

Moa (2010) and Mao et al. (2010) have done research on the effects of whipping on the fatigue and extreme load. Conclusion was that whipping contributes about 30 % to fatigue loading of the estimated 2,800 TEU container vessel. The influence on extreme loads was left open for further studies.

Heggelund et al. (2011) have performed full scale measurements for fatigue and extreme loading on a post panmax container vessel. Strain on a 8,600 TEU vessel has been measured amidship over a period of 20 months. The measurements have been evaluated and compared to the design rules applied for the vessel, concluding that the vibrations dominate the fatigue damage. It is observed for the extreme loading that in harsh conditions the value is well above the design level for the hogging condition. Additionally the damping of the ship seems to be higher, than for other ship types, causing the loads to decay faster.

Storhaug et al. (2010) have performed model test with a 13,000 TEU container ship. Aim was to estimate the fatigue and extreme loading caused by whipping and springing. The model tests have been performed at MARINTEK. The model was divided into four rigid elements connected by three flexible joints. This ensured, that the model is able to vibrate in the governing two-node mode. Several sea states and wave directions have been tested, corresponding to typical trading routes. Outcome is that the vibration load is the dominating fatigue load at midship with 65 %. The extreme loading exceeds the IACS design values and further investigations are required.

In addition Storhaug et al. (2011) have done tests on the same model in bow quartering seas.

The results regarding the effect of different wave encounter angles have been evaluated. The outcome shows, that the heading direction to the wave does not effect the influence of whipping loads. Thus a change of the course, does not effect the whipping loads.
More recently Barhoumi and Storhaug (2014) have evaluated measured strain data on a 8,600 TEU container vessel. The measured effect of fatigue loading from whipping is assessed to be 57 %. The rule based extreme loads has been exceeded by up to 48 % at aft quarter length. For further rule development the recommendation is to keep realistic loading situations, caused by seamanship in perspective to avoid over conservative class rules.
Kahl et al. (2014) have evaluated full scale measurements on board a 4,600 TEU Panmax and a 14,000 TEU Post-Panmax container vessel. The results for the fatigue design are between 41 % and 73 % influence from hull girder vibrations.
Andersen and Jensen (2014) have published an assessment of measured strain data on 9,400 TEU container vessel. The outcome is, that quasi-static wave loads and high frequency effects can have roughly the same magnitude. Additionally in moderate conditions the design values for extreme loading can be exceeded. The results of this paper will be one of the project's main components and will be discussed in more depth in the next section.
Andersen (2014) compared strain measurements from the 14,000 TEU, 9,400 TEU, 8,600 TEU and 4,400 TEU ships mentioned earlier. The response of the 9,400 TEU vessel with a bow flare angle of 45 degrees and the 8,600 TEU vessel with a bow flare angle of 58 degrees have been compared. The response was very different and the bow flare angle was assumed to be one important parameter.
Storhaug (2014) summed up the performed work so far. He describes the previously mentioned measurements and verifications of the findings. He states the problems by using model test and strain measured data on real ships. It is pointed out, that so far the effect of whipping loads is not fully developed.

2.3. Measured strain data on a container vessel

Andersen and Jensen (2014) have recently published an investigation of measurements of hull girder stresses on an Ultra large container carrier (ULCC). The estimated vessel was the

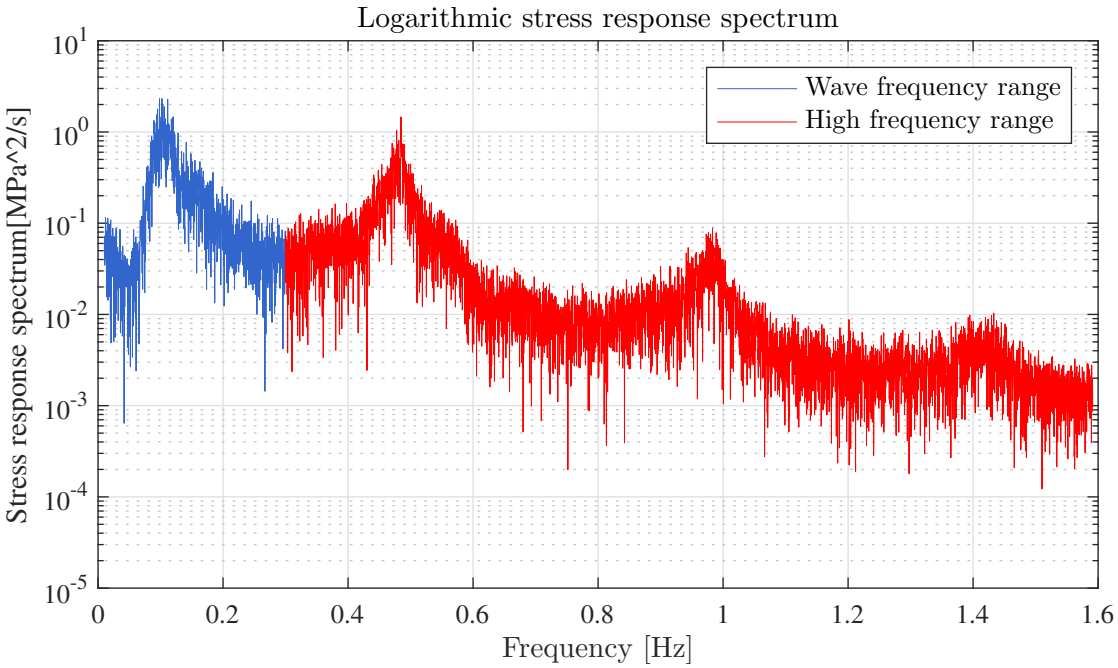

Figure 2.3.: FFT of the measured strain data on a 9,400 TEU ULCC in a sea state with a significant wave height of eight meter on a logarithmic scale. (Andersen and Jensen, 2014)

9,400 TEU container ship.

The strain data has been measured on 02 October 2011 when the ship went through a storm while sailing about ten knots in a sea state with significant wave height around eight meters. The strain has been measured using two long-base strain gauges in the passageway amidship. The stress measured at starboard and port has be averaged to exclude torsional and horizontal loads.

A FFT has been performed on the measured strain series. Four peaks are visible in Figure 2.3, corresponding to the most common loading frequency. The signal is considered between the borders of 0.01 Hz and 1.6 Hz according to the DNV-RC (2011) recommendations. The frequency range from 0.01 Hz to 0.3 Hz is called the Low Frequency (LF) range, the frequency range from 0.3 Hz to 1.6 Hz is called the High Frequency (HF) range. The peak in the LF range displays the wave load frequency, whereas the range above 0.3 Hz displays the whipping contribution. Herein the two node mode can be estimated at 0.48 Hz and the three node mode at 0.99 Hz.

By using a FFT and their inverse it is possible to switch between time and frequency domain.

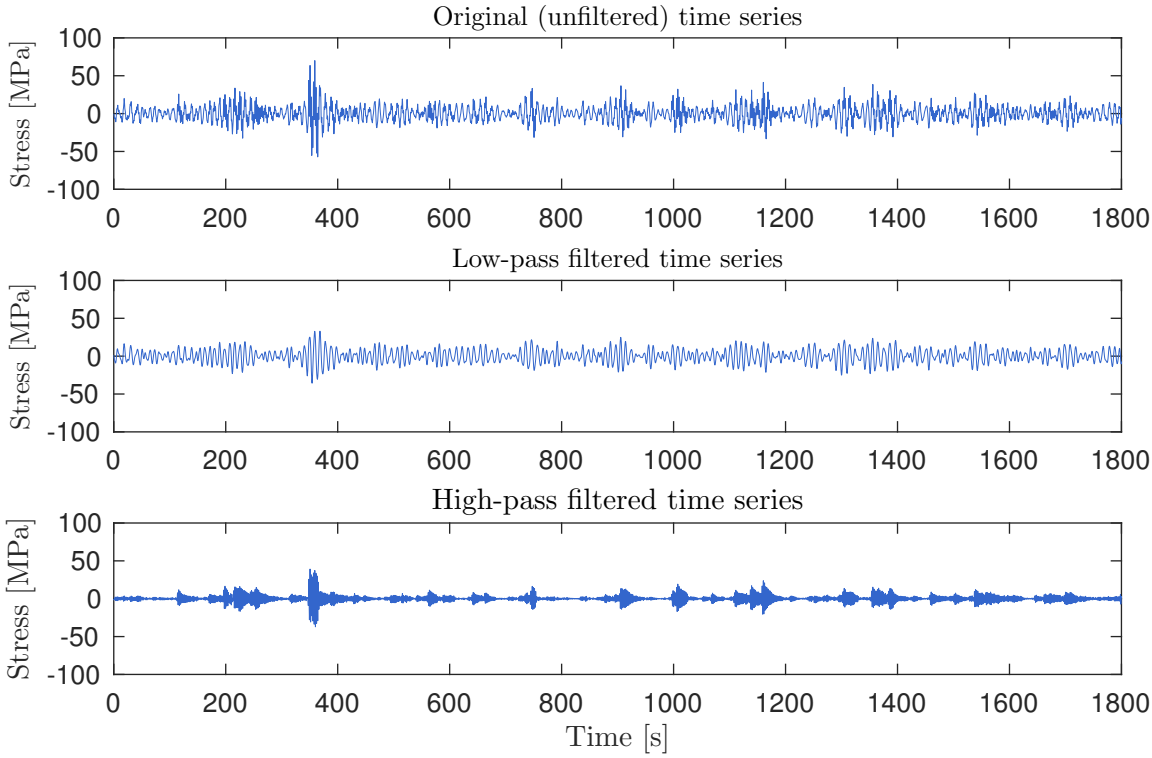

Figure 2.4.: Time series of the measured strain data over 30 minutes. The unfiltered series is shown as well as the low-pass filtered time series and the high-pass filtered time series. (Andersen and Jensen, 2014)

Advantage hereby is the ability of erasing certain frequencies of the time series. In Figure 2.4 the unfiltered time series as well as the filtered LF and HF range is shown. For the wave loads it can be seen, that the magnitude of the stress varies, but is always present over the time. For vibration loads, it can be seen how the load start abrupt and decays thereafter again. The average load level is low, but the peak loads are high.

Comparing the magnitude of the wave loads and the dynamic loads, for their peak values, e.g. at second 350, the stress is roughly of same magnitude. Andersen and Jensen (2014) have compared further the measured stresses with the allowed stress for the container ships according to the classification society rules. The measured loads exceed the design values during the peaks already in this moderate sea state.

2.4. Prediction of whipping loads

So far it is known, that dynamic effects have an influence on the fatigue load and might influence the extreme load. Thus the estimation of whipping loads is a topic of great interest. The estimation of slamming loads has already been defined by von Karman in 1929 and has been improved by Wagner in 1932 (Faltinsen, 1990). Consequently the exercise is to estimate from known slamming loads, the corresponding whipping loads.

Research at Danish Technical University (DTU) has been performed to combine strip theory developed by Salvesen et al. (1970) with hydro elasticity. Based on the perturbation method by Jensen and Pedersen (1978), Xia et al. (1998) present a non-linear time domain strip theory accounting for hydrodynamic memory effects. The "momentum slamming" force is included. The ship is modelled with Timoshenko beams and allows rigid body motion. The beam model combined with the non-linear hydro elasticity model makes it possible to predict vibration loads.

Andersen and Jensen (2012) have used the in-house strip theory code SHIPSTAR and compared the results with model tests in regular waves. The tests have been performed with a flexible model ship at CEHIPAR, Spain. For longer wavelength, both methods are applicable. For shorter wavelengths the results are poorer. Nonetheless is the method able to simulate momentum slamming.

More recently Computational Fluid Dynamic (CFD) is used for the whipping prediction. Seng and Jensen (2012) compared slamming loads received by a free surface Navier-Stokes equation with the results of non-linear strip theory. Further Seng et al. (2012a) compared strip theory with a CFD solver in terms of whipping loads. Even though the CFD method is the more advanced method, strip theory reveals similar accurate results. For reasons of comparison, again the model test are consulted, showing good agreement for long crested waves.

Seng et al. (2012b) have applied a direct three-dimensional, fully non-linear numerical calculation in a realistic wave environment. The method of a model correction factor approach is proposed, to apply the complex processes of hydro elasticity in strip theory. This improves the accuracy of strip theory, especially for bow quartering sea and following seas.

Seng and Jensen (2013) applied the model correction factor approach and worked out difficulties using it with strip theory. Since strip theory is not able to include radiation effects, it is likely to detect slamming in the stern of the vessel, even though in reality this is not the case. Thus recommendation is to use a modified aft model to avoid this pitfall.
In a nutshell, strip theory is improved to account for the effect of hydro elasticity. Further CFD is used to improve the accuracy of the strip theory results.

2.5. Influence of Rigid Body Motion in Ultimate Strength Analysis

When investigating the post collapse region of a hull girder, it is important to estimate the influence of rigid body motion. During the collapse of a 350 meter long ship, the ends experience a big change in draft even for small angles. The increasing buoyancy will force the midship section to lift and generate moment capacity. This will define the severity for a failure of the hull girder.
Xu et al. (2011a) have developed a new approach for the dynamic collapse behaviour. The basic model contains two rigid body elements and a rotational spring connecting both parts at the hinge. Strip theory is further used to apply the loads. It shows, that the collapse increases rapidly until unloading occurs. Tank tests have been performed to prove the results. Herein a specimen links both rigid parts and defines the collapse behaviour. Of special interest is the extend to which the ship collapses until equilibrium is reached.
Xu et al. (2011b) have improved the existing strip theory model and compared it with effects which will occur in reality. Focus is put on post ultimate strength. Effects such as development of buckling pattern, a higher capacity drop and stiffness recovery when unloading due to residual capacities have been discussed.
Iijima et al. (2011) have performed model test to validate the non-linear strip theory including a plastic hinge. Outcome is that the hull girder collapses rapidly unless unloading due to rigidity occurs. As well that the severity of the collapse is highly depending on the capacity drop after failing.

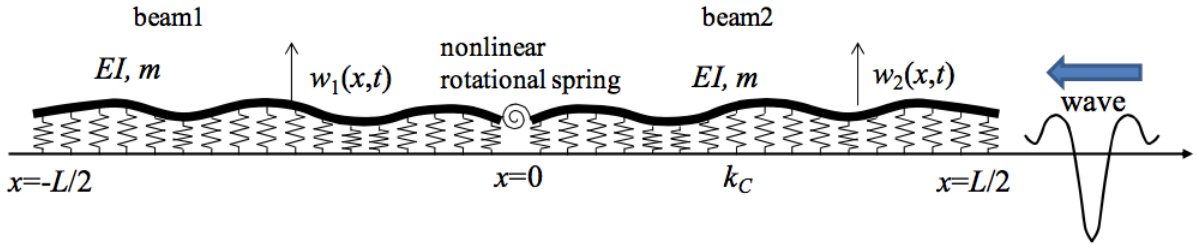

Figure 2.5.: Extension of the rigid body motion model, using flexible beams to model the rigid part of the vessel. The collapse region is displayed by a non-linear rotational spring. The beams are embed on springs. (Iijima and Fujikubo, 2012)

Xu et al. (2012) have performed a parametric study on the post buckling behaviour. The dynamic collapse is characterised by the eigenvalue. Whereas the eigenvalues are depending on the moment of inertia and the stiffness. The latter is highly dependent on the restoring forces from hydrostatic pressure and rigidity of the structure.

An extension for very large floating structures is done by Iijima and Fujikubo (2012). The definition of rigid elements is not sufficient enough due to hull girder flexibility. An approach with flexible ends is developed, but more sophisticated models should be consulted.

Xu et al. (2014) have replaced the non-linear spring with a finite element approach. The loads have been applied using the developed strip theory method. The bending moment on the finite element model is applied using Multi Point Constraint (MPC) elements at the height of the neutral axis. The FEM shows good agreement with the developed strip theory approach for the total collapse of the structure.

Summing up, strip theory has been combined with a plastic hinge and a finite element model. This enables the estimation of the post collapse path for the ship. Several methods have been applied to increase the accuracy of the non linear spring and the rigid body parts.

2.6. Finite Element Modelling

Finite Element Analysis (FEA) has been performed from several authors on different subjects. Amlashi (2008) has built a model of the midship section of a Bulk carrier. He used a 1/2 + 1 + 1/2 cargo hold model (Amlashi and Moan, 2008). The longitudinal parts of the middle cargo hold are defined with non-linear material. The other parts are modelled with linear material.

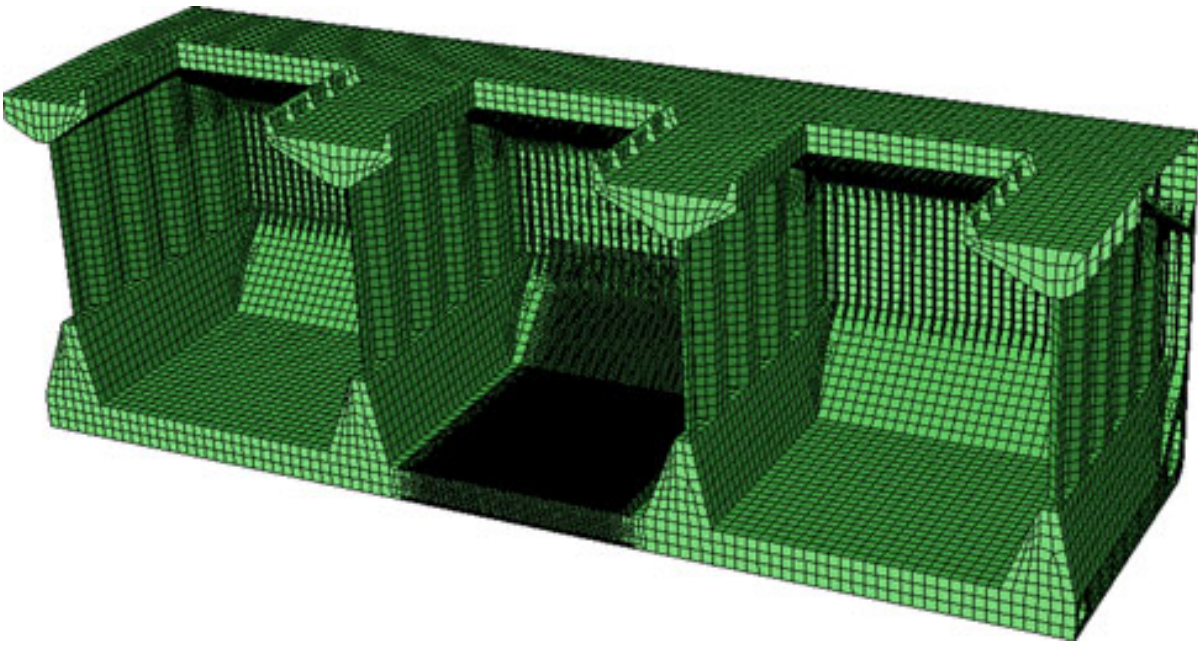

Figure 2.6.: Three cargo hold model of a bulk carrier. Mesh defined in ABAQUS/CAE. Modified version of the Amlashi (2008) model, used by Shu (2010), taken from Shu and Moan (2012).

A bilinear material model is chosen for the non-linear part of the model. The program used for the analysis is ABAQUS/Standard. The S4 shell elements have been chosen. These are four node general purpose, finite membrane strain shell elements. This element has been compared with the S4R element, using reduced integration with hourglass control and the S4R5 which is a thin shell, reduced integration with hourglass control, using five degrees of freedom per node element (Abaqus User Manual IV, 2012). The results gave little variation between the different elements and thus the S4 was chosen. Additionally a mesh convergence study was performed. Different mesh sizes have been applied over the length of the model. Using a fine mesh for the estimated "failure" region and a relatively coarse mesh for the surrounding area.

Further work with a similar model has been performed by Shu (2010). Due to difficulties at the boundaries for the 1/2 + 1 + 1/2 cargo hold model, a three cargo hold model is chosen. The element as well as the mesh size are taken over from the previous work done. Geometrical imperfections have been included for the plates and stiffeners. The total amount of Degree of Freedom (DoF) for the model is 990,000. The model is shown in Figure 2.6. Clearly

visible is the refine midship area of the model. For both models only the port side has been designed. Symmetric boundaries have been applied to reduce the number of DoF. For the application of the external loads have the programs VERES and WASIM been used. VERES is based on 2D strip theory and WASIM is based on 3D Rankine panel method.

2.7. *MSC Napoli* Accident

On the 18th January of 2007 the 4,419 TEU container vessel *MSC Napoli* suffered structural hull girder failure in the English Channel. The ship was sailing with wind of storm force measuring between 10 and 11 on the Beaufort scale. The wave height was between 5 and 9 meters with a wave period of 9 to 10 seconds. The wave length was 150 meters and the water depth 80 meters (Marine Accident Investigation Branch, 2008).
The hull girder collapsed right behind the engine front bulkhead, in the area of the engine room. Intensive research have been done to determine the triggers of failure. The ship was classified under Det Norske Vertitas AS (DNV) rules. Thus DNV as well as Bureau Veritas SA (BV) investigated this matter. Both methods will be presented within this section.
The DNV method described in Marine Accident Investigation Branch Annex A-D (2008) has been performed in the following steps:

1) Hydrodynamic Wave Load analysis using DNV's wave load tool WASIM

2) Global linear stress analyses with fine mesh in examined area using DNV's finite element program SESAM

3) Non-linear stress and ultimate capacity analysis with fine mesh in examined area using ABAQUS.

The still water bending moment has been analysed using the software package Naval Architecture Package (NAPA) based on strip theory, from the actual loading condition. The wave loads have been analysed for linear and non-linear effects in WASIM. Two different wave scenarios have been estimated to define a possible load range. Whipping loads have been mentioned as an additional factor, increasing the load.

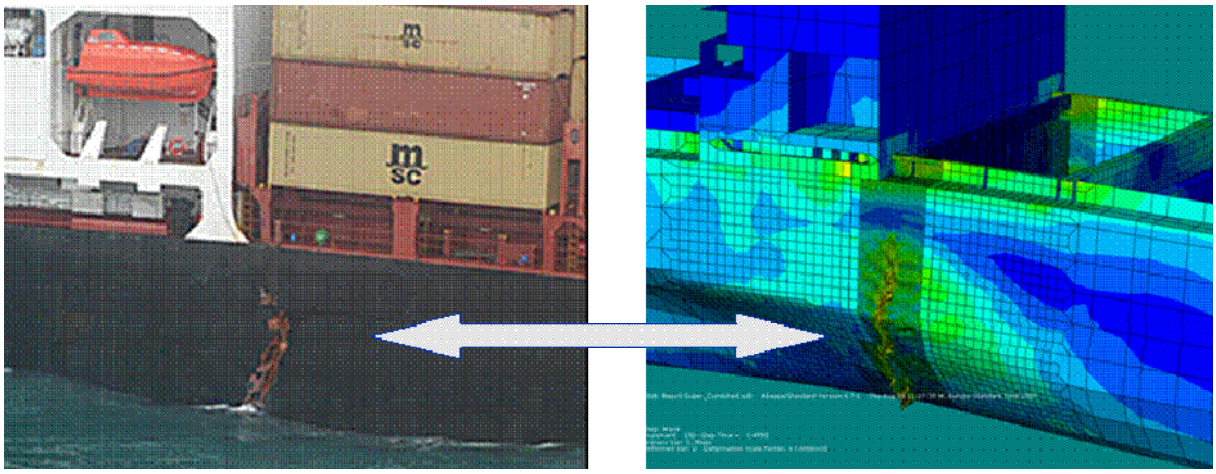

Figure 2.7.: Comparison between the collapsed *MSC Napoli* hull and the calculated failure using the non-linear finite element program ABAQUS. (Marine Accident Investigation Branch Annex A-D, 2008)

The loads from WASIM have been transferred onto the linear SESAM Model and equilibrium solved. The stresses have been found close to the yield stress and the results have been transferred onto the non-linear ABAQUS model.

The global model has been defined as linear except of the engine part, which has been defined as a non-linear super element using very fine mesh. The determination of the fine mesh area will be discussed later in this thesis. Small imperfections have been included in order to capture the real buckling and collapse behaviour.

The non-linear material has been defined as a bilinear material curves. Three different material sets have been used:

1) Lower 5 % quantile yield stress

2) Mean value yield stress

3) Upper 5 % quantile yield stress.

The lower 5% quantile yield stress are rule based values. This will in 95 % underestimate the structure and a higher value is more realistic. The calculations result in different ultimate capacities, corresponding to the yield stress levels.

Comparing the capacity range with the estimated load range, reveals a certain overlap. In this area, the capacity is lower than the load and failure occur. The collapse pattern received

in ABAQUS has been compared with the real collapse pattern. Figure 2.7 shows a good agreement for the model. The loss was in this case caused by insufficient rules of DNV. The rules have been changed and the hull girder capacity has been increased thereafter.
BV uses a more simplified approach. The conditions at time of the accident are interpolated from data of the hindcast model provided by the British government. A Jonswap spectrum is used to determine the most likely sea state.
Whipping loads are estimated in matter of measuring slamming forces in a time domain analysis and receiving a whipping response. The result is, that the load is increased by 30 % when slamming loads are considered. The calculation however does have a number of uncertainties, namely: structural damping, speed, heading, wave spectrum and mass distribution.
A finite element model of the engine room area is modelled in ABAQUS. The material is chosen to follow the Ramsberg-Osgood theory. The yield and tensile strength are defined according to the design values. Riks method is used. Finally the ultimate structural capacity is defined and evaluated. The angle of the ultimate capacity is found to be 10^{-3} radiant. Taking uncertainties as whipping into consideration a collapse is possible.

2.8. *MOL Comfort* Accident

On 17th June 2013 the 8,110 TEU container vessel *MOL Comfort* broke near the midship section into two pieces. Pictures of the ship can be seen in the problem description. The ship was sailing with a speed of 17 knots in a sea state with a significant wave height of 5.5 meter, wave period of 10.3 seconds and wind of force 7 Beaufort. The accident happened in the Indian Ocean on a voyage from Singapore to Saudi Arabia. The ship was classified under Nippon Kaiji Kyokai (ClassNK).
After the accident ClassNK published and interims investigation report (Sumi et al., 2013) and a final report (Sumi et al., 2013) about the loss of the ship. The ship experienced severe collapse of the bottom structure at the midship section. After the accident six sister ships and four similar ship have been examined in the affected bottom area. In five of the six sister ships and in one of the four similar ships deformations in the bottom area were found. The out of plane deformation has been in the area of the section weld and has been on average

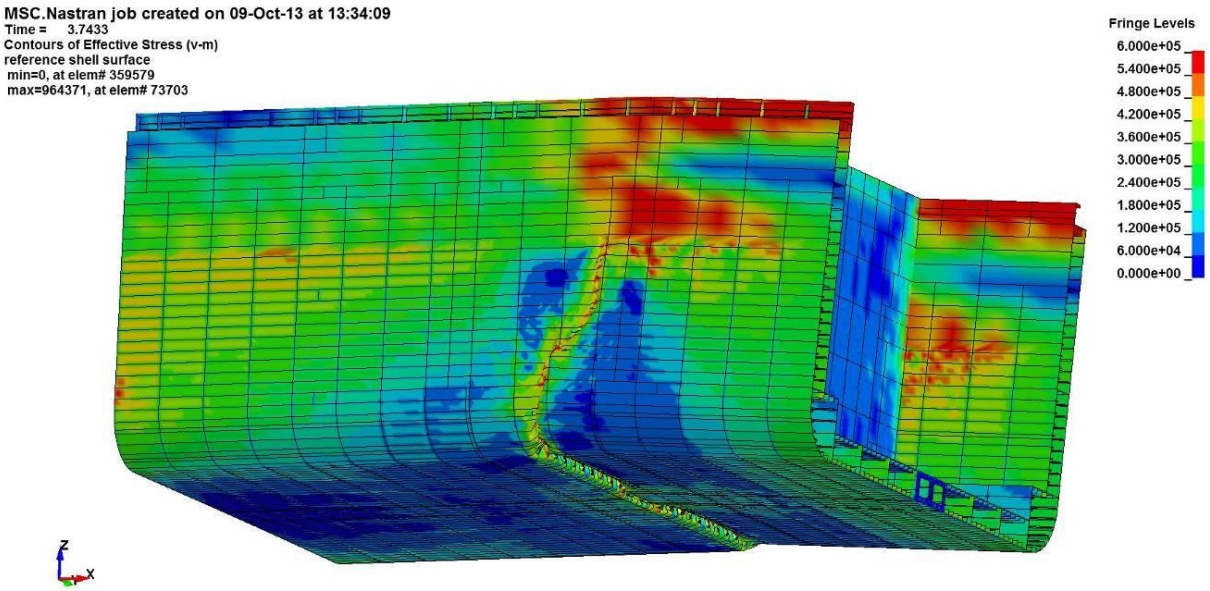

Figure 2.8.: Deformed model of the *MOL Comfort* loaded higher than the ultimate strength. (Sumi et al., 2013)

20 millimetre but deformations up to 60 millimetre have been measured.

The *MOL Comfort* was at the time of the accident five and a half years old. Intensive work has been put into the estimation of the load strength. Further a 1/2 + 1 + 1/2 cargo hold model was build. First a model of a bottom panel has been build and analysed. The effect of transverse and longitudinal stresses on the panel has been estimated. As well the effect of residual stresses have been analysed.

For calculating the ultimate capacity of the section, the LS-DYNA code, using an explicit solver, has been used. The following loads have been applied:

1) Gravitation Force for steel weight

2) Hydrostatic Pressure

3) Container Loads

4) Allowable still water bending moment

5) Wave-induced pressure

6) Wave induced Vertical Bending Moment (VBM)

7) Additional VBM.

The additional VBM was increased until the hull girder collapsed. Thus the ultimate capacity can be estimated by looking at the load displacement curve. The failed hull girder can be seen in Figure 2.8. The outcome is, taking all uncertainities into account, that a failure of the hull girder is possible.

2.9. Ultimate Strength Design Rules

IACS UR-S (2016, S11A.5) defines rules for hull girder ultimate strength, given by:

$$\gamma_S M_S + \gamma_W M_W \leq \frac{M_U}{\gamma_M \gamma_{DB}}. \tag{2.1}$$

With γ denoting partial safety factors and M vertical hull bending moments. The equation is divided into three parts. Where the left hand side of the equation is the load part. The still water bending is denoted with S, the wave bending with W. On the right hand side of the equation is the capacity. Having the ultimate capacity denoted with U and two safety factors covering material, geometric and strength prediction uncertainties M and double bottom bending effect DB. The new amendment IACS UR-S (2016, S11A.6.3) states, that each classification society must take the effect of whipping into account. The way of inclusion is left open to the classification societies.

3. Methodology

The aim of this thesis is to verify the influence of dynamic load effects, such as whipping, on the hull girder. Several classification societies have published a recommendation, as this might be done. The influence factors will be compared with the results of this thesis. To evaluate the effects, a certain strategy must be defined. In the following, the modelling of loads, structure and finally verification of the results is discussed.

3.1. Modelling the Loads

As mentioned in Chapter 2 several researches have been performed to use strip theory, for including whipping loads. Effort has been performed to use CFD to improve the results. (Seng and Jensen, 2013) The structural and hydrodynamic damping is hard to predict and has a big influence on the contribution of dynamic effects (Iijima et al., 2011). Additionally strip theory does not account for radiation effects and requires a special definition of the vessels stern. (Seng and Jensen, 2013)

Alternatively the loads can be applied by using model test data, or strain measurements on a container vessel. Heggelund et al. (2011) mentioned, that the damping of vibrations depends on size of the vessel. Generally container vessels have higher damping due to interaction of the cargo. In model testing it is hard to achieve a high enough damping rate for large container vessels, thus whipping loads might be too high. (Storhaug et al., 2010)

The best way of applying loads with a realistic whipping contribution is to use measured strain data. The author is fortunate to be able to use the strain data evaluated in Andersen and Jensen (2014). The data is transferred from stresses into a bending moment and further

scaled in magnitude to reach certain values of interest. To reduce the required calculation time a suitable wave is picked out of the measured set to represent an extreme event. To estimate the effect of the dynamic collapse a longer time period is used.

3.2. Modelling the structure

For the definition and calculations of the structure the program ANSYS is chosen. Due to a lack of data a container vessel in dimensions close to the estimated ship is designed. Main focus is to match the eigenfrequencies of the 9,400 TEU ship used in the load data. The program POSEIDON is used to design a suitable midship section according to the regulations of the GL

Several studies have proven the use of finite element analysis valid for the analysis of the ultimate capacity of the hull girder. On the one hand the model needs to have a certain size, to neglect influence of boundaries. On the other hand it must be sufficiently simplified to reduce calculation time. A first approach on the model size is taken according to the *MOL Comfort* survey. This ensures symmetry conditions in the longitudinal direction and ensures steady deflections between the cargo holds and the bulkheads. Only the starboard side is modelled and symmetry condition in transverse direction is applied as well.

The dynamic collapse is the main consideration of the thesis. Thus dynamic effects need to be considered. For this matter it is important that the ship has the same eigenfrequencies as the load data. This can be done by defining masses in the extensions of the ship. They account for the mass of the ship and container loads. The eigenfrequencies are known from Andersen and Jensen (2014). The ship in water will have to deal with the effect of added mass. Thus the external weights are scaled until the structure has the corresponding wet eigenfrequencies. To avoid the masses to create a bending moment on the structure, loads are applied to ensure equilibrium.

A loading scenario is developed, including static and dynamic external pressure, container and tanks. Since the inertia of the masses are important for the dynamic behaviour, containers are defined as masses instead of loads.

Intensive research has been done on the ultimate collapse behaviour of ships. To account

for the relaxation effect of "rigid" body motion the procedure of Iijima and Fujikubo (2012) is followed, by applying beam elements in the extension of the shell model. These beams are constrained by springs in vertical direction to account for the change in displacement.
The provided load data is applied at the ends of the shell model using MPC elements. The effect of the rigid body is measured and excluded for the collapse behaviour.

3.3. Planning and verification of work

To reach the goal of estimating the dynamic collapse several steps need to be considered on the forehand. The finite element method is chosen for the work. Since this numerical method does not necessarily reflect realistic behaviour it is required to validate the result with analytical solutions. First evaluations are performed with a simple plate. The analytical results are given by the Euler buckling loads and the concept of effective width which will be introduced later. Additionally the semi analytical program PULS by DNV is used to compare the results. Also the effect of different parameters e.g. materials, added mass, imperfections, etc. on the structure can be checked with this simple model.
When the method is validated, the midship section can be designed and modelled. For a non linear buckling analysis it is necessary to include imperfections. These imperfections are obtained from an eigenvalue analysis of the "crash" section. Important for the dynamic collapse later on is the representation of the correct eigenfrequencies. These will be modelled by beam elements at the rigid ends.
With this set up it is possible to calculate the static collapse of the structure. An incremental method provided by POSEIDON is used to compare the results. Next the incremental collapse using wave data with the whipping loads can be estimated. A load level will need to be estimated at which plasticity occurs. With this level defined, several waves will be loaded onto the structure and the dynamic collapse can be estimated. The whole process can be seen in Figure 3.1.

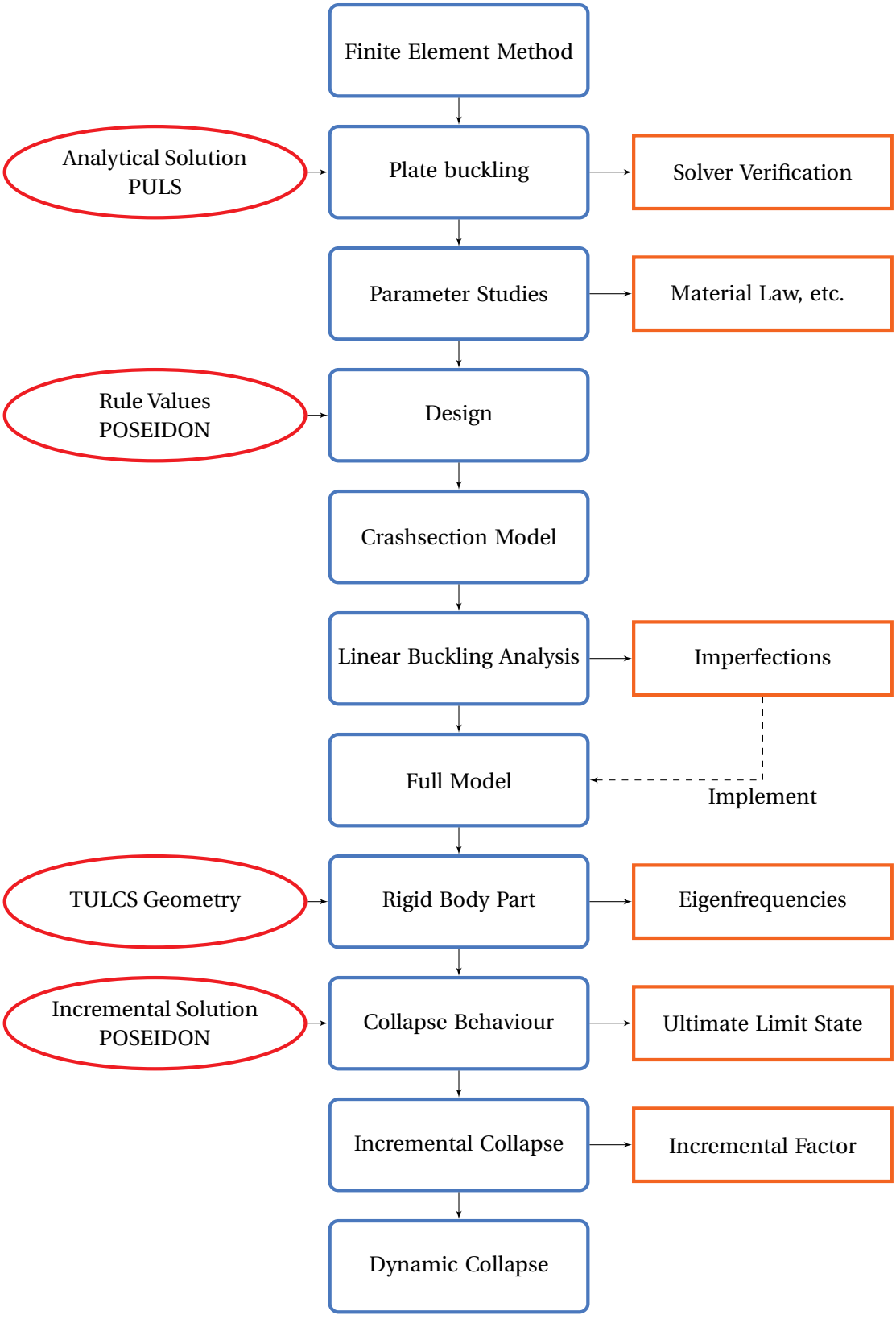

Figure 3.1.: Flowchart steps necessary to estimate the dynamic collapse of the structure.

4. Individual Studies

For the studies a midship section is designed. The design is further transferred to a finite element model. The following section will outline the thoughts and theories used for the model.

4.1. Coordinate & Unit System Definition

One of the most important set ups for a model is always a clear definition of the used coordinate system and units, ANSYS allows both to be manually defined by the user. The coordinate system is chosen, using a typical naval architecture approach. With the x-axis pointing forward starting at the aft perpendicular, the y-axis point to the port side of the vessel starting at centreline and the z-axis pointing upwards beginning at the basis. Where the basis is defined as height of the bottom, without the bottom plating. The reference system is shown in Figure 4.1.

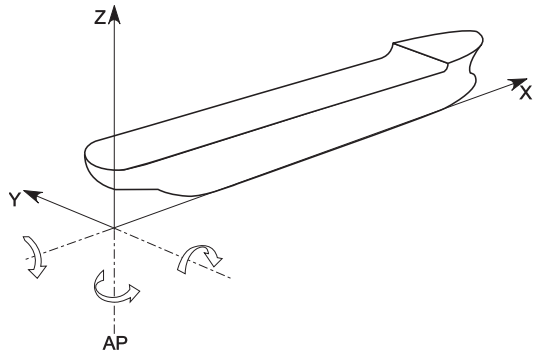

Figure 4.1.: Global coordinate system and direction of rotations of the ship. (IACS UR-S, 2016, S11A, Fig.:2)

Table 4.1.: Units and combined units used in the model. The measurement system is set to use SI-Units. The values are the input values for ANSYS.

Property	Unit name	Combined Unit	SI-Unit(s)
Mass	kilogram	-	kg
Length	meter	-	m
Time	second	-	s
Force	newton	N	kg·m/s
Moment	newton · meter	Nm	kg·m^2/s
Stress	pascal	Pa	N/m^3

The local coordinate system for the elements is defined as the global one. This ensures a consistent definition of the coordinates.
Next step is the definition of the unit system. The SI-Unit system is chosen. The main dimensions are given as kilogram, meters and seconds. Properties such as force, moment and stress will have units combined from several single SI-Units. The full input table can bee seen in Table 4.1.
It should be noted that IACS and thus GL, DNV, DNVGL and POSEIDON use for force and moments the units kN and kNm respectively. It is also common to use millimetre instead of meter in naval architecture, these pitfalls will be considered.

4.2. Estimated Ship

As already mentioned the ship is defined by the author. Therefore the main dimensions could be chosen freely. In response to the accidents of the *MSC Napoli*, the accident of the *MOL Comfort* and the strain data taken from the TULCS ship, the main dimension are chosen. The main dimensions are shown in Table 4.2.
The next decision is which classification society rules should be used in order to estimate permissible loads on the ship. Due to previous experiences the GL classification society is chosen. The class sign is thereafter given by:

Classification : GL +100A5 Rules: January 2016

Container ships are designed in a similar way so as to carry the standardized cargo TEU and

Table 4.2.: Main Dimensions of the *MSC Napoli*, *MOL Comfort*, TULCS project ship and the designed ship.(Marine Accident Investigation Branch Annex A-D, 2008) Sumi et al. (2014) (Andersen and Jensen, 2014) (Andersen, 2014)

Property	Symbol	*MSC Napoli*	*MOL Comfort*	TULCS	Ship	Unit
Class	-	DNV	ClassNK	BV	GL	-
Length over all	L_{oa}	275.66	-	349.00	350.00	m
Rule Length	L_{Rule}	-	-	329.70	340.00	m
Length btw. pp.	L_{PP}	261.40	302.00	333,40	330.00	m
Breadth	B	38.18	45.60	42.80	46.00	m
Draft	D	21.50	25.00	25.00	25.00	m
Depth	T	13.50	14.50	14.50	14.50	m
Block Coefficient	C_B	0.609	-	0.66	0.66	-
Max. Displacement	∇	82,052	-	136,559	149,674	m^3
Max. velocity	V	24.10	25.25	25.40	25.00	kn
Container Capacity	-	4,419	8,110	9,400	10,500	TEU
Deadweight	-	62,277	-	113,000	120,000	ton

Table 4.3.: Main dimension of a TEU and a FEU, an ISO 20' Container and an ISO 40' Container.

Property	TEU	FEU	Unit
Length	6,058	12,192	mm
Width	2,438	2,438	mm
Height	2,591	2,591	mm
Height HC	2,896	2,896	mm
Average loaded weight	7,000	14,000	kg

Fourty foot equivalent unit (FEU). The dimensions are shown in Table 4.3. The cargo hold is designed to accommodate at the midship section sixteen container besides each other. The stack will be nine container height with the out most row only eight.

After a sketch of the midship section is defined, caused by geometric considerations the next step is to estimate the bending moment and shear forces acting on the section. Therefore several sources have been consulted. As earlier mentioned the still water and wave bending moment must be estimated. The still water bending moment is usually found by calculating the required loading conditions, which represent the most severe cases. In this case, no hydrodynamic model is developed and a coarser method is chosen. DNVGL Rules (2016) has developed a formula to estimate the still water loads in a rough estimation. The calculation is given in Section B.2 and the results are shown in Table 4.4.

Table 4.4.: Vertical still water and wave rule bending moment according to GL, DNVGL and the POSEIDON design tool. (GL Rules, 2015) (DNVGL Rules, 2016)

Property	Rule	Symbol	Value	Unit
Still Water Shear Force positive	DNVGL	Q_{SWpos}	8.7435e+04	kN
Still Water Shear Force negative	DNVGL	Q_{SWneg}	-8.7435e+04	kN
Still Water Bending Moment Hogging	DNVGL	M_{SWh}	5.7707e+06	kNm
Still Water Bending Moment Sagging	DNVGL	M_{SWs}	-3.7849e+06	kNm
Wave Bending Moment Hogging	GL	M_{WVh}	6.7529e+06	kNm
Wave Bending Moment Sagging	GL	M_{WVs}	-8.0561e+06	kNM
Wave Bending Moment Hogging	DNVGL	M_{WVh}	6.7529e+06	kNm
Wave Bending Moment Sagging	DNVGL	M_{WVs}	-8.0708e+06	kNm
Wave Bending Moment Hogging	POSEIDON	M_{WVh}	6.7447e+06	kNm
Wave Bending Moment Sagging	POSEIDON	M_{WVs}	-8.0463e+06	kNm

Table 4.5.: Moment of inertia, neutral axis and section moduli for the final design of the ship.

Property	Symbol	Value	Unit
Moment of Inertia	I	732.351	m^4
Neutral Axis above base line	-	12.204	m
Section Moduli Top	W_{top}	51.517	m^3
Section Moduli Bottom	W_{bot}	60.008	m^3

For the wave bending moment three different methods are applied. Since the wave bending moments according to the DNVGL is calculated for the still water bending moment, the value is compared with the old GL rule values. POSEIDON calculates additional wave loads based on the main dimensions. The three moments in Table 4.4 are of the same magnitude. The values coincide and the POSEIDON set is applied.

Based on the predefined dimensions are the plate thicknesses and stiffeners modelled. The overall midship properties can be seen in Table 4.5. The detail design of the midship section is shown in Figure 4.2. The profiles of the structure are further defined in Table 4.6. Two different material models are applied but will be discussed in the next section.

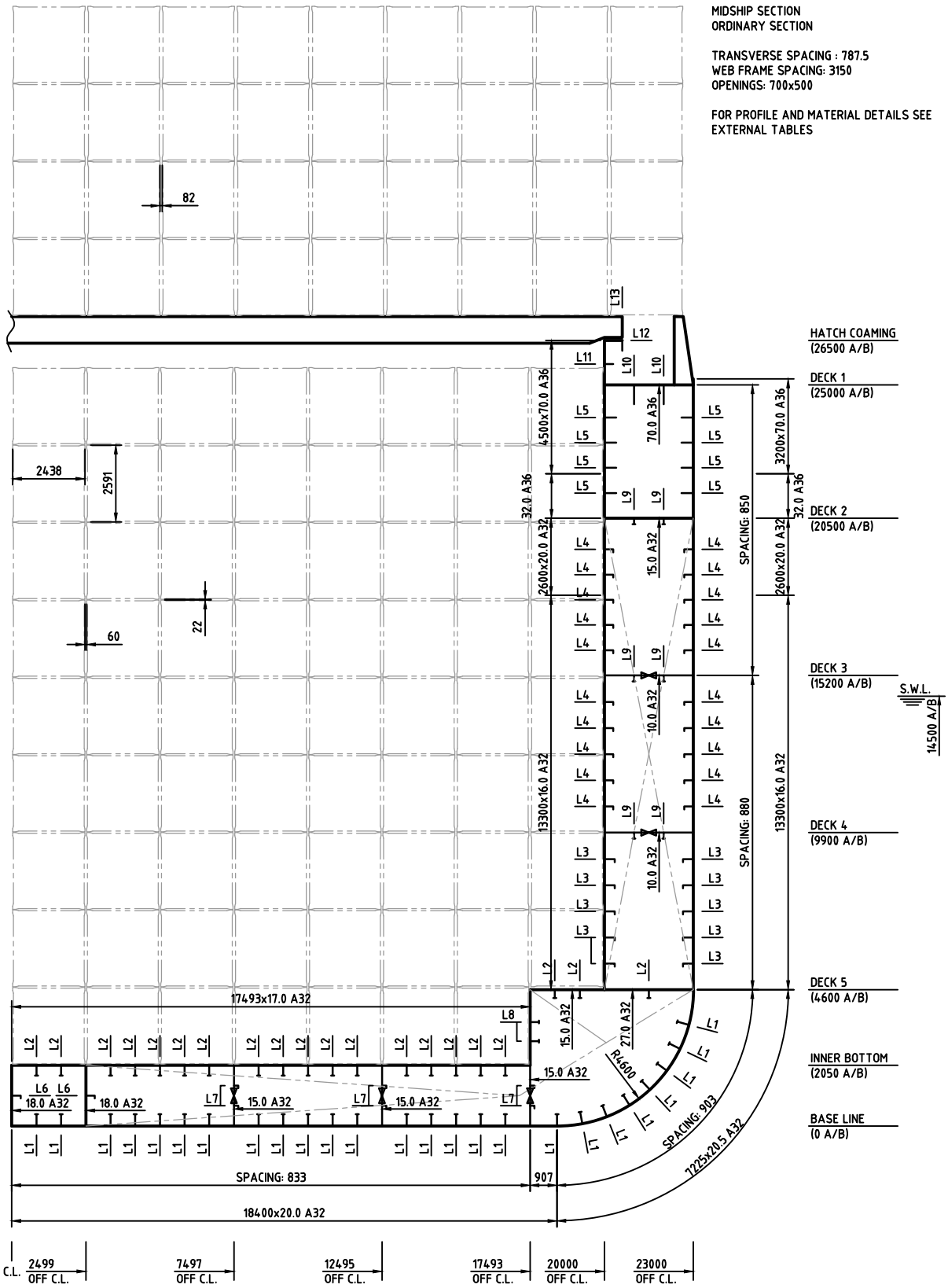

Figure 4.2.: Midship section of the defined ship. The stiffeners are defined in Table 4.6. The material properties are defined in Table 4.8.

Table 4.6.: Profile Table of the used stiffeners in the midship section in Figure 4.2 of the estimated ship.

Number	Type	Dimensions	Material
L1	Tee-bar	450 x 15 + 100 x 20	A32
L2	Tee-bar	300 x 15 + 100 x 20	A32
L3	Tee-bar	350 x 15 + 100 x 20	A32
L4	Tee-bar	300 x 15 + 100 x 20	A32
L5	Flat-bar	400 x 70	A32
L6	Angle-bar	300 x 10 + 90 x 10	A32
L7	Angle-bar	150 x 10 + 90 x 10	A32
L8	Angle-bar	300 x 15 + 100 x 20	A32
L9	Tee-bar	200 x 10 + 90 x 15	A32
L10	Flat-bar	650 x 80	A36
L11	Flat-bar	300 x 80	A36
L12	Flat-bar	600 x 70	A36
L13	Flat-bar	350 x 70	A36

4.3. Material Properties

The choice of a suitable material model is studied. Wherein several facts are of consideration. The linear steel model is given on Table 4.7. The two properties for a linear material are the Youngs modulus defining the stress/ strain relation and the Poisson ratio defining the transverse axial expansion of the material. In the plastic region are three effects taking place:

1) Yield criterion

2) Hardening rule

3) Flow rule

Plasticity occurs when the yield stress in a material is exceeded and the object starts to deform (Yield criterion). If plasticity is increased, the material starts to harden (Hardening Rules). Additionally the material starts to move inside of the elements (Flow rule). (Moan, 2003b)

Before starting to discuss different material models, it is necessary to define the different stress-strain relations. It is distinguished between true and engineering strain. In the engineering stress-strain relation necking of the material is already considered. The difference can

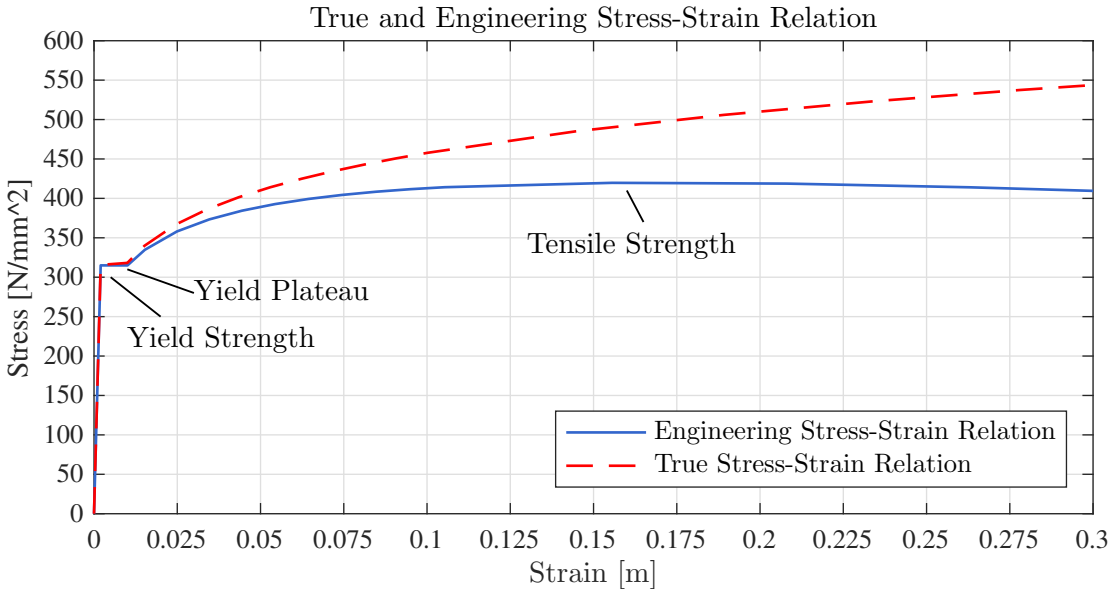

Figure 4.3.: True and Engineering stress-strain relation and definition of the terms yield strength, yield plateau and tensile strength of the A32 material using the Power law.

be seen in Figure 4.3. The lower capacity of the engineering curve is caused by the change of the material cross section, causing higher stresses for the true curve. The conversion is given by Storheim (2016, Eqn.:3.11-3.12) by:

$$\epsilon_{true} = \ln\left(1+\epsilon_{eng}\right) \tag{4.1}$$

$$\sigma_{true} = \sigma_{eng} e^{\epsilon_{true}} \tag{4.2}$$

In this thesis three different material models are discussed: elastic perfectly plastic, bilinear hardening model and Power law. In Figure 4.4 are all models shown in an engineering stress strain relation. The simplest approach is the elastic perfectly plastic approach. In this model material hardening is neglected and the ultimate strength is equal to the yield strength. Thus after yielding the material has no remaining capacity.

DNV-RP-C208 (2013) recommend a bilinear hardening model. In there hardening is taken into account as a linear proportionality. An advantage with this model is the simplicity, because only three points need to be defined to determine the stress-strain relationship. The starting point is given by the yield strength and the path is linear until the ultimate capacity is reached, at the corresponding strain. The stress level stays constant when the ultimate ca-

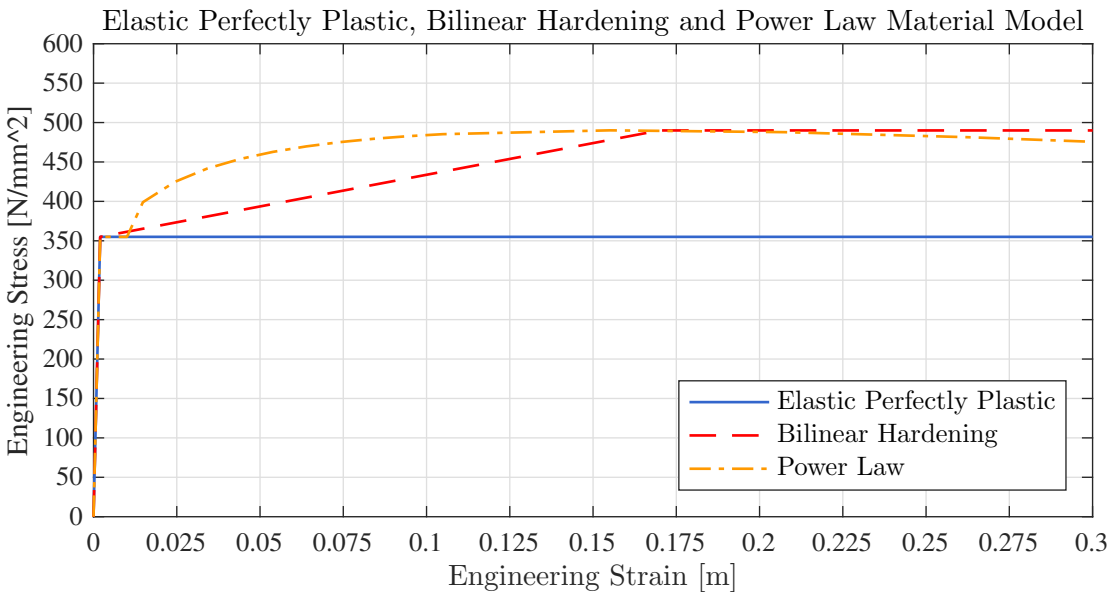

Figure 4.4.: Elastic perfectly plastic material model, biliniear material hardening model and the Power law shown in an engineering stress-strain diagram for the A36 material.

Table 4.7.: Linear material properties for steel according to IACS UR-W (2016, UR-W11 Tab.: 7)

Property	Symbol	Value	Unit
Youngs' Modulus	E	210	GPa
Poisson ration	ν	0.3	-

pacity is reached.

Storheim (2016) has performed intensive studies with crash simulations and suggested a more advanced material model. The model uses the Power law defined by:

$$n = \ln(1 + \epsilon_{UTS}) \tag{4.3}$$

$$K = \sigma_{UTS}(e/n)^n \tag{4.4}$$

with e the base natural logarithm. The true stress is calculated using:

$$\sigma_{true} = K \cdot \epsilon_{necking}^{n_{modified}} \tag{4.5}$$

Table 4.8.: Non-linear material properties according to IACS UR-W (2016, UR-W11 Tab.: 7) and calculated Power law parameters.

Grade	Min σ_y [MPa]	σ_{UTS} [MPa]	$\epsilon_{fracture}$ [%]	$\epsilon_{necking}$ [%]	$\epsilon_{plateau}$ [%]	$n_{modified}$	K
A32	315	440-570	22	18	-1	0.157	657.17 E6
A36	355	490-630	21	17	-1	0.148	753.83 E6

Table 4.9.: Elongation $\epsilon_{necking}$ in dependence of the material grade and component thickness according to IACS UR-W (2016, UR-W11 Tab.: 7).

Thickness mm	Grade	≤ 5	>5 ≤ 10	>10 ≤ 15	>15 ≤ 20	>20 ≤ 25	>25 ≤ 30	>30 ≤ 40	>40 ≤ 50
Elongation $\epsilon_{necking}$	A32	14	16	17	18	19	20	21	22
%	A36	13	15	16	17	18	19	20	21

The model has been validated with material tests and gave good results. Additionally he suggests to include a plateau of 1 % to increase the accuracy.

For all of these models, the yield stress and for the latter models the tensile stress and the necking strain are required as inputs. In reality these values vary greatly between different steel manufactures and batches. Thus a decision has to be made to define the required values. Storheim (2016) has estimated the distributions for these values based on data from VanDerHorn and Wang (2011). The statistical properties are given in Table 4.10 and shown in Figure 4.5. The yield stress can be distributed by using a log normal distribution:

$$f\left(x,\mu,\sigma\right) = \frac{1}{x\sigma\sqrt{2\pi}}\, e^{-\frac{\left(\ln\left(x\right)-\mu\right)^2}{2\sigma^2}} \tag{4.6}$$

with the mean defined as m and the standard deviation as v given the two statistical parameters:

$$\mu = \left(\frac{m}{\sqrt{1+\frac{v}{m^2}}}\right) \tag{4.7}$$

$$\sigma = \sqrt{\ln\left(1+\frac{v}{m^2}\right)}. \tag{4.8}$$

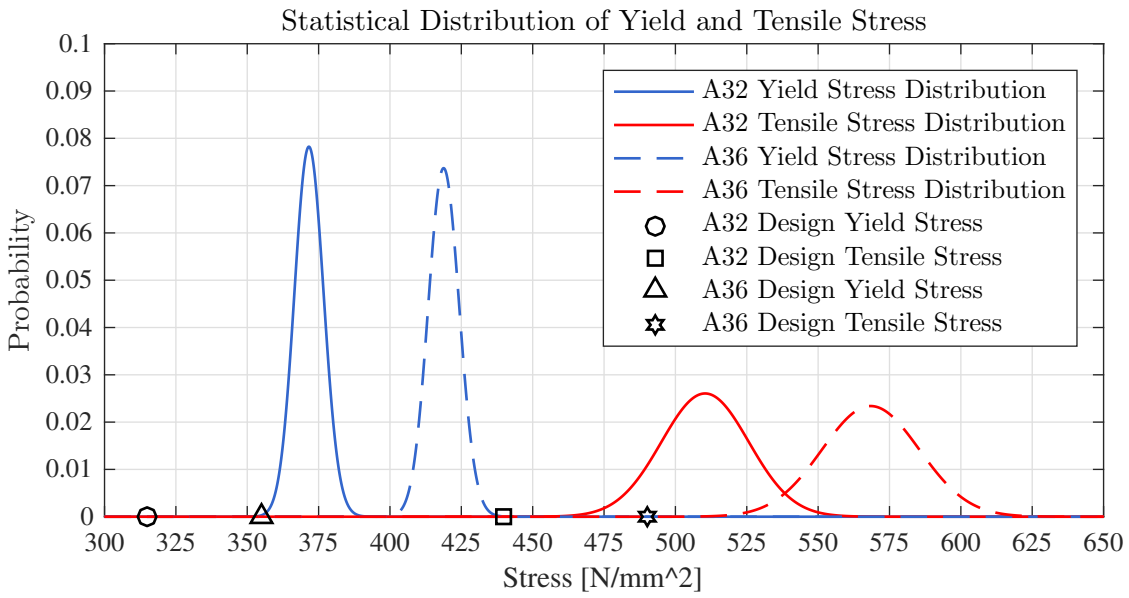

Figure 4.5.: Statistical material values plotted according to the suggestion by Storheim (2016) based on data of VanDerHorn and Wang (2011), using the values in Table 4.10.

The tensile strength and the necking strain are distributed according to a normal distribution:

$$f\left(x,\mu,\sigma\right) = \frac{1}{\sigma\sqrt{2\pi}}\, e^{-\frac{\left(x-\mu\right)^2}{2\sigma^2}} \tag{4.9}$$

with the mean μ and the standard deviation σ. Finally the Coefficient of Variation (COV) is defined by:

$$COV = \frac{\sigma}{\mu} \tag{4.10}$$

and states the dependency between mean and standard deviation.

It should be noted that the design values are particularly smaller than the mean values of the steel. Using the mean value as stress and strain values might reveal the most realistic set of values. Using this method would reveal non-conservative results and is not considered. Since the result of this work should be comparable with the developed design rules, a design approach should be followed. This includes using reasonably conservative values.

IACS UR-W (2016) has defined the required material properties. As already mentioned within

Table 4.10.: Statistical material properties evaluated by Storheim (2016) based on data of VanDerHorn and Wang (2011).

Property	Symbol	Mean	COV	Distribution
Yield Strength	σ_y	$1.18 \cdot \sigma_y$	0.06	Log-normal
Tensile Strength	σ_{UTS}	$1.16 \cdot \sigma_{UTS}$	0.03	Normal
Elongation	ϵ	$1.35 \cdot \epsilon$	0.08	Normal

the rules, the classical linear material properties are defined in Table 4.7. Additionally the non-linear material properties are defined. These are shown in Table 4.8. Specifically the necking strain $\epsilon_{necking}$ which is additionally dependent on the thickness of the material. Table 4.9 shows the different values. To simplify the model, one value is picked for all thicknesses. The most important part is the bottom part, thus the corresponding value for this region is picked. With the bottom plates being 20 mm and the stiffeners 15-20 mm of thickness an elongation of 18 % and 11 % respectively for the different materials is chosen.
Another effect to be discussed is the strain rate effect. The strain rate effect increases the yield stress to certain level in correlation with a change in strain. DNV-RP-C208 (2013) state, that the material models defined by IACS can be used for strain rates up to $0.1s^{-1}$. For higher strain rates the Cowper-Symonds (CS) might be used. Given by DNV-RP-C208 (2013, Eqn.:8):

$$\sigma_{dynamic} = \sigma_{static}\left(1 + \left(\frac{\dot{\epsilon}}{C}\right)^{\frac{1}{p}}\right) \tag{4.11}$$

with $\dot{\epsilon}$ the strain rate and C and p are the material parameters. DNV-RP-C208 (2013) and Jones (2012) give similar values for high strength steel, whereas DNV has more conservative values. Storheim (2016) stated, that neglecting strain rate effects give a conservative result. However using strain-rate hardening is uncertain. A calibration might be applicable after first calculations are performed. In this first step, strain rates are not included in the calculations. This ensures the conservatism of the calculation, as well keeping in mind, that strain rate effects are neglected in the new DNVGL rule set.

4.4. Element Choice & Meshing

One of the most important decisions is the use of the element type and the corresponding meshing of the model. The presented calculations in Chapter 2 are taken as reference. The methods of Amlashi (2008), Shu and Moan (2012), Xu et al. (2014), Marine Accident Investigation Branch Annex A-D (2008), Marine Accident Investigation Branch Annex E-G (2008) and Sumi et al. (2014) are compared in Table 4.11.

Additionally different regulations are consulted such as GL Guidelines (2011), DNV-RP-C208 (2013), DNVGL Rules Part 3 Chapter 7 (2016), DNVGL Rules Part 3 Chapter 8 (2016), DNVGL-CG-0128 (2015) and DNVGL-CG-0153 (2015).

In most cases the FEM program ABAQUS is used. For the time domain calculation of the *MOL Comfort* and the crash simulations performed by Storheim (2016) the explicit solver LS-DYNA have been used. In ABAQUS have either the element S4 or S4R have been used. The S4 element is a "4-node general-purpose shell, finite membrane strains" whereas the S4R is a "4-node general-purpose shell, reduced integration with hourglass control, finite membrane strains" (Abaqus User Manual IV, 2012, P.:29.6.7–1). Storheim (2016) used LS-DYNA with Belytschko-Lin-Tsay shell elements. The element is a 4-node shell using one integration point and is the recommend element for most applications (ANSYS LS-DYNA, 2009, P.:8-12). No information is given about the elements used in the *MOL Comfort* report. These elements all have four nodes. In this thesis the corresponding element is the SHELL181 element. ANSYS uses different element description than ABAQUS and LS-DYNA, thus no direct comparison can be made. For ABAQUS elements the difference is the reduced integration with hourglass control in the elements. ANSYS Element Reference (2009) recommends for shell structures, to use the "Reduced integration with hourglass control" option for the structure. Anyhow for stiffener webs the "Full integration with incompatible modes" is endorsed. The recommendation will be followed in thesis and the element with the respectively recommended key option is used. The number of integration points for elements experiencing plastic strains is automatically increased from 3 to 5.

An alternative approach, not discussed in this thesis is the use of Idealized structural unit method (ISUM) elements by Fujikubo and Kaeding (2002). The elements are especially de-

Table 4.11.: Comparison of the work performed by Amlashi (2008), Shu and Moan (2012), Xu et al. (2014), Marine Accident Investigation Branch Annex A-D (2008), Marine Accident Investigation Branch Annex E-G (2008) and Sumi et al. (2014) with respect to methods, elements mesh, material models and loads. (* counted from figure, - not known, ✓applied, ✗not applied)

Property Institution	Amlashi NTNU	Shu NTNU	Xu et al. NTNU	MSC Napoli DNV	MSC Napoli BV	MOL Comfort ClassNK
Program						
Program	ABAQUS	ABAQUS	ABAQUS	ABAQUS	ABAQUS	MARC/LS-DYNA
Solver method	Riks	Implicit	Riks	-	Riks	Implicit/Explicit
Meshing "crash" area						
Element	S4	S4	S4R	S4	-	-
Global Size [m]	0.1	0.1	0.1	0.15	-	0.1
Between Longitudinal Stiffeners [n]	5	5	9	5-6	6*	9*
Between Transverse Webs [n]	15	15	26	6*	8*	6*
Longitudinal Stiffener web [n]	5	5	4	3*	2*	5*
Longitudinal stiffener flange [n]	2	2	2	1*	1*	2*
Height of girder [n]	21	21	28	19*	12*	26*
Material						
Material Model	Bilinear	Bilinear	EPP	Bilinear	Ramsberg-Osgood	EPP + Hardening
Yield Stress	Design	Design	Design	3 Sets	Design	Average
Size						
Extend of Model	1/2+1+1/2	1+1+1	1 Web	Global	Local	1/2+1+1/2
Number of DoF non linear [n]	-	-	541,00	$1.06 \cdot 10^6$	-	-
Number of DoF linear [n]	-	-	541,000	$1.22 \cdot 10^6$	330,498	-
Loads						
Gravitation	✓	✓	✓	✓	✓	✓
Static Pressure	✓	✓	✓	✓	✓	✓
Dynamic Pressure	✓	✓	-	DNV	BV	ClassNK
Bending Moment	Increased	Increased	Strip Theory	WASIM	BV	Increasing
Residual Stresses	-	✗	✓	✗	✗	Factor
Whipping Loads	✗	✗	✗	✗	BV Model	Factor

veloped to represent the occurring buckling modes and to simulate the buckling and collapse behaviour of plate panels. The advantage of these elements is the reduced calculation time compared with regular finite elements.
Another important factor of the finite element model is the mesh size. The mesh size in this work has been orientated on the *MOL Comfort* investigation. For the crash section a fine mesh with a size 100 mm x 100 mm is used. The surrounding area is meshed using an element size of 200 m x 200 mm. Above the neutral axis a global element size approach is used, which will be explained later. The fine mesh size is based on several previous calculations. Only the DNV *MSC Napoli* investigation uses a different approach of a mesh size of 150 mm x 150 mm. Also super elements are used and the transitions zone has been defined differently. In crash simulations Storheim (2016) has used an element size of 100 mm x 100 mm. The choice of 100 mm x 100 mm seems reasonable. A mesh convergence study is performed later on and will prove this assumption.
The area above the neutral axis is meshed using a global mesh approach. The rules therefore are given by Johansen and Bratbak (2015) with:

- 2 x 2 meter mesh
- Usually 8-node Shell elements and 3-node beams
- as quadratic elements as possible, maximal ration 5:1
- lumped stiffeners should follow the actual stiffener direction as close as possible
- primary girders modelled with shell elements should have 2 or more elements over the height

Additionally in the global mesh area stiffeners are not defined as shell elements but as beam elements. The element BEAM188 is chosen. The 2-node element corresponds with the definition of the shell elements.
Using several different mesh size will create the struggle of connecting the elements. The approach used in this thesis is to use triangular elements. A typical mesh transition using triangular elements can be seen in Figure 4.6. The advantage with this method is, that the mesh size is doubled with each row of triangular elements.

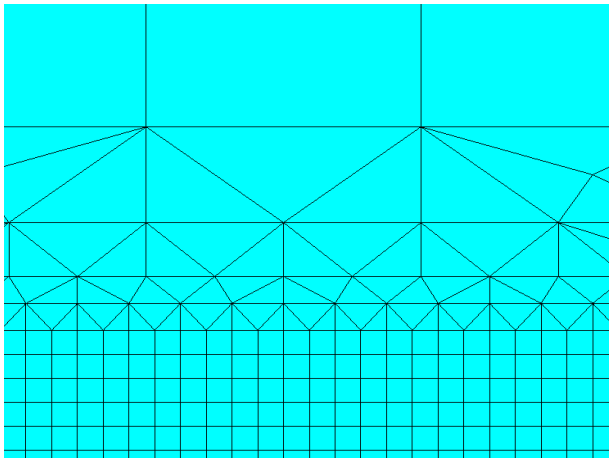

Figure 4.6.: Typical mesh transition using triangular elements

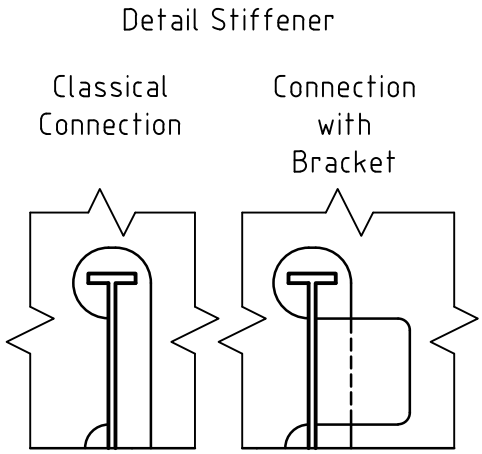

Figure 4.7.: Typical stiffener connection to transverse bulkhead

Another point to discuss is the connection of the longitudinal stiffeners. It is worth taking a look at the connections in reality. Typical stiffener to transverse bulkhead connections are shown in Figure 4.7. In both connections only the web of the stiffener is attached to the bulkhead and the flange is free. Only for watertight bulkheads, the flange will be connected to the bulkhead to close the gap between the two compartments. For reasons of simplicity only the open bulkhead approach is considered. In the meshing, only the flange is connected with the transverse components and the flange is connect in longitudinal direction only and free to rotate at the bulkheads.

4.5. Model Size

In Table 4.11 it becomes obvious that different approaches for the model size have been chosen. Care should be taken in considering bulk carriers and container vessels as different ship types. Amlashi and Moan (2008) used a 1/2 + 1 + 1/2 model for the model but encountered problems regarding the boundaries. Therefore Shu and Moan (2012) used a 1 +1 + 1 approach. Both considered the distance of three webs for the non linear material part. DNV and BV have used smaller non-linear models and as well Xu et al. (2014) used only one web distance for the model.

Fricke and Bronsart (2012) have made analysis on a panel and the influence of its length. A

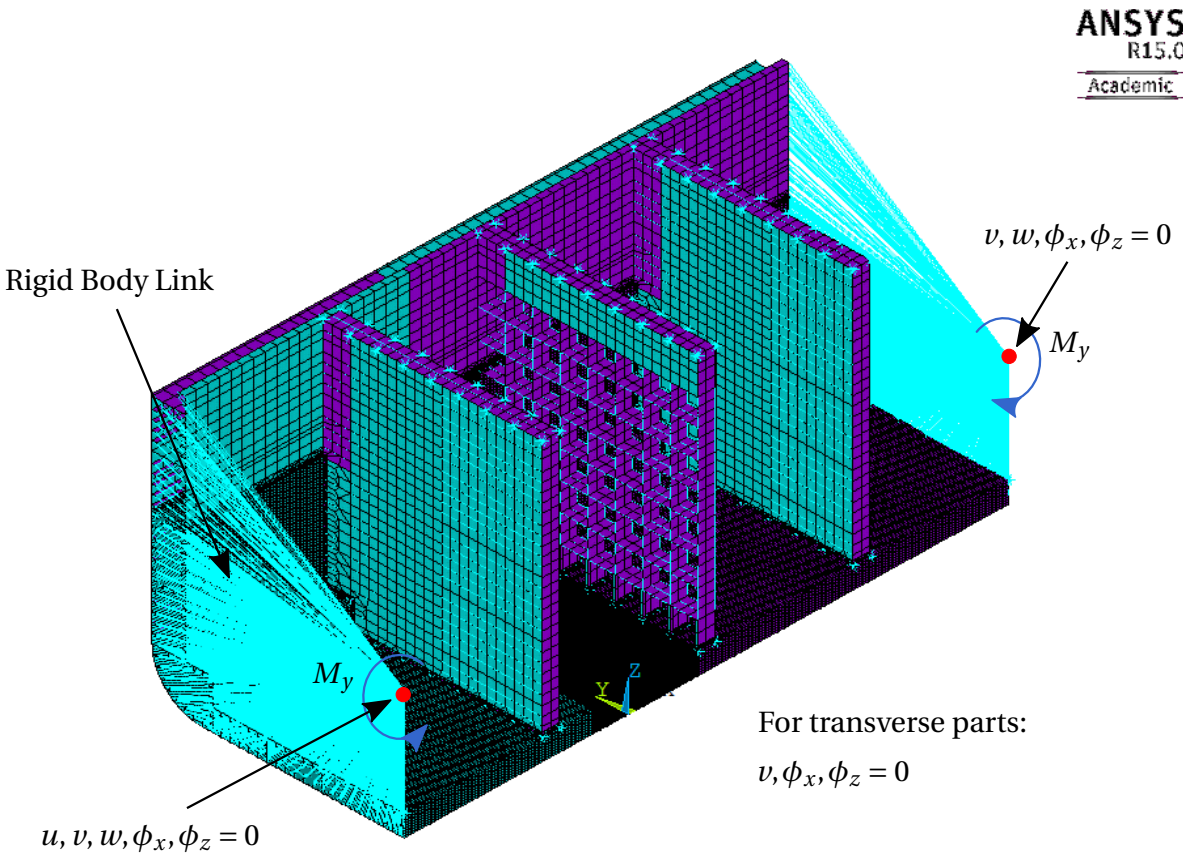

Figure 4.8.: Full model size over 1/2 + 1 + 1/2 cargo holds. Showing the boundary conditions and the rigid body links with the applied bending moment.

panel with only one web distance is predicting an unrealistic high ultimate capacity, due to wrong boundary conditions. Thus the model should be bigger than one web distance.

Different to a bulk carrier are the bulkheads on a container ship. Older designs will have open bulkheads through the whole ship. According to International Maritime Organization (IMO) rules it is forbidden to carry fuel in the shell. Thus typical container vessels using every second cargo hold closed bulkheads to store the bunkers. Access through the containers is still given by the remaining open bulkheads. This causes irregular bending shapes, due to the change in stiffness of the bulkheads. For the *MOL Comfort* investigation a 1/2 + 1 + 1/2 model is chosen, which usually refers to a 4 hold model. The approach is followed and the model is shown in Figure 4.8 . Due to calculation time and technical limitations a reduction of the model is considered at later stages.

Table 4.12.: Applied magnitude of imperfections for stiffened panels according to the maximum allowed values given by DNV-OS-C401 (2013, Tab.: 2-1).

Property	Symbol	Value	Unit
Plates between stiffeners or girders	δ_{plate}	0.5 % $\cdot b$	m
Stiffener or girder webs relative to the plate plane	$\delta_{stiffener,op}$	1.5 % $\cdot l$	m
Stiffener or girder flanges relative to the web plate	$\delta_{stiffener,ip}$	1.5 % $\cdot l$	m

4.6. Application of Imperfections

Imperfections are of high importance for buckling problems. An initially perfect finite element, loaded in the axial direction will never buckle, since no trigger is present. Thus imperfections need to be included. Several ways are known for including imperfections in elements. Imperfections can be defined by using out of plane loads or small deflections of the initial node and force the plate in a certain buckling behaviour. The latter is the more accurate one and is applied in this thesis.

Two methods would be applicable to apply deformations on the plate elements. The typical pattern is given by (Leira, 2014):

$$w = \delta \sin\left(\frac{m\pi}{l}\right) x \sin\left(\frac{n\pi}{b}\right) y \tag{4.12}$$

with m and n are integers which determine the number of sinus half waves over the plate length and breadth respectively. This method works well for simple structures. The application of imperfections on the stiffeners and longitudinal bulkheads is troublesome

This thesis uses a more simplified approach. An eigenvalue or linear buckling analysis is performed on the structure. Choosing several suitable eigenmodes for different parts of the structure. Adding several eigenmodes, leads to a superposition of the displacement of the modes and to an overall deformed initial condition.

The magnitude of the applied imperfections is orientated on the maximum allowed deviation of the component to the design value. The magnitudes are shown in Figure 4.12.

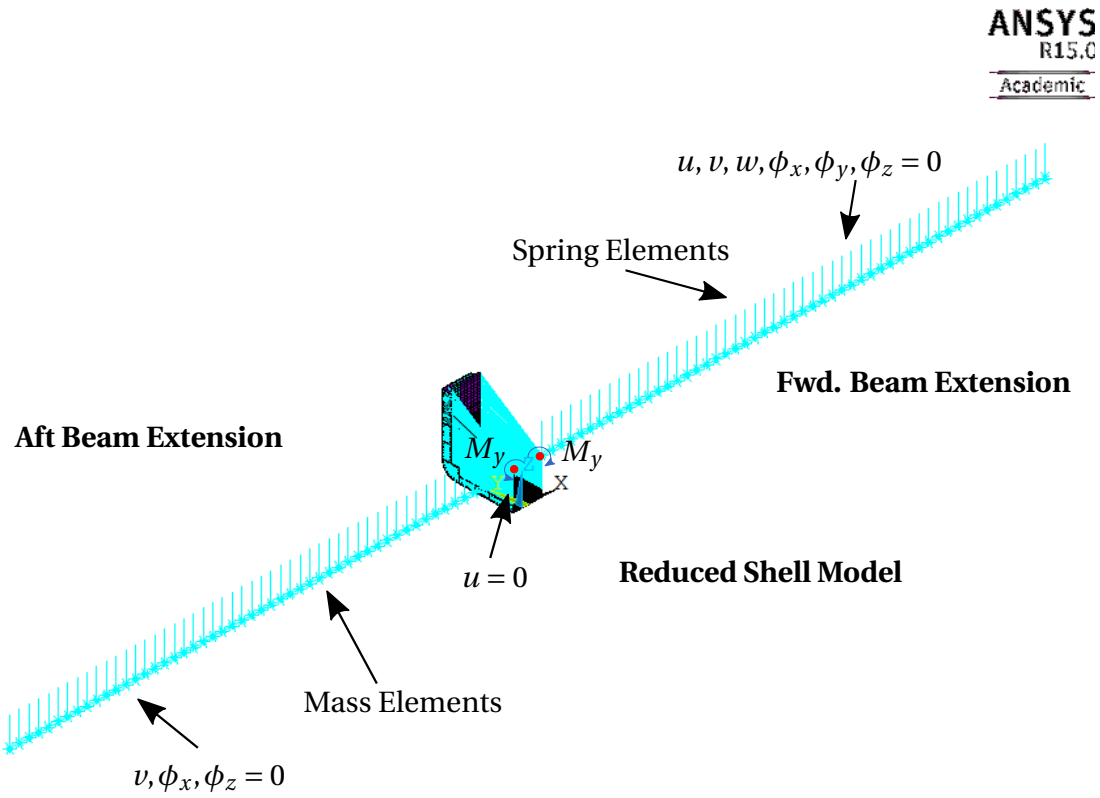

Figure 4.9.: Reduced shell model, with forward and aft beam extensions, consisting of mass and spring elements and the respective boundary conditions.

4.7. Inertia and Rigid Body Motion Effects

The main point of view in this thesis is the dynamic collapse behaviour. Vibrations on the hull girder are occurring at the eigenfrequency of the vessel. This makes it necessary to create a model which possess the same eigenfrequencies as the real ship.

The ends of the ship are modelled using beam elements. The length of the beam element is four times the longitudinal spacing. The distribution over the ship length is assumed according to the body plan in Figure D.1. The stiffness of the beams is gradually reduced to the ends according to Figure D.2. The mass is applied according to the volume distribution of the ship according to Figure D.3. Additionally loads have been applied to the masses to avoid an influence on the bending moment. Figure 4.9 shows the full model, with the beam extensions. For the final model is a reduced shell model is chosen. Main consideration of

Table 4.13.: Natural frequencies of the TULCS vessel and the defined ANSYS model. The values are separate into dry and wet frequencies, accounting for the effect of added mass. (Andersen and Jensen, 2014)

Property	TULCS Dry	TULCS Wet	ANSYS Dry	ANSYS Wet	Unit
Vertical bending 2-node	0.67	0.47	0.67	0.47	Hz
Vertical bending 3-node	1.38	0.98	1.48	1.05	Hz

this change was the overall time consumption during the calculations.

The natural frequencies for the ships have been given in Andersen and Jensen (2014) and can be seen in Table 4.13. The dry and wet frequencies are given. The difference is roughly $\sqrt{2}$. Considering Equation 4.13 is the added mass coefficient is two. The mass in the model is applied with the factor of two to account for the added mass effect. The stiffness is thereafter reduced until the desired eigenfrequency is reached. The main focus is on the 2-node mode, whereas the 3-node mode has a deviation of 7 %. The natural frequency formulation is given by Larsen (2014) by:

$$\omega_0 = \sqrt{\frac{\overline{k}}{\overline{m}}} \tag{4.13}$$

Additionally the effect of rigid body motion is accounted for. Springs are attached to the modelled masses. The stiffness of springs is given by Faltinsen (1990) with:

$$k_{spring} = C_{33} = A_{waterplane} \cdot \rho \cdot g \tag{4.14}$$

Additionally damping should be applied on the springs, to stabilize the model. Faltinsen (1990) gives the following approach:

$$B_{33} = \rho \left(\frac{A_3}{|\eta_3|} \right) \frac{g^2}{\omega^3} \tag{4.15}$$

with the strip area A_3 the heave motion η_3 and the wave frequency ω. Heave motion as well as wave frequency are unknown for the scaled set. For reasons of simplification is the

following approach is chosen:

$$c_v = \xi \cdot 2 \cdot \sqrt{(M + A)\, K} \tag{4.16}$$

with the damping coefficient c_v, the damping ratio of critical damping ξ, mass of the strip M, added mass of the strip A and the stiffness K. The damping ratio is assumed to be in range of 2 % and mass, added mass and stiffness are already defined for the mass and spring system.

5. Theory

The following chapter provides an insight into the applied methods and formulas. The depth of explanation differs according to the relevance of the topic. A short description of the FEM is given and the applied solution methods. This chapter should give a rough overview, for a deeper description, corresponding literature should be consulted.
In the following section $(\underline{\underline{\_}})$ denotes a matrix and $(\underline{\_})$ denotes a vector. A simple derivative with respect to time t is shown by $(\dot{})$ and a double derivative of t is shown by $(\ddot{})$ respectively. Derivations with respect to certain directions are written out.

5.1. Hull Girder Failure

Structural failure occurs in several different ways. The direction of the load is of importance. The two considered cases on a ship are sagging and hogging. This means that the upper and lower fibre experience either compression or tension. Loaded under latter, failure of the plate will appear when the stress exceeds the yield level and the material starts yielding. The limit state under compression might be reached earlier depending on the slenderness of the structure. The stress deflection curve for a structure experiencing extreme loading in compression is shown in Figure 5.1. The girder is loaded until failure. In the pre-buckling region, the deflection is linear and follows the linear deformation of the material defined by Young's modulus. Exceeding the elastic buckling level brings the plate into the post buckling range. Mechanisms acting are linear buckling of the plate. When buckling exceeds the elastic range, yielding of the components occurs and the structure loses faster capacity until the ultimate capacity is reached and the structure can no longer take the load.

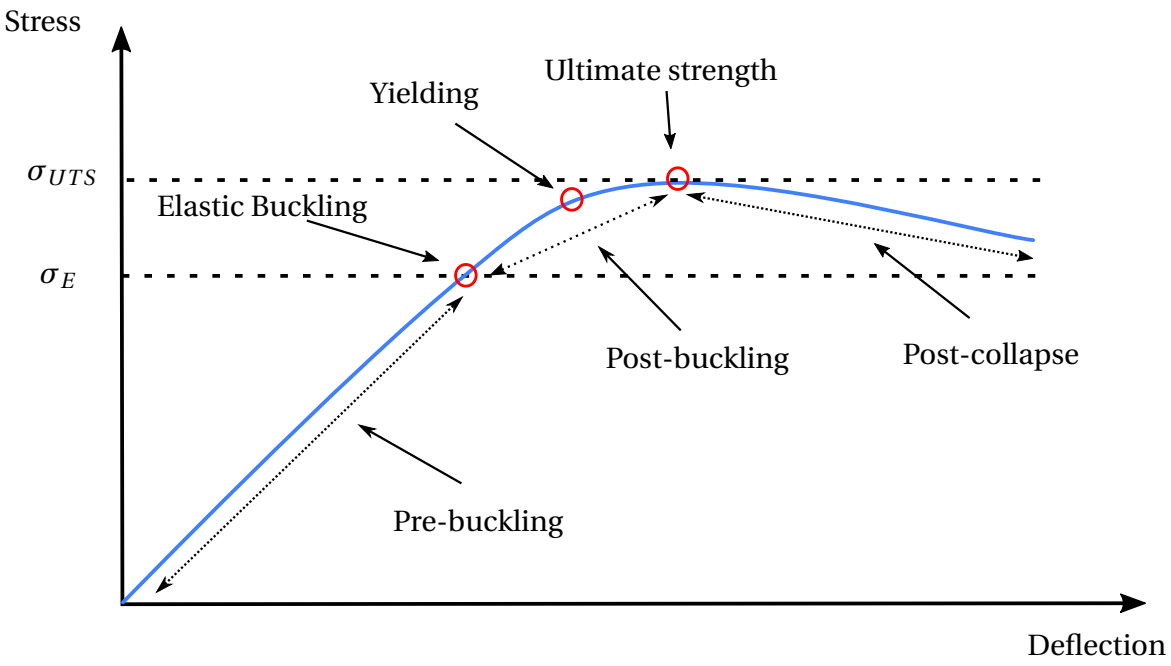

Figure 5.1.: Typical stress-deflection or load-deflection curve. Defining Euler strength and ultimate strength as well as the regions pre-buckling, post-buckling and post collapse. (Brubak, 2016)

The behaviour examined is the collapse in hogging condition. Thus buckling of the bottom structure will define the ultimate capacity. This suggests to take a deeper look into the buckling behaviour of panels.

5.1.1. Buckling Failure Modes

The bottom panels of the ship can fail in several different ways. Figure 5.2 shows the most common failure modes of a panel. The modes can be described as follows:

- *Overall grillage buckling* (not shown) failure of longitudinal and transverse components of the girder
- *Overall global buckling* (a) failure of plate and stiffeners usually happens with weak stiffeners
- *Local plate buckling* between stiffeners (b) usually leads to unloading of the plate and loading of stiffeners

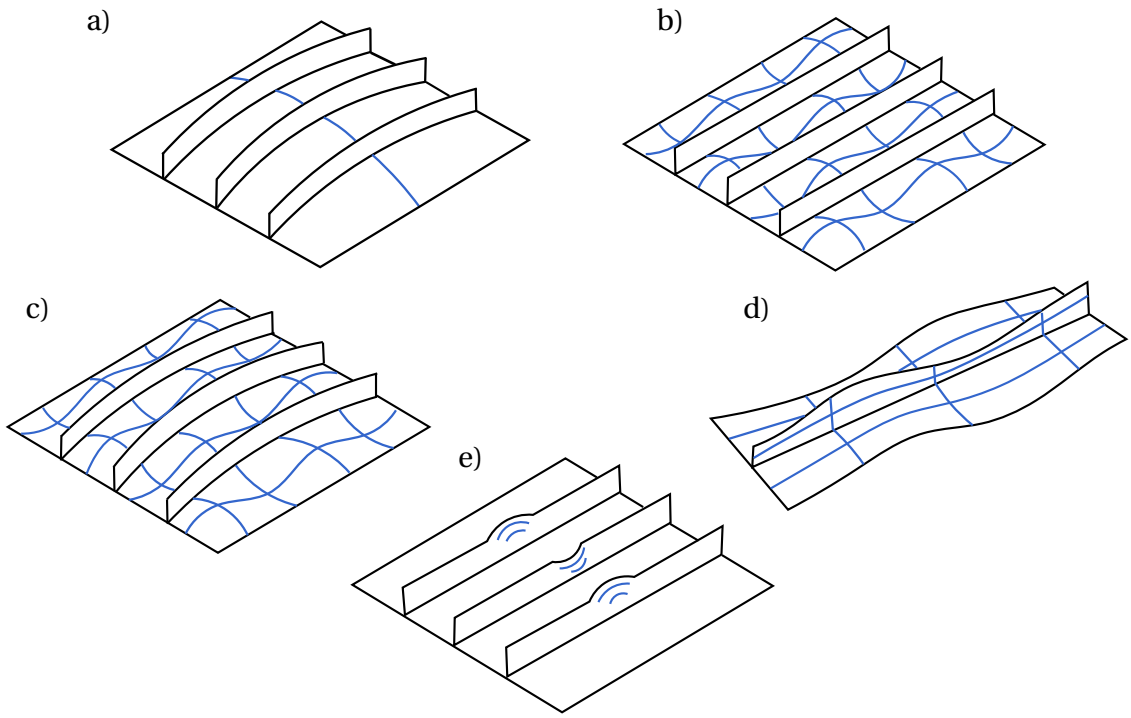

Figure 5.2.: Illustration of different buckling modes of a stiffened panel. (Khosravi and Sedaghati, 2008, Fig.:1)

- Combination of interframe flexural buckling of the effective plate and the associated longitudinal stiffener (c)
- *Tripping failure of stiffeners* (d) rotation of the slender stiffeners forces deformations in the plate and causes a loss of capacity
- *Restrained torsional buckling of stiffeners* (e) in this case without effect on the plate

An overall grillage buckling is very unlikely to happened, since structural regulations usually prevent this failure. The expected failure mode is initially case (b) where unloading of th plate increases the load of stiffeners until failure of the stiffeners occur (c). (Amdahl, 2013)

5.1.2. Effect of Boundaries

Not the whole ship can be modelled in total, only smaller parts of special interest are examined. When examining a single plate or a panel, the structure is always part of a bigger

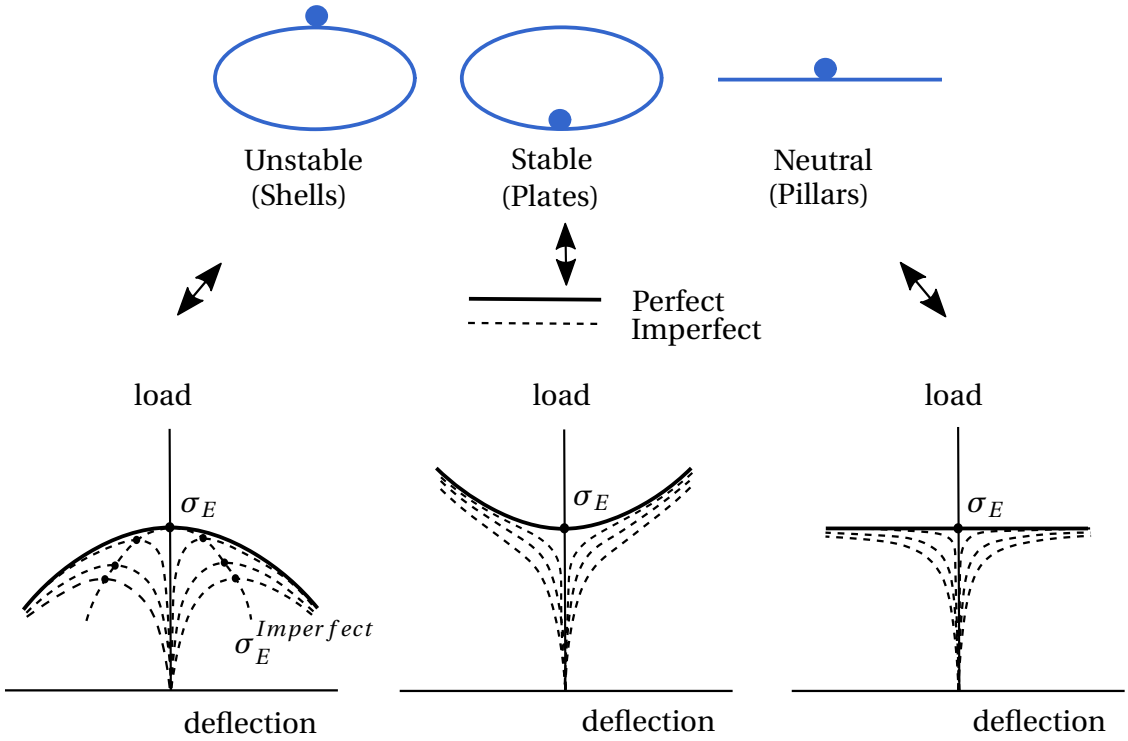

Figure 5.3.: Effect of imperfections on unstable, stable and neutral components. (DNVGL Rules Part 3 Chapter 8, 2016, Fig.:2)

component. The challenge is to define the boundaries as if the surrounding parts are defined as well.

Besides the well known symmetry and anti-symmetry conditions in buckling analysis it is common to use constrained and restrained boundaries. A plate or panel is usually defined between stiffer elements such as stiffeners or longitudinal or transverse web frames. Failure of the bottom region will cause the plate or panel to fail before the other parts do. Thus the boundaries stay in line during failure. Straight edges with in-plane motions are called constrained and with fixed in-plane displacement are called restrained respectively. The method which should be applied depends on the structure's surroundings. Generally the constrained method is used in buckling calculations.

5.1.3. Effect of Imperfections

Uncertainties arises from the topic of imperfections. When an initially perfect finite element plate is exposed to axial pressure, the plate is compressed. For this plate, no buckling would occur, since no trigger is given, forcing the plate to deflect in either of its normals. Imperfections can be introduced in several ways. Out of plane loads are an option to force the structure to buckle, or small initial deflections in the assumed final buckling shape. In reality a structure will never be perfect. Imperfections are introduced by microscopic material defaults and assembly and/or welding deformations.
The effect of imperfections on different structure types is shown in Figure 5.3. Shell structures are unstable components once buckling occurs the structure collapses totally. The initial imperfections have a huge effect on the ultimate strength of the unit. Pillars are neutral components. Once the buckling limit is reached the required load stays equal. Plate elements are stable structures. Once the buckling load is exceeded the plate has still capacity preventing the total collapse.

5.2. Verification Methods

The used finite element analysis is a numerical method and thus simplifies the real processes. Applying a simplified methodology also requires a way of verifying the received results. The used models are presented in following.

5.2.1. Analytical Solution

The buckling load for simple initially perfect plates can be estimated. The formula accounts for the elastic buckling load of the plate and is given by Amdahl (2013, Eqn.:3.7):

$$\sigma_E = \frac{\pi^2 E}{12\left(1-\nu^2\right)}\left(\frac{t}{b}\right)^2 \cdot k. \tag{5.1}$$

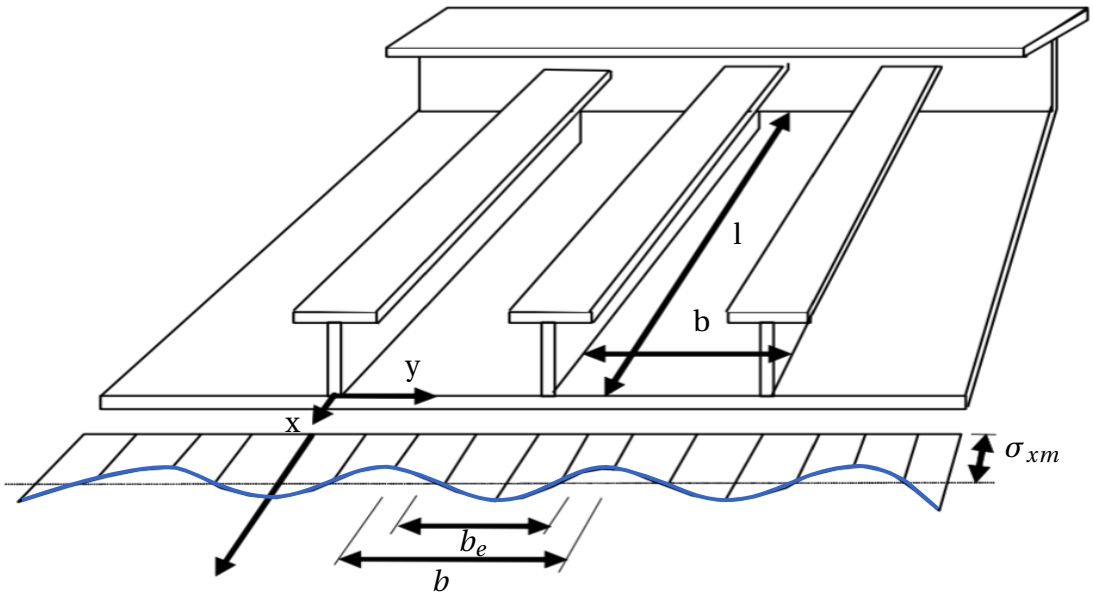

Figure 5.4.: Concept of effective width. When buckling in the single plates occurs, the stress is redistributed on the stiffeners. The capacity of the stiffeners is defined by the stiffener itself and the effective width of the plate. (Amdahl, 2013)

The derivation of the the equation can be found in Section A.1. In the equation the Young's modulus E and the Poisson's ratio ν represent the material properties. The thickness t and the breadth b the plate proportions. The coefficient k is depending on the aspect ratio, the applied load and on the boundary conditions of the plate. Typical value for k is 4, for a simply supported plate under axial loading. For a plate with clamped boundaries a k equal to 7 might be used.

One of the main difficulties is the consideration of realistic boundary conditions for the plate embedded in a panel. In a hull girder panel it is most likely, that the plate starts to buckle. However, this is not the ultimate capacity. After initial plate buckling, the stiffeners will start taking axial load. To capture this effect the concept of effective width is developed. The relationship is defined by (Amdahl, 2013, Eqn.:3.23):

$$\frac{b_e}{b} = \frac{\sigma_{xm}}{\sigma_y} = \begin{cases} \frac{2}{\beta} - \frac{1}{\beta^2} & \beta \geq 1 \\ 1 & \beta \leq 1 \end{cases} \tag{5.2}$$

Where b_e is the effective width and σ_{xm} is the corresponding stress. The equation is only dependent on the plate slenderness parameter β, defined by (Amdahl, 2013, Eqn.: 3.24):

$$\beta = \frac{b}{t}\sqrt{\frac{\sigma_y}{E}} \tag{5.3}$$

The plate slenderness parameter is dependent on the geometrical dimensions and the material properties. The process is shown in Figure 5.4. When unloading of the plates occur, the stress is redistributed to the stiffeners and the overall critical buckling load is increased. Despite the two mentioned techniques a few other methods which will be shortly introduced. The Johnson-Ostenfeld formula has been developed to account for the effect of plasticity of slender plates. The slenderness ratio is defined by (Amdahl, 2013, Eqn.:3.14):

$$\bar{\lambda} = \sqrt{\frac{\sigma_y}{\sigma_E}} \tag{5.4}$$

The corresponding buckling stress is defined by (Amdahl, 2013, Eqn.:3.14):

$$\sigma_{cr} = \phi \cdot \sigma_y \tag{5.5}$$

with ϕ, the Johnson-Ostenfeld parameter, defined by(Amdahl, 2013, Eqn.:3.17):

$$\phi = \begin{cases} 1 - \dfrac{\bar{\lambda}^2}{4} & \bar{\lambda}^2 \leq 2 \\ \dfrac{1}{\bar{\lambda}^2} & \bar{\lambda}^2 \geq 2 \end{cases} \tag{5.6}$$

The Johnson-Ostenfeld parameter depends only on the slenderness ratio. Another approach has been developed by DNV. A difference is made in here if buckling of the structure impairs the functionality . The Serviceability limit state (SLS) is defined to avoid all kinds of deformation, whereas the Ulitmate limit state (ULS) allows for smaller deformations of the structure. Since deformations in the bottom area of a container vessel do not effect the functionality the ULS equation given by (Amdahl, 2013, Eqn.:3.22):

$$\sigma_{ult} = \frac{\sigma_y}{\bar{\lambda}\sqrt{2}}, \quad 1.0 < \bar{\lambda} \leq 5.0 \tag{5.7}$$

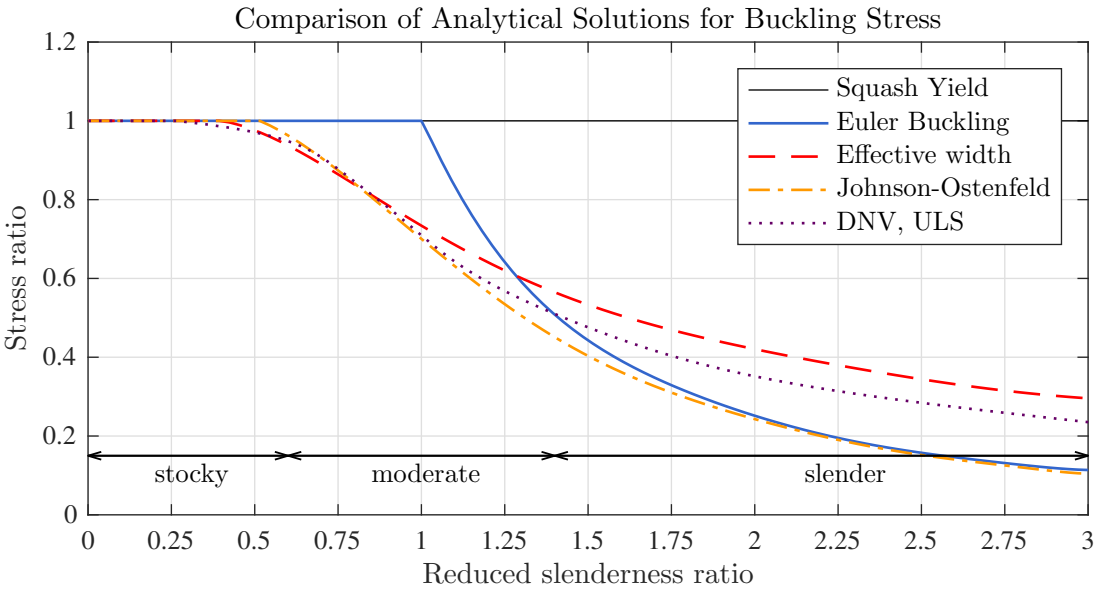

Figure 5.5.: Comparison between the different analytical solutions for the buckling stress. Comparing Euler buckling, with the effective width concept, Johnson-Ostenfelds formula and the DNV ULS formula. Plotted for the reduced slenderness $\bar{\lambda}$ and the stress ration σ_c/σ_y. (Amdahl, 2013, Fig.:3.9) (DNVGL-CG-0128, 2015, Fig.:3)

The different limit states are shown in Figure 5.5. As well the different classifications of slenderness $\bar{\lambda}$ can be found in the graphic. The structure can range from (DNVGL-CG-0128, 2015):

- Stocky structures $\bar{\lambda} < 0.6$
- Moderate slender structures $0.6 < \bar{\lambda} < 1.4$
- Slender structures $1.4 < \bar{\lambda}$

5.2.2. Semi Analytical Solution PULS

PULS is a program developed by DNV for buckling code check of plain and stiffened panels. The program supports three different elements. An unstiffened plate (U3), a stiffened panel (S3) and a stiffened plate with non-regular geometry (T1). The first two elements are used in this thesis. Linear deformations of the elements are allowed, plastic deformations not. Imperfections are introduced in the model to account for geometrical and material imper-

fections. (DNV PULS, 2006). PULS follows four design principles:

- Estimation of extreme Loads
- Acceptation of buckling deflection
- Do not accepts permanent buckles in plates
- Ensureing strong stiffeners

The considered elements are using von Karmen and Marguerre's non-linear plate theory. The equilibrium is established by use of the energy method, the principle of virtual work and stationary potential energy. The discretization of the deflections is done by the Rayleigh-Ritz method. Finally the equation is solved by using an incremental perturbation procedure with arc-length control. (Brubak, 2016)

5.2.3. Ultimate Capacity POSEIDON

The design tool POSEIDON includes a method to calculate the ultimate capacity of the midship section. The approach follows the GL guidelines for the ultimate vertical bending moment given in GL Rules (2015, R.I,P1,C.5,S.5,E.5) by:

$$\left| M_{SW} + \frac{\gamma_{WV} M_{WV}}{c_S} \right| \leq \left| \frac{M_U}{\gamma_R} \right| \tag{5.8}$$

with the partial safety factors defined as:

$$\gamma_{WV} = 1.2 \quad ; \quad \gamma_R = 1.2 \tag{5.9}$$

and the distribution factor $c_S = 1$ for the midship section. Calculation of the ultimate state is shown in POSEIDON User Manual (2016) and given by:

$$US = \frac{\left| M_{SW} + \frac{\gamma_{WV} M_{WV}}{c_S} \right|}{\left| \frac{M_U}{\gamma_R} \right|} \leq 1. \tag{5.10}$$

In the incremental method used is the curvature step by step increased until the post collapse region. The calculation works for the hogging and sagging condition.

5.3. Finite Element Method Theory

The FEM is used for the the analyses. The model is divided into several elements, i.e. the finite elements. The main equation solving a system is given by (Cook, 1995, Eqn.:1.6-6):

$$\underline{\underline{K}}\,\underline{r} = \underline{R} \tag{5.11}$$

With the stiffness matrix $\underline{\underline{K}}$, displacement vector $\underline{r}$ and nodal load vector $\underline{R}$. This holds true for calculations with small displacements and linear elastic materials. Since the dynamic collapse behaviour should be estimated, non-linearities and transient effects need to be accounted for.

5.3.1. Non-linearity

To be able to evaluate the collapse behaviour non linear effects need to be considered. Three non-linearities are known:

- Non linear material properties
- Non linear geometries
- Contact problems

The latter is not used in this thesis, the other two are included. The used material properties have been described earlier. Non linear geometries are occurring when large deformations are present. The deformations causing a change in stiffness of the structure. Thus Equation 5.11 need to be changed into (Moan, 2003a, Eqn.:12.6):

$$\underline{\underline{K}}\left(\,\underline{r}\,\right)\underline{r} = \underline{R} \tag{5.12}$$

where $\underline{\underline{K}}\left(\underline{r}\right)$ is called the secant stiffness. The secant stiffness is a combination of the linear stiffness matrix $\underline{\underline{K_0}}$ and the geometric stiffness $\underline{\underline{K_G}}$ written as:

$$\left(\underline{\underline{K_0}} + \underline{\underline{K_G}}\left(\underline{r}\right)\right)\underline{r} = \underline{R}. \tag{5.13}$$

The stiffness matrix is now dependent on the displacement of the different elements. Thus an update for every single substep is necessary.

5.3.2. Transient Effects

Two additional effects are important to capture the dynamic behaviour of a structure. Inertia and damping need to be included in the calculation to build a realistic model. The derivation of the dynamic equation of motion can be found in section A.2, revealing the full equation of motion by:

$$\underline{\underline{M}}\,\underline{\ddot{r}}(t) + \underline{\underline{C}}\,\underline{\dot{r}}(t) + \underline{\underline{K}}\,\underline{r}(t) = \underline{\underline{R}}(t) \tag{5.14}$$

with the mass matrix $\underline{\underline{M}}$ and the damping matrix $\underline{\underline{C}}$ added through the already introduced equation. Applying stress stiffening effects yields the following equation:

$$\underline{\underline{M}}\,\underline{\ddot{r}}(t) + \underline{\underline{C}}\,\underline{\dot{r}}(t) + \underline{\underline{K}}\left(\underline{r}(t)\right)\,\underline{r}(t) = \underline{\underline{R}}(t) \tag{5.15}$$

5.3.3. Mass Matrix

In the calculations a consistent mass matrix is chosen. The mass matrix for the whole structure is given by (Langen and Sigbjörnsson, 1979, Eqn.:5.3):

$$\underline{\underline{M}} = \sum_i \underline{\underline{a_i}}^{\mathsf{T}}\,\underline{\underline{m_i}}\,\underline{\underline{a_i}} \tag{5.16}$$

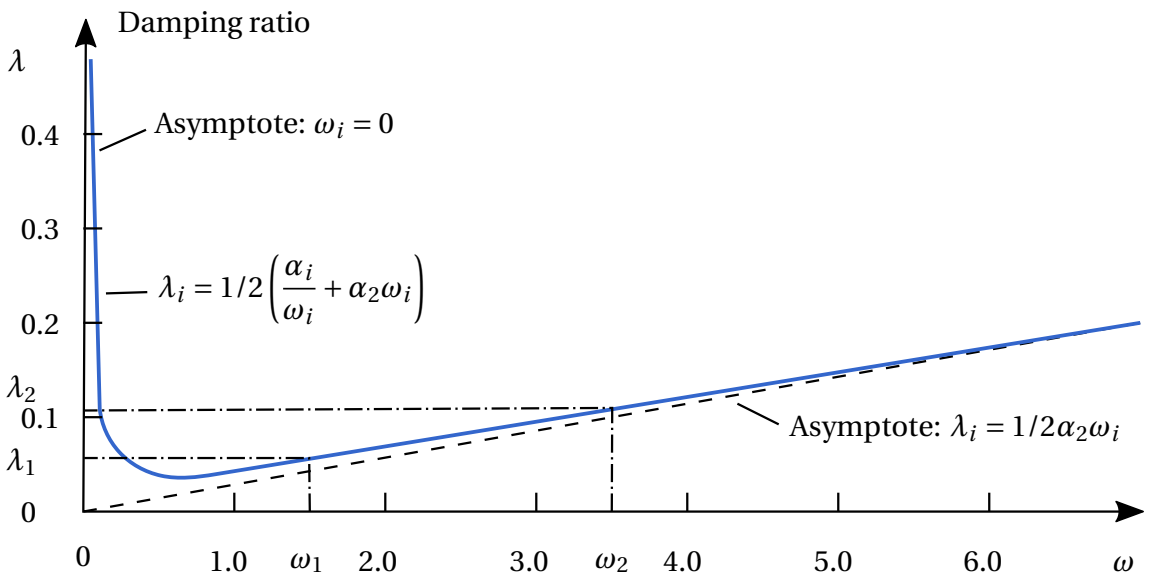

Figure 5.6.: Full Newton-Raphson iteration scheme, which is recommended for non-linear transient finite element calculations. (Moan, 2003a, Fig.:12.27)

with the connectivity matrix $\underline{\underline{a_i}}$ and the consistent mass matrix for each element is defined by (Langen and Sigbjörnsson, 1979, Eqn.:5.1):

$$\underline{\underline{m}} = \int_V \rho \underline{N}^\mathsf{T} \underline{N} \mathrm{d}V \tag{5.17}$$

with the material density ρ and the vector of shape functions $\underline{N}$, which will be defined later.

5.3.4. Damping Matrix

Damping can be defined in several different ways. The approach in this thesis is to use Proportional or Rayleigh damping. The damping therein is dependent on the mass and stiffness matrix given by Langen and Sigbjörnsson (1979, Eqn.:9.46):

$$\underline{\underline{C}} = \alpha_1 \underline{\underline{M}} + \alpha_2 \underline{\underline{K}} \tag{5.18}$$

with the two damping coefficients α_1 and α_2. The dependency can be seen in Figure 5.6. The graph follows the two asymptotes, along the y-axis and along the x-axis. The damping ratio

is further defined as (Langen and Sigbjörnsson, 1979, Eqn.:9.47):

$$\xi_i = \frac{1}{2}\left(\frac{\alpha_1}{\omega_i} + \alpha_2\omega_i\right) \tag{5.19}$$

with the damping ratio ξ_i and the eigenfrequencies ω_i. The coefficients α_1 and α_2 can be calculated by using two eigenfrequencies and the corresponding critical damping given by Langen and Sigbjörnsson (1979, Eqn. (9.48)):

$$\alpha_1 = \frac{2\omega_1\omega_2}{\omega_2^2 - \omega_1^2}\left(\lambda_1\omega_2 - \lambda_2\omega_1\right) \tag{5.20}$$

$$\alpha_2 = \frac{2\left(\omega_2\lambda_2 - \omega_1\lambda_1\right)}{\omega_2^2 - \omega_1^2} \tag{5.21}$$

However in most practical structural problems the mass damping coefficient α_1 is ignored and the structural damping defined by (ANSYS Structural Analysis Guide, 2009):

$$\alpha_2 = 2\frac{\xi_i}{\omega_i} \tag{5.22}$$

This is shown in the figure as the x-axis asymptote.

5.3.5. Stiffness Matrix

The stiffness matrix is defined similar to the mass matrix given by (Langen and Sigbjörnsson, 1979, Eqn.:2.5):

$$\underline{\underline{K}} = \sum_i \underline{\underline{a_i}}^{\mathsf{T}}\ \underline{\underline{k_i}}\ \underline{\underline{a_i}} \tag{5.23}$$

with $\underline{\underline{a_i}}$ the already introduced connectivity matrix and the individual local stiffness matrix $\underline{\underline{k_i}}$ in global coordinates. The local stiffness matrix is transformed into global coordinates by (Langen and Sigbjörnsson, 1979, Eqn.:2.3b):

$$\underline{\underline{k}} = \underline{\underline{T}}^{\mathsf{T}}\ \underline{\underline{\overline{k}}}\ \underline{\underline{T}}. \tag{5.24}$$

The transformation matrix $\underline{\underline{T}}$ changes the local stiffness matrix $\underline{\underline{\overline{k}}}$ from local to global coordinates. The local stiffness matrix is defined by (Moan, 2003a, Eqn.:3.34):

$$\underline{\underline{\overline{k}}} = \int_V \underline{\underline{D}}^{\mathsf{T}} \, \underline{\underline{B}} \, \underline{\underline{D}} \mathrm{d}V \tag{5.25}$$

with the stiffness $\underline{\underline{D}}$ and the strain-displacement matrix $\underline{\underline{B}}$. The generation is shown for the common used 4-node shell elements. ANSYS uses for all plates Mindlin-Reissner theory or thick plate theory. The strain-displacement relation is based on the linear material properties and given by (Moan, 2003a, Eqn.:7.30):

$$\underline{\underline{D}} = \frac{E}{1-\nu^2} \begin{bmatrix} 1 & \nu & 0 & 0 & 0 \\ \nu & 1 & 0 & 0 & 0 \\ 0 & 0 & \frac{1}{2}(1-\nu) & 0 & 0 \\ 0 & 0 & 0 & \frac{1}{2k}(1-\nu) & 0 \\ 0 & 0 & 0 & 0 & \frac{1}{2k}(1-\nu) \end{bmatrix} \tag{5.26}$$

The stiffness is defined by (Moan, 2003a, Eqn.:7.32):

$$\underline{\underline{B}} = \begin{bmatrix} \underline{0} & -z\dfrac{\partial \underline{\underline{N}}}{\partial x} & \underline{0} \\ \underline{0} & \underline{0} & -z\dfrac{\partial \underline{\underline{N}}}{\partial y} \\ \underline{0} & -z\dfrac{\partial \underline{\underline{N}}}{\partial y} & -z\dfrac{\partial \underline{\underline{N}}}{\partial x} \\ \dfrac{\partial \underline{\underline{N}}}{\partial x} & \underline{\underline{N}} & \underline{0} \\ \dfrac{\partial \underline{\underline{N}}}{\partial y} & \underline{0} & -\underline{\underline{N}} \end{bmatrix} \tag{5.27}$$

with the shape functions $\underline{\underline{N}}$. For the used SHELL181 element the shape function is given by (ANSYS Element Reference, 2009):

$$\underline{\underline{N}} = \left[\frac{1}{4}\left(1-\frac{x}{a}\right)\left(1-\frac{y}{b}\right), \frac{1}{4}\left(1+\frac{x}{a}\right)\left(1-\frac{y}{b}\right), \frac{1}{4}\left(1+\frac{x}{a}\right)\left(1+\frac{y}{b}\right), \frac{1}{4}\left(1-\frac{x}{a}\right)\left(1+\frac{y}{b}\right) \right] \tag{5.28}$$

with a the half width and b the half plate length and the coordinates x and y on the plate. The coordinate system with the nodes and degrees of freedom can be seen in Figure 5.7. The

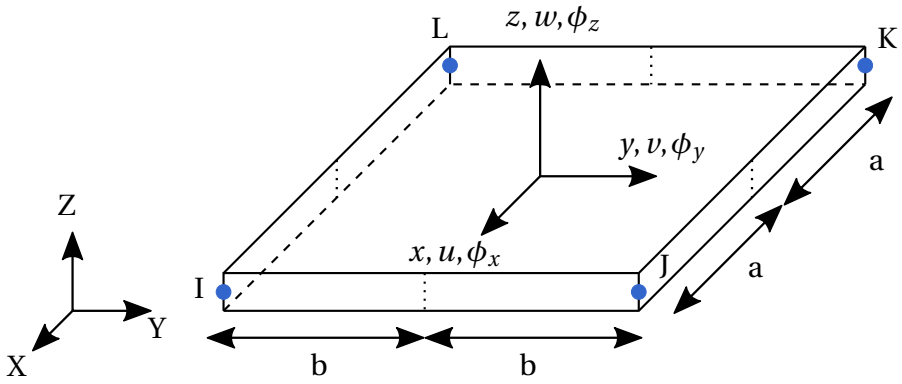

Figure 5.7.: Degree of freedom and node definition of a shell element in local and global coordinates. (ANSYS Element Reference, 2009)

four nodes are defined by I, J, K, L, the coordinate system utilizes x, y, z and the degrees of freedom are denoted $u, v, w, \phi_x, \phi_y, \phi_z$.

5.4. Finite Element Analysis Solver

The defined system containing the different components can be solved in different ways, to receive various results. Four different solvers are introduced in the following to determine the required values.

5.4.1. Eigenfrequency Solver

A modal analysis can calculate the eigenfrequencies of the system. The general eigenvalue problem for the model is defined by (Langen and Sigbjörnsson, 1979, Eqn.:4.3):

$$\left(\underline{\underline{K}} - \omega^2 \underline{\underline{M}}\right) \underline{\phi} = 0 \tag{5.29}$$

with the circular frequency ω and the mode shape vector $\underline{\phi}$. More typical is the consideration of the special eigenvalue problem. The transformation from the general into the special

eigenvalue problem is shown in Section A.3. The derivation yields:

$$\left(\underline{\underline{A}} - \lambda_i \underline{\underline{I}}\right) \underline{x} = 0 \tag{5.30}$$

The system can be solved by the Rayleigh-Ritz method. The application in ANSYS is shown in Listing G.1. The input is given as an ANSYS Parametric Design Language (APDL) input file. The subspace method with a frontal solver is used as recommended by ANSYS.

5.4.2. Linear Static Solver

A linear static solver is used for simple checks of the structure and is required for the linear buckling analysis as well. The static solver uses the inverse of the stiffness matrix. Noted should be that ANSYS uses a frontal solver, a variation of the gauss elimination, to avoid inverting the stiffness matrix. Equation 5.11 is solved by:

$$\underline{r} = \underline{\underline{K}}^{-1} \underline{R} \tag{5.31}$$

The APDL code is shown in Listing G.2.

5.4.3. Linear Buckling Solver

For a linear buckling analysis Equation 5.13 is reconsidered. A linear buckling analysis solves for the load required to start linear deformations. The equation looks as follows:

$$\left(\underline{\underline{K_0}} + \underline{\lambda}\,(P)\, \underline{\underline{K_G}}\right) \underline{r} = 0 \tag{5.32}$$

with the buckling load multiplier$\underline{\lambda}$ depending on the applied load P. The system can be solved by using the determinant and solving for $\underline{\lambda}\,(P)$. Finally P can be estimated and the different buckling loads, for the respective buckling modes can be estimated by:

$$\det\left(\underline{\underline{K_0}} - \underline{\lambda}\,(P)\, \underline{\underline{K_G}}\right) \tag{5.33}$$

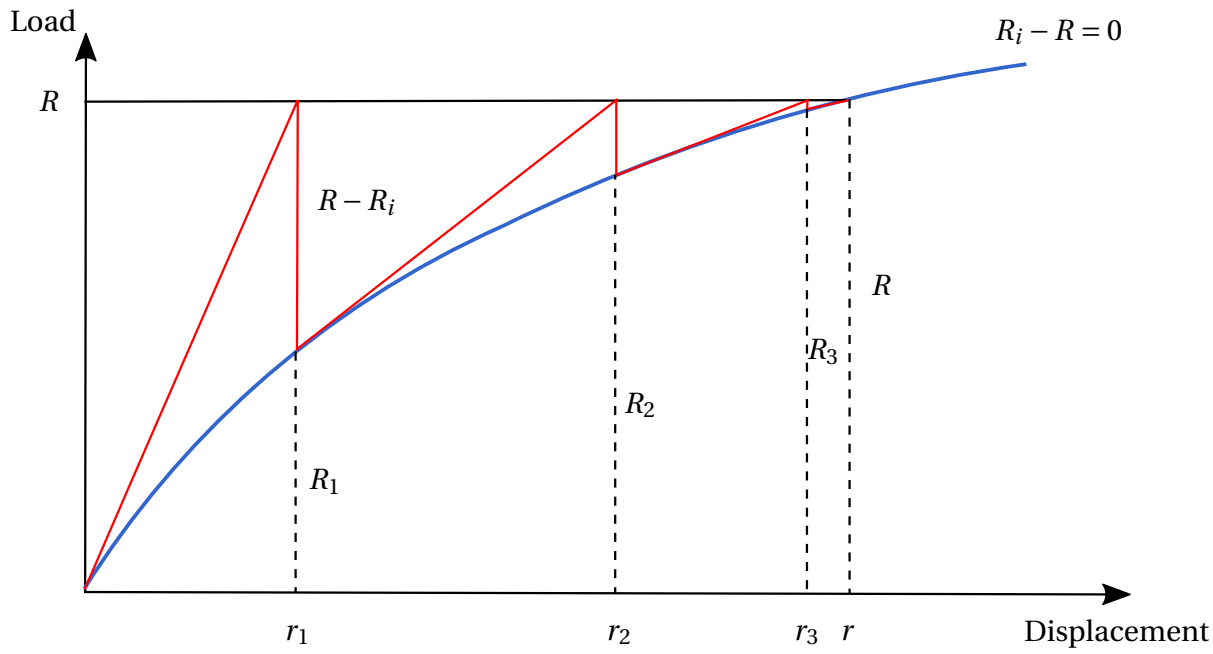

Figure 5.8.: Full Newton-Raphson iteration scheme, which is recommended for non-linear transient finite element calculations. (Moan, 2003a, Fig.:12.27)

The input file for ANSYS is shown in Listing G.3. ANSYS needs to solve the static system first before it can estimate the buckling load. In this example the first 2,500 buckling modes are extracted to be able to find suitable imperfection patterns.

5.4.4. Transient Solver

Solving non linear systems requires special solution methods. For static calculations the Riks method might be used, which is not considered in this work. In this thesis the non linear transient solver using the full Newton-Raphson iteration method is applied. The load displacement curve in Figure 5.8 is non-linear, thus an iterative approach must be followed. The algorithm can be written as (Moan, 2003b):

$$x_{n+1} = x_n - \frac{f(x_n)}{f'(x_n)} \tag{5.34}$$

Applied on the finite element problem, the equation looks like:

$$\underline{r_{n+1}} = \underline{r_n} - \underline{\underline{K_I}}^{-1} \left(\underline{r_n}\right) \left(\underline{R_{int}} - \underline{R}\right) \tag{5.35}$$

or:

$$\underline{r_{n+1}} - \underline{r_n} = \Delta \underline{r_{n+1}} = \underline{\underline{K_I}}^{-1} \left(\underline{r_n}\right) \left(\underline{R_{int}} - \underline{R}\right) \tag{5.36}$$

The aim is, to find an equilibrium between the internal forces $\underline{R_i}$ and the external forces $\underline{R}$. The stiffness matrix is updated for each step until the convergence criterion is reached. The final formulation is given by (Moan, 2003b, Eqn.:12.98a):

$$\underline{R} - \underline{R_{int}} = \underline{\underline{K_{I(n)}}} \, \Delta \underline{r_{n+1}} \tag{5.37}$$

The application in ANSYS is shown in Listing G.4. Additionally to the activation of the full Newton-Raphson method, several other adjustments must be made. Automatic time stepping is activated, allowing the program to include several substeps based on the complexity of the system. Additionally the load is ramped, which means, that high loads can be split into several steps to reach equilibrium. The maximum number of substeps is set to 1,000. For unstable structures it might occur that for one substep the system can not find equilibrium. In this case the solver will ignore this substep and continue with the next step. Often equilibrium is reached in the next step and the result might be considered to right. Another important factor is the output values. Huge models create huge amounts of data for several steps and substeps. Since only a few values are usually needed the output is redefined.

5.4.5. Distributed ANSYS

On the personal computer, ANSYS 15.0 is used. To be able to solve larger systems the HPC VILJE of NTNU is used. The specifications of the cluster have been mentioned in the introduction. For calculations on several cores and nodes a special application exists, ANSYS Distributed (Distributed ANSYS Guide, 2009).

Using two different ANSYS applications causes difficulties. ANSYS Distributed does not support the MPC element MPC184 with a direct elimination method. Alternatives are discussed in the following section. The second unsupported feature is the arc-length method or Riks method. The arc-length method allows the investigation into the post collapse region in a non linear static analysis excluding transient effects. The method could have been used for comparisons and validation of the transient results.

5.4.6. Multi Point Constraint

The bending moment acting on the ship section is applied at the ends of the model. A master node is defined at the hight of the neutral axis of the section and the corresponding bounded points are connected as slaves using multi point constrained. ANSYS offers several possibilities to do so. The RBE3 element defines a load distributing element, which is in a strict sense non rigid body connection and causes problems due to deformations of the boundaries. The CERIG element is however a rigid connection. Unfortunately the element does not support large deformations, which occur in a buckling analysis.
The preferred element to use would be the MPC184. Two calculation options within the element formulation are given, the direct elimination method and the Lagrange multiplier method. As already mentioned is the direct elimination method not supported by ANSYS Distributed, which would usually be the recommended method to use, the Lagrange multiplier method is troublesome with overconstrained problems. In this case, the method reveals zero pivot messages and causes convergence difficulties.
A last alternative is to use very stiff beam elements connecting the master and slave nodes. The BEAM181 element is used. Care should be taken with the definition of the Youngs modulus. It is important the restrain all elements to avoid shifts between the different elements. Difficulties arise due to excessively stiff elements causing pivots in the stiffness matrix and causes convergence difficulties. A stable Youngs modulus with a factor 10^6 higher than steel is chosen.

5.4.7. Convergence Problems

When solving non linear problems convergence problems might occur. Convergence problems describe the state when the system can not be solved to find equilibrium. This can be caused by an insufficiently constrained model with rigid body motions. If this is not the problem, it can be caused by a few elements behaving in a non realistic manner and causing large displacements. The calculation is thereafter forced to terminate. This behaviour can have several triggers.
A first approach is to include reasonable damping in the model, which stabilises the calculations. Extreme displacements are damped and the structure moves in a closed manner. If the error still occurs the fault can be overcome by use of any of these methods:

- Change time and/or time stepping
- Change number of substeps
- Switch between stepping or ramping of loads
- Change of convergence tolerances

Experiencing convergence errors does not necessarily suggest input errors. In some cases just the combination of several parameters causes the calculation to fail. Generally it should be ensured that the loads be applied gently and the number of substeps and the substeps size is small enough to solve the system. (PADT, 2012a) (PADT, 2012b)

5.5. Whipping Rule Values

As already mention IACS defined in their new IACS UR-S (2016) rule set, coming into force on the 1st July 2016, the inclusion of whipping loads. The way is left open to the respective classification societies. The methods of the different institutions are presented in following.

5.5.1. DNV

DNV published as the first classification society regulation for the inclusion of whipping loads. In DNV-CN-No.30.12 (2013) an extension to the partial safety factor method is suggested. It should be mentioned, that these rules are now out ruled, since the DNVGL rule set came in force the 1st January 2016. The rule is valid for container ships with:

1) Length between perpendicular > 350 m

2) Bow flare angle > 55°

3) Vessel design speed at 85 % MCR > 25 knots

The equation has been extended by the partial safety factor for whipping loads γ_{WH} and the partial safety factor for the dynamic collapse γ_{dU} are introduced as:

$$\gamma_S M_S + \left(\gamma_W + \left(\gamma_{WH} - \gamma_W\right)\gamma_{dU}\right) M_W \leq \frac{M_U}{\gamma_R}. \tag{5.38}$$

With γ_R defined by:

$$\gamma_R = \gamma_M \gamma_{DB}. \tag{5.39}$$

The safety factors are defined as follows:

$$\gamma_S = 1.0 \quad ; \quad \gamma_W = 1.2 \quad ; \quad \gamma_{dU} = 1.0 \quad ; \quad \gamma_M = 1.1 \quad ; \quad \gamma_{DB} = 1.0. \tag{5.40}$$

The safety factor for whipping is given by:

$$\gamma_{WH} = 1 + k_1 \left(L + k_2\right)\left(V + k_3\right)^2 \left(\tan\left(\alpha \frac{\pi}{180}\right) + k_4\right) \quad ; \quad \gamma_{WHmin} = 1.3 \tag{5.41}$$

With

$$k_1 = 4.83 \cdot 10^{-7} \quad ; \quad k_2 = 1,100 \quad ; \quad k_3 = 4.1 \quad ; \quad k_4 = -0.19$$

5.5.2. DNVGL

DNVGL has overtaken most of the former DNV rules. However some parts have changed. The special treatment of container ships is defined in DNVGL Rules Part 6 Chapter 1 (2016). The rules provided by DNVGL-CG-0153 (2015) contain special considerations for whipping loads. The validity range is given by:

1) Block coefficient in the order of 0.6 to 0.7

2) Speed in the range of 20 to 29 knots

3) Length in the range of 90 to 400 meters

The partial safety factor approach is given by:

$$\gamma_S M_S + \left(\gamma_W + \left(\gamma_{WH} - \gamma_W\right)\gamma_{dU}\right) M_W \leq \frac{M_U}{\gamma_M \gamma_{DB}}. \tag{5.42}$$

with the partial safety factors defined as:

$$\gamma_S = 1.0 \quad ; \quad \gamma_W = 1.2 \quad ; \quad \gamma_{dU} = 0.9 \quad ; \quad \gamma_M = 1.05 \quad ; \quad \gamma_{DB} = 1.1 \tag{5.43}$$

The partial safety factor for the whipping loads is given by:

$$\gamma_{WH} = 1 + c_L \left(3.8 \cdot 10^{-7} \left(L + 1100\right) \left(V + 4.1\right)^2 / \tan\alpha - 0.19\right) \geq \gamma_W \tag{5.44}$$

with the distribution factor c_L given with 1 for the midship position.

5.5.3. Bureau Veritas

BV-NR-583 (2015) have introduced three additional service features "WhiSp1", "WhiSp2" and "WhiSp3". The designed ship will fall into the category "WhiSp1" and only a linear fatigue assessment is required. An ultimate strength assessment including dynamics effects is only required for ships $L_{PP} \geq 350m$ in class "WhiSp2". Since the fatigue calculation is not part of this thesis it is neglected. For larger ships, the inclusion of whipping loads is done by

considering in the used wave load estimation tool VERISTAR HOMER.

5.5.4. ClassNK

ClassNK, the society which classified the *MOL Comfort* has introduced a new rule set. In the ClassNK Rules (2015) container ships over 150 m length will use the following partial safety factor approach:

$$\gamma_S M_S + \gamma_W M_W \leq \frac{M_U}{\gamma_M \gamma_{DB}} \tag{5.45}$$

The partial safety factors are defined as:

$$\gamma_S = 1.0 \quad ; \quad \gamma_W = 1.2 \quad ; \quad \gamma_M = 1.05 \quad ; \quad \gamma_{DB} = 1.15 \text{ (hog)} \quad ; \quad \gamma_{DB} = 1.0 \text{ (sag)} \tag{5.46}$$

For ships not less than 300 meter is a different approach followed:

$$\gamma_S M_{Smax} + \gamma_{Wh} M_{W-Hog-Mid} \leq M_{U\_DB} \tag{5.47}$$

with the partial safety factors defined as:

$$\gamma_S = 1.0 \quad ; \quad \gamma_{Wh} = 1.5 \tag{5.48}$$

The value for M_{U_DB} must be estimated directly by the classification society. The defined loads are calculated in the same way, as for smaller ships.

5.5.5. American Bureau of Shipping

American Bureau of Shipping Inc. (ABS) has defined with ABS Guidance Notes (2014) their own guidance note on the effect of whipping loads on container carriers. The partial safety

factor concept is given by:

$$\gamma_S M_{Smax} + \gamma_{Wh} M_{W-Hog-Mid} \leq \frac{M_{U\_DB}}{\gamma_R} \tag{5.49}$$

with the partial safety factors given as:

$$\gamma_S = 1.0 \quad ; \quad \gamma_R = 1.1 \tag{5.50}$$

The partial safety factor is the maximum value of the approach for the wave loads $\gamma_W = 1.05$ or an approach resulting from the calculated whipping loads. Whipping loads are additionally included in the wave moment M_W. ABS has developed a closed form approach to estimate whipping loads and prorate them with the wave bending moment. This approach exceeds the capacities of this thesis and is not further investigated.

5.5.6. Lloyds Register

Lloyds Register Ltd. (LR) has developed a class notation "WDA" for the assessment of whipping loads. The longitudinal strength procedure is described in LR Rules (2016). In the rules correction factors for the Ship Right program have been developed. These values can't be compared directly with the previous ones and will not be investigated further.

6. Results

The first part of the chapter deals with the verification of the chosen method on a simple plate. Thereafter, the effect of different parameters on the plate is shown. Finally the ultimate capacity of the hull girder is determined and the time history load is applied.

6.1. Simple Plate and Panel validations

In a first step, a simpler model is compared with an analytical and a semi analytical method. The purpose is to get a general feeling about the finite element method and to validate the results and show weaknesses and limitations of the chosen approach.

6.1.1. Comparison of Analytical, PULS and FEM Results

For the verification of the applied finite element method a simple plate is used. The dimensions are chosen to be of same magnitude as the inter frame bottom plates. This results in a length of 3.15 meter, a width of 0.833 meter and a thickness of 0.02 meter. In this study the material A32 is taken and hardening is applied by using the Power Law. The aspect ration of the plate is 3.7815. The slenderness ratio given by Equation 5.4 is $\overline{\lambda} = 0.8484$. The plate is a moderate slender structure according to Figure 5.5.
The numeric result is compared to the yield level σ_y, the Euler buckling stress σ_e, the Johnson-Ostenfeld Method σ_{cr}, the DNV ultimate strength method σ_{ult} and the method of the effective width σ_{xm}. Additionally the plate is modelled in the DNV program PULS and evaluated. The maximum stress under axial loading is evaluated.

Table 6.1.: Comparison of ultimate capacity for a simple plate with a width of 0.833 meter and a length of 3.15 meter with constrained edges. Calculated by the yield level, Euler buckling, Johnson-Ostenfeld assumption, ultimate strength method, the method of effective width, PULS and ANSYS.

Method	σ_y	σ_e	σ_{cr}	σ_{ult}	σ_{xm}	σ_{PULS}	σ_{ANSYS}	Unit
Stress	315.00	437.65	258.32	262.54	269.50	273.00	271.91	MPa
Deviation	13.68	37.87	5.26	2.40	0.89	0.40	1	%

The plate is modelled in ANSYS and loaded in the longitudinal direction. The boundaries on the short edges are modelled by using multi point constrains. The boundaries on the long edges are defined as constrained. Imperfections are implemented using an eigenvalue analysis on the forehand. As expected, by an aspect ratio close the four, the first eigenvalue consists of four half waves and is shown in Figure F.1 in the appendix. The imperfections are applied with the maximum allowed magnitude according to DNV-OS-C401 (2013). The displacement controlled calculation are performed until the plate is well inside the post collapse region. The maximum value of the load-displacement curve is shown in Table 6.1. The final deflections are shown in Figure F.2 in the appendix.

Comparing the results according to their deviation of the ANSYS values, shows that the Euler buckling load is much higher than the expected value. Considering Figure 5.5 the plate is in the moderate slender range and the Euler buckling load is out of the range. The yield stress level is well above the buckling stress level, thus buckling occurs and need to be considered.

The Johnson-Ostenfeld result reveals a deviation of 5.26 % and the ultimate strength concept reveals a deviation of 2.4 % to the ANSYS result. These values are not very satisfying, but might be considered as an indication of valid results. However the most accurate approach, Faulkners method, gives an error of 0.89 %. More sophisticated is only the semi analytical method used in PULS. The results are close to match with an error of 0.4 %. Thus the method of effective width, PULS and ANSYS reveal trustworthy results.

The comparison is performed for several thicknesses. The best convergence could be found for the already examined thickness. In the range between 15 millimetre and 35 millimetre the results are within 5 % difference and thus valid. Below 15 millimetre thickness the results start to diverge. This happens for all three considered values in Figure 6.1. This can

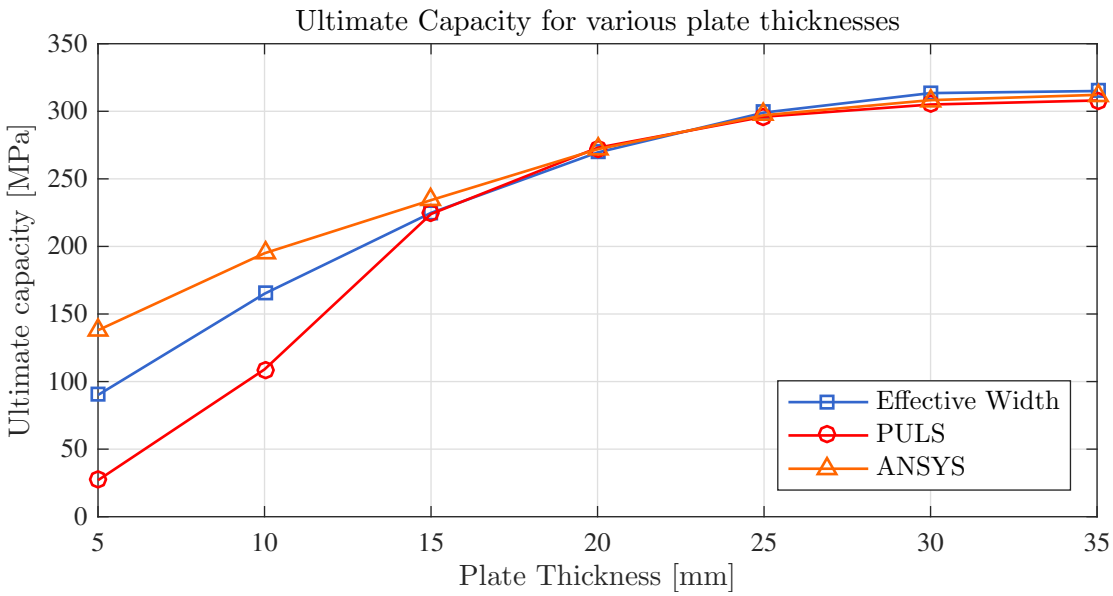

Figure 6.1.: Comparison of ultimate capacity of the plate of the effective width method, PULS and ANSYS. The thickness of the plate with a length of 3.15 meter and a width of 0.833 meter is varied.

have several influencing factors. However in the considered region only shell elements with a thickness higher then 15 millimetre are used. Therefore the matter is not further investigated.

6.1.2. PULS results

The results generated with the semi analytical approach used in PULS are already shown. The outcome of PULS gives similar results to the non linear finite element approach. Both methods are using a similar approach but the formulation of the elements is different. This explains the good correspondence and the verification as well.

PULS offers the possibility to check the limit state for combinations of axial and transverse loadings. The bottom structure will experience loads in axial and transverse directions from external pressure. The results for load combinations can be seen in Figure 6.2. The first graph shows the considered plate with pinned boundaries. The curve shows a cubic behaviour for the combined loading conditions. The capacity under axial thrust remains constant as long as it is the dominating load. The ultimate capacity deflection pattern for the pinned plate can be seen in Figure E.1.

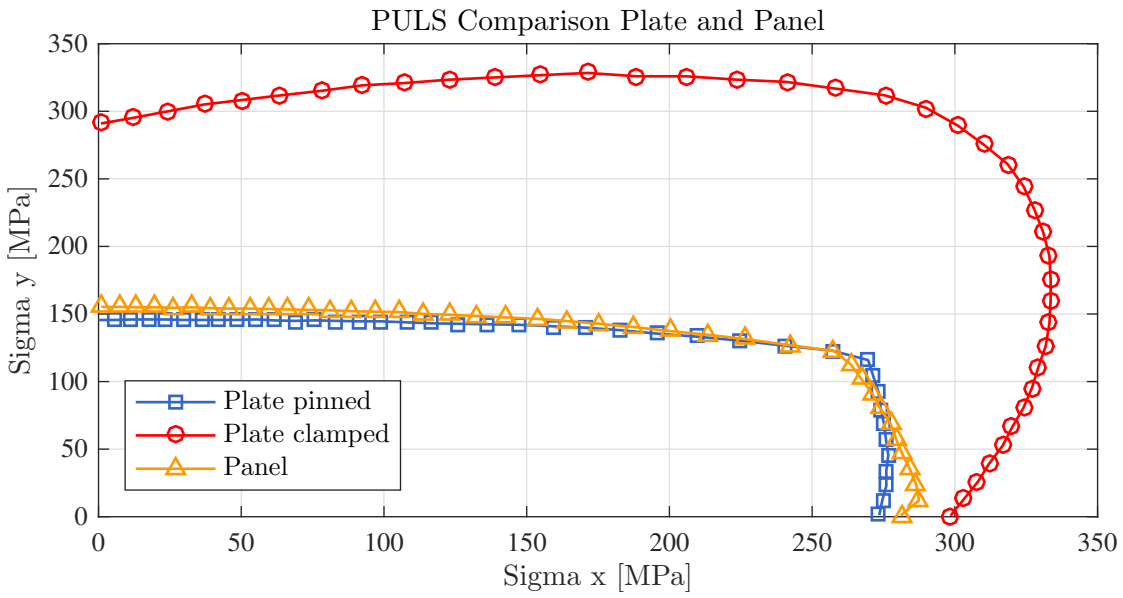

Figure 6.2.: PULS results for the plate of length 3.15 meter, 0.833 meter width and a thickness of 0.02 meter with clamped and pinned boundaries loaded under biaxial load. As well as the result for a panel of 3.15 meter length and 4.998 meter width and five mounted tee-bar profiles of 450x15+100x20 mm loaded under biaxial stress is given.

The combined load case for the same plate with clamped boundaries has a different shape. The capacity under pure axial pressure is slightly higher than for the pinned plate. The effect of the different boundary condition is especially visible when biaxial loading is applied. Generally shows the plate a higher capacity for transverse and combined loading then the pinned plate. Additionally the deflection pattern changed into six half waves as seen on Figure E.2. This does not corresponds with the aspect ratio of the plate.

PULS gives the opportunity to design a whole panel. A typical bottom panel including six plates and five stiffeners is modelled. The biaxial loading curve is shows high correspondence with the simple plate result. PULS includes two different sets of imperfections on the panel. The local imperfections are shown in Figure E.3 and the global imperfections in Figure E.4. The ultimate capacity pattern is a combination of both, dominated by the local deformations. The stiffeners are failing due to tripping and the plate shows the local plate deflection with four half waves over the plate length. The deflection pattern in Figure E.5 might give an outlook on the expected failure of the hull girder.

In a nutshell the pinned plate and the panel do not show drops in their capacity as long as

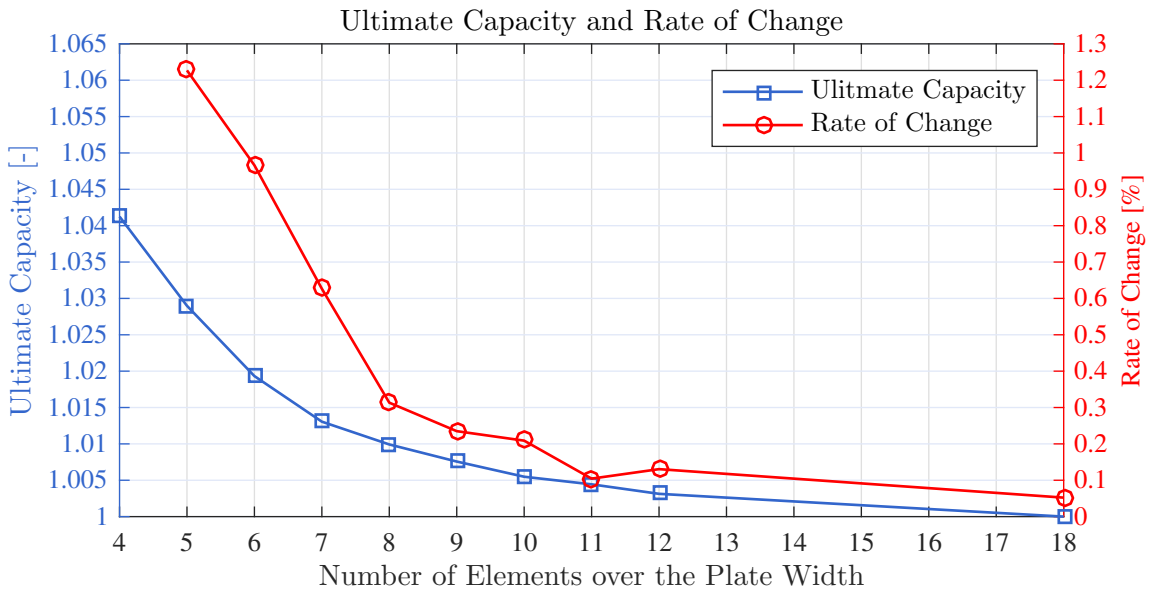

Figure 6.3.: Mesh sensitivity study of the simple plate with length 3.15 meter, 0.833 meter widths and 0.02 meter thickness. The results shown are the non-dimensionalized ultimate capacity and the rate of convergence.

the longitudinal load is the dominating force. The effect of transverse loads will be neglected in following. The matter is not further investigated. The panel failure gives an assumption of the expected limit state of the midship section.

6.1.3. Mesh Convergence Study

For each finite element problem a mesh convergence study should be performed. The normal way is to decrease the mesh size and measure the displacement or maximum stress. A typical convergence criterion is that the rate of change is below 5 %. For this thesis the approach is changed. The most critical element measurement is the number of element over the transverse of the plate. Thus this number is increased. Measured and compared is the ultimate capacity of the plate.

Figure 6.3 shows the non dimensional ultimate capacity. With finer mesh the capacity decreases constantly. The deviation between the first and the last step is less than 4.5 %. The rate of change for the second step is already 1.25 % which is below 5 %. This can be explained by the already very fine mesh of the structure. Thus the normal mesh convergence criterion is not be applied in this case. A mesh size of nine elements over the width is chosen which

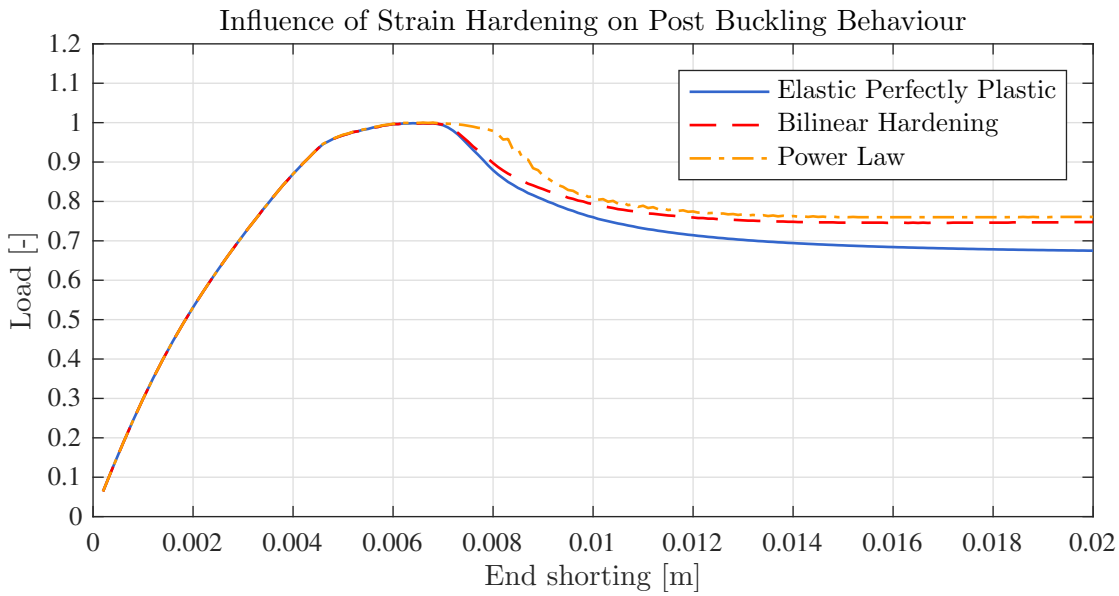

Figure 6.4.: Influence of elastic perfectly plastic, bilinear and power law hardening on the post buckling behaviour of a simple plate.

corresponds to an element size of 100x100 millimetre. This is based on comparisons with other studies.

6.2. Case Study on a Simple Plate using FEM

After the applied method is verified the influence of several parameters on the buckling and post collapse behaviour is estimated.

6.2.1. Influence of Material Hardening

The influence of the already discussed different non-linear material models should to be evaluated. All three models are applied in ANSYS. The plates are pushed far into the post collapse region to evaluate the results. The load-displacement curves are shown in Figure 6.4. The pre- and post-buckling curve are equal for all three material models. Differences are occurring in the post-collapse region. Including hardening with the DNV recommended bi-linear model gives the plate a higher post collapse capacity than the elastic-perfectly plastic model. Increasing a simple hardening model increases the remaining capacity of the plate

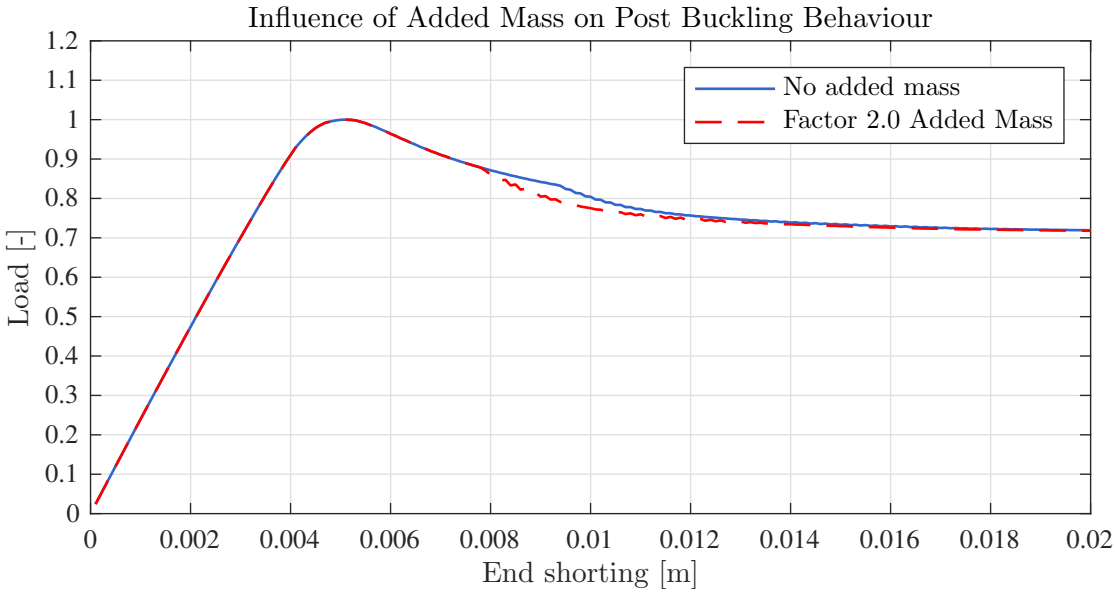

Figure 6.5.: Influence of added mass on the collapse of a simple plate under axial loading.

compared with the elastic perfectly plastic model. The Power law increases the plates capacity directly after the collapse, but nearly follows the bilinear hardening model afterwards.

6.2.2. Influence of Added Mass

In dynamic analysis for marine structures, added mass is a topic of concern. The added mass factor for the load is defined as two. This factor is as well applied for the bottom plates. The mass of the plate is multiplied by the factor 2. Noted should be that neither external pressure or gravitational acceleration are considered in this test case. The two load - displacement curves are shown in Figure 6.5.

The graphs are identical until the post collapse region. After collapse the plate with higher mass continues to collapse faster compared to the lighter plate. Both paths are matching after a while again at the same capacity. Thus only the last part of the unloading path is influenced by added mass. In general added mass has a minor influence on the static case, but might come in play in the dynamic case.

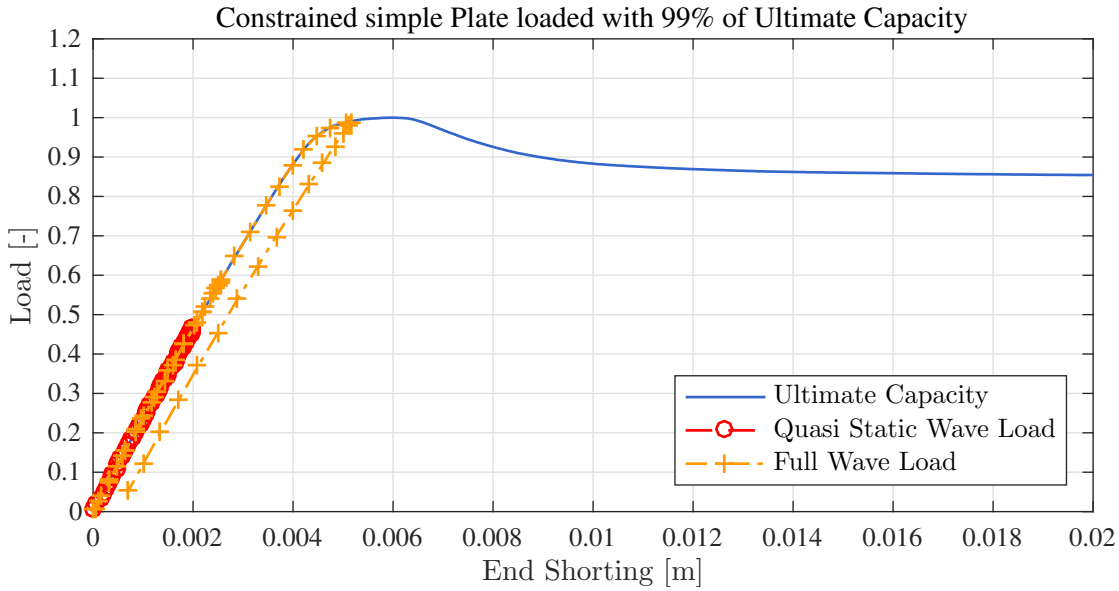

Figure 6.6.: Load-displacement curve for the simple plate. Displacement controlled loaded into the post collapse region and load controlled loaded under quasi-static and full wave loads.

6.2.3. Influence of Dynamic Loads

In a first test the simple plate is loaded with the set of measured strain data. Two load sets are herein considered, the quasi static wave load set and the full wave load set including whipping effects. The full wave loads is scaled with the maximum load being equal to 99 % of the ultimate capacity of the plate. In the quasi-static load set is the high frequency range filtered out. The result in Figure 6.6 shows clear plastic deformations of the plate. The unloading path is clearly shifted to the right hand side of the ultimate capacity path. This calculation is not very meaningful, since the plate does not have the same inertia as the ship. Nonetheless shows the test the expected result for the midship section.

6.3. Full Model Results

Finally the ship is modelled in ANSYS. Due to calculation time considerations several models appear in the following section. The five used models are listed below:

1) "Full Model", 4 cargo hold model (Figure F.4)

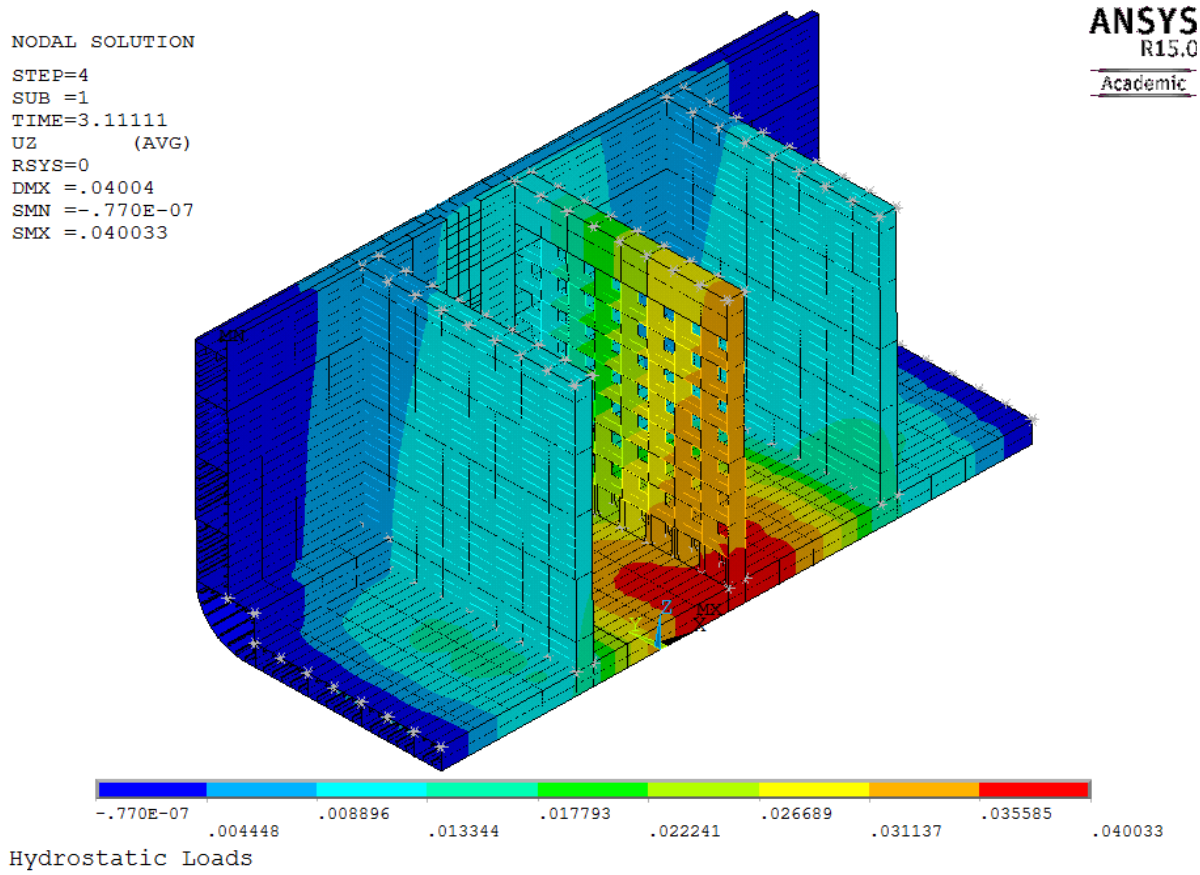

Figure 6.7.: Vertical deflection of the four cargo hold model "Full Model" loaded under static and dynamic wave pressure.

2) "1 Web Model" or "Crash Section" according to the 1 Web length (Figure F.5)

3) "3 Web Model" according to the 3 Web length (Figure F.6)

4) "Rigid Body Model", 3 Web model with the effect of rigid body motion (Figure F.7)

5) "Floating Model", 3 Web model with inertia and effect of rigid body motion (Figure F.7)

The section starts with estimation of the ultimate capacity of the models and continues with the consideration of dynamic effects.

6.3.1. Static Case on full Model

In a first step the effect of hydrostatic loads on the four cargo hold model is checked. Hydrostatic loads include the hydrostatic and hydrodynamic pressure. The vertical deflection of

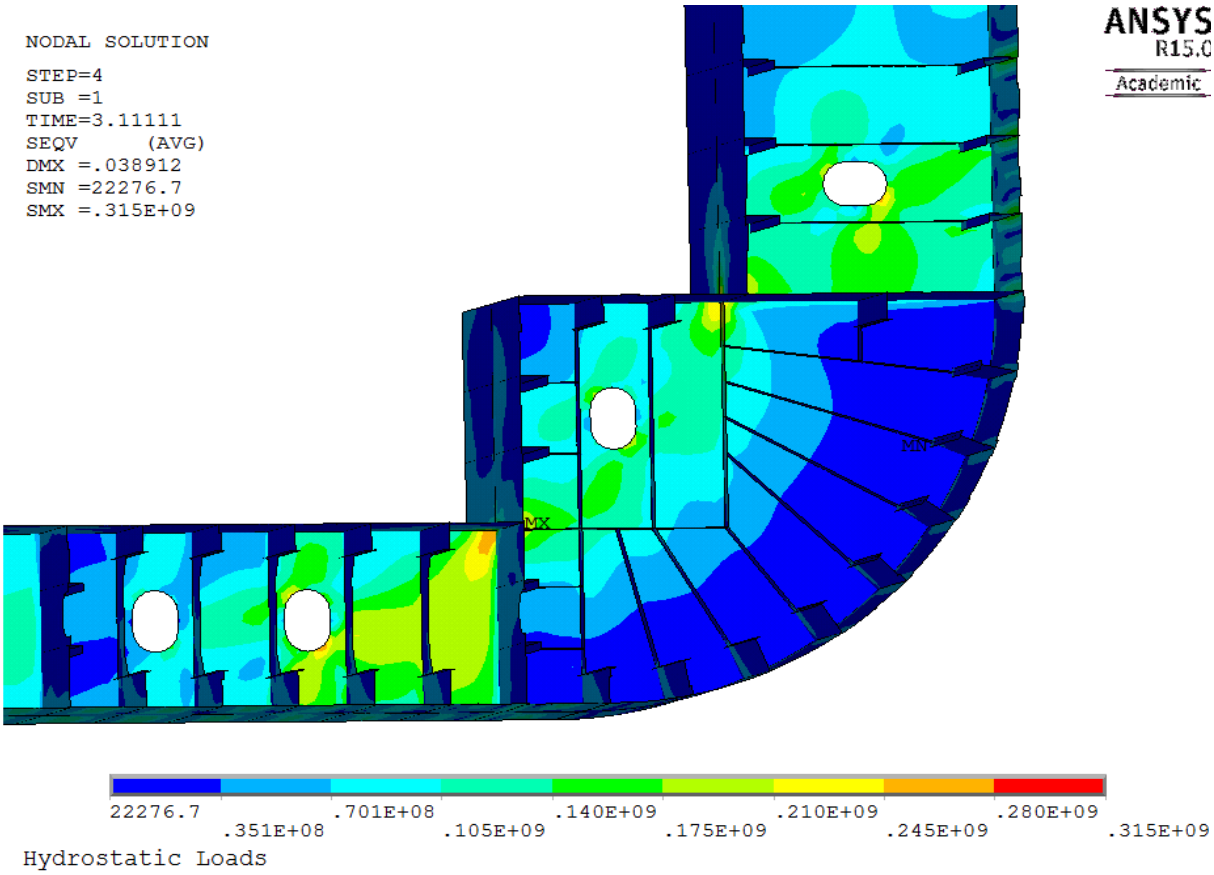

Figure 6.8.: Detail of the von Mises stress distribution on an open web frame in the non-linear part.

the loaded model is shown in Figure 6.7. The different stiffness of the open and closed bulkheads can be seen as the weaker open bulkhead allows more vertical deflection. Whereas the closed bulkheads keep the hull nearly at base level. The maximal deflection is 4 centimetres. The stress level, when considering the von Mises stress is at a reasonable level. In the bottom area the maximum stress is with 100 MPa far from the yield level. The stress in other parts of the structure is even lower. Higher stresses occur in the corners where the container masses are applied. Because of the coarse modelling these areas are singularities and cause theoretically infinitive high stresses. The stiffeners of the open bulkhead are modelled as beam elements. However the connection between the inner bottom and the bulkhead is done by shell elements. This reduces the peak stress and gives more reasonable results. The modelled shell elements are distributing the loads in the transverse direction. The stress is remarkably reduced and brought to an acceptable level.

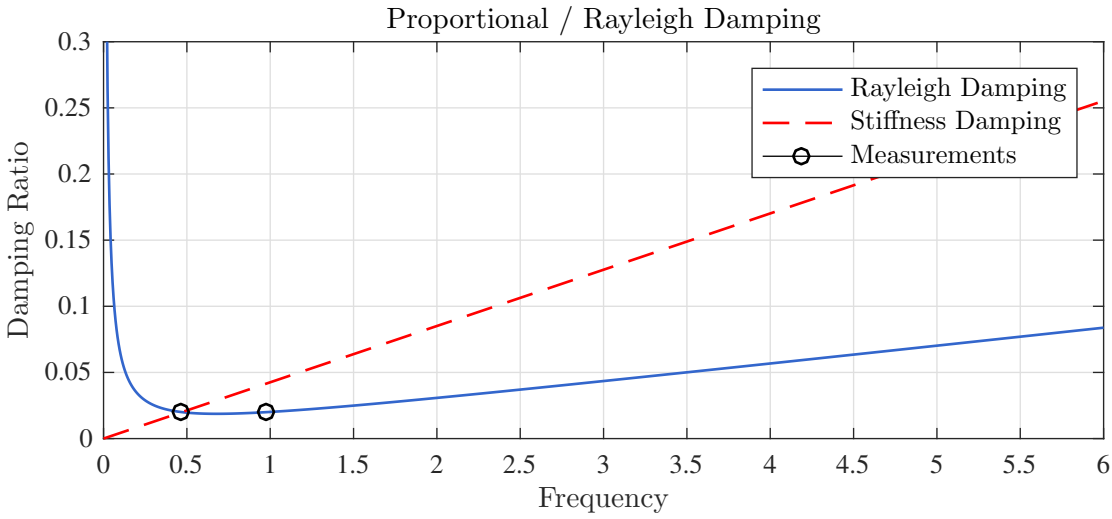

Figure 6.9.: Comparison between Rayleigh damping and pure stiffness damping applied for the eigenfrequencies of the 2 node and 3 node mode with a critical damping ratio of 2 %.

The maximum stress in the model is 406 MPa. This stress is well above the yield level and causes plasticity. The peaks occur at the transition of the double bottom and the side tank. Figure 6.8 shows the von Mises stress at an open web frame. The stress is in both corners remarkably too high. On the one hand might the stress peaks arise from the geometrical singularity, on the other hand the average stress is in this region already relatively high. In reality should this matter be examined, especially with regards to torsional loads might the web be insufficiently strong. For the calculation in this thesis has the plasticity only minor influence and is accepted.

6.3.2. Influence of Structural Damping

Before taking a look at the intensive transient calculations it is necessary to include structural damping in the system to avoid divergence difficulties. The concept of proportional damping is already discussed in section 5.3.4. The application of reasonable values is always difficult. The two required measurements are taken as the eigenfrequencies of the two and the three node mode. The damping ration for this two frequencies is orientated on the findings of Andersen and Jensen (2014). A critical damping between 1 % and 3 % is assumed and in a first approach the damping is set to 2 %.

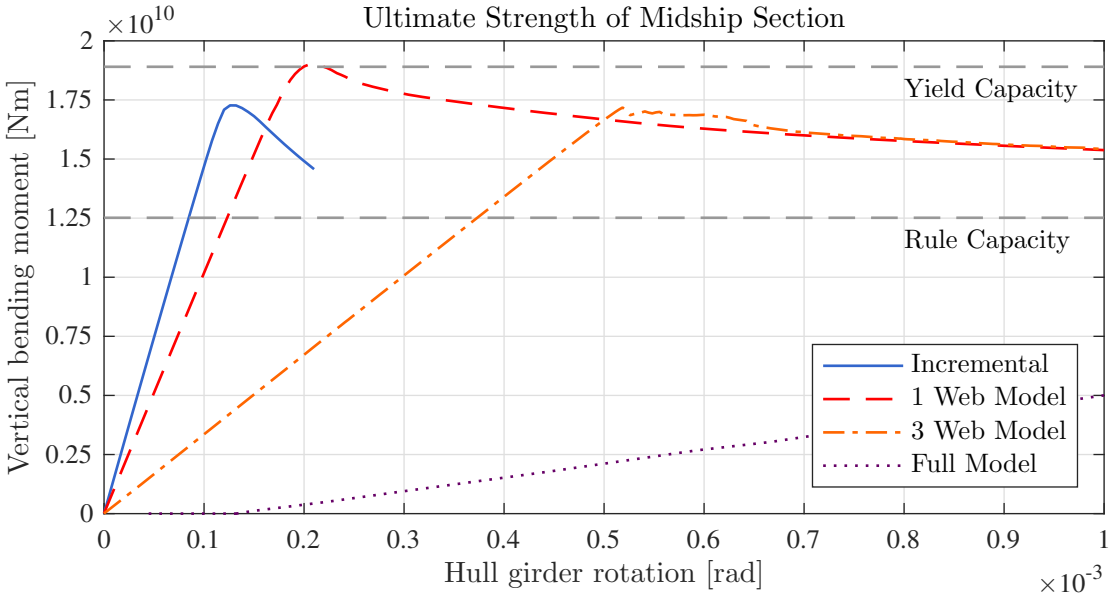

Figure 6.10.: Moment-rotation curve for the ultimate strength of the midship section for the 1 Web Model, the 3 Web Model and the Full Model. Additionally the incremental result obtained by POSEIDON,the rule loading and the yield capacity are shown.

The second decision is to choose the simplified stiffness damping, defined by only one frequency or the full proportional damping approach. The stiffness damping carries the risk of the overestimation of very low frequency loads. Thus the full proportional damping is applied defined by $\alpha_1 = 0.0127$ and $\alpha_2 = 0.0276$.

6.3.3. Ultimate Capacity of the Midship Section

After the static consideration the Full Model is gradually loaded with a hogging bending moment, until the hull girder collapses. The required computational time exceeds a reasonable time limit by far. A smaller 1 Web and a 3 Web model are considered and loaded. Also the program POSEIDON is used to calculate the ultimate state with the incremental method. The Results are shown in Figure 6.10.

No result could be reached for the Full Model, due to several instability problems and time computational. Only the pre buckling part of the the calculation is solved. The ultimate capacity for the 1 Web and 3 Web is calculated. First point of interest are the different slopes of the pre buckling parts. This is caused by the way the deflection is measured. Measuring at

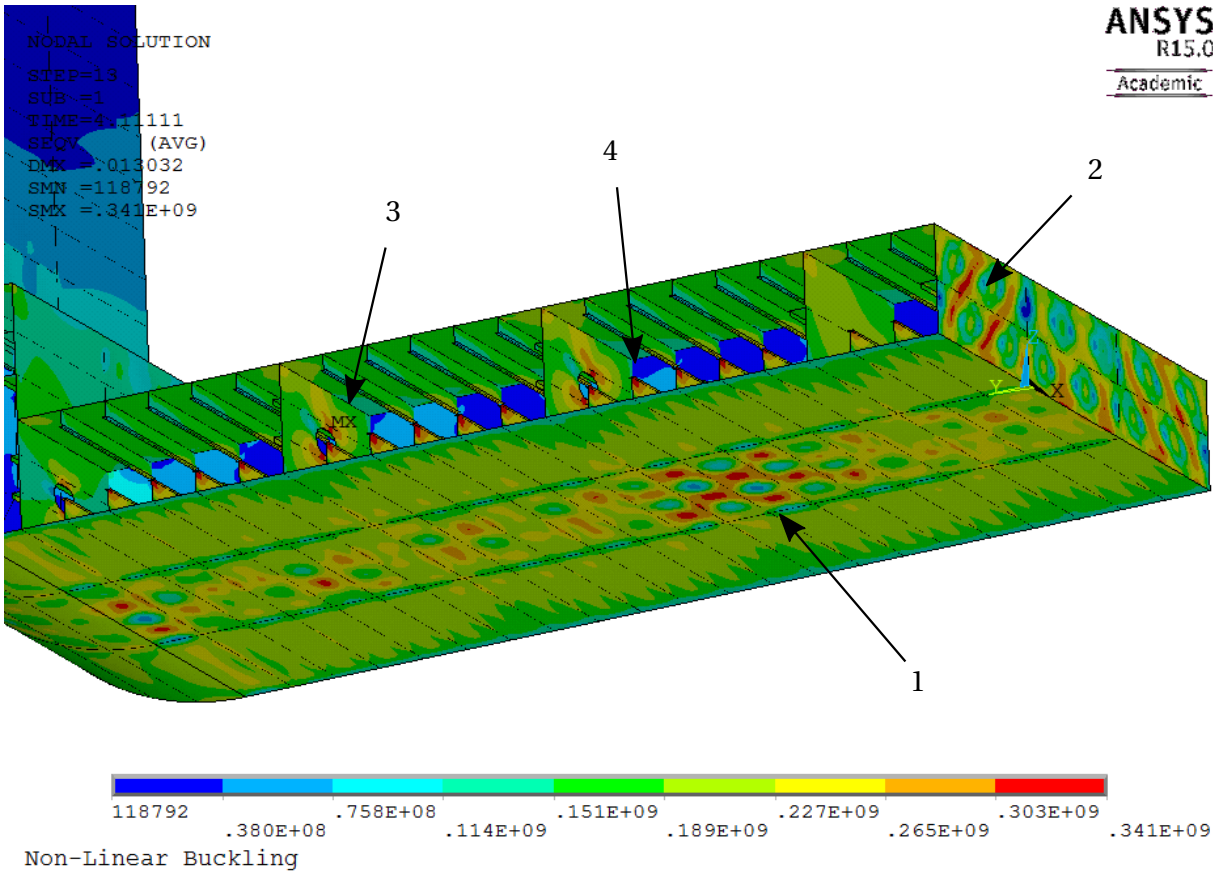

Figure 6.11.: Von Mises stress at the bottom of the 3 Web Model with the GL rule load applied looking forward.

the same points where the moments are applied will include the stiffness of the model. Thus a longer model will be weaker than a shorter one.

Of interest are the maximum ultimate capacities of the two models. Suspicious for the 1 Web model is the fact that the ultimate strength exceed the yield strength level. This is caused by influence of the boundaries. The behaviour is matching with the results received by Fricke and Bronsart (2012). The clamped boundaries close to the considered areas are over predicting the ultimate capacity. Thus the 1 Web model is non-conservative and not suitable for this thesis.

The 3 Web model gives more reasonable values. The ultimate capacity is in a valid range. Comparing the maximum value of the incremental result with the FEM result shows a difference of 0.5 %. This is a very good match for both values. A second check is done by comparing the FEM ratio between yield and buckling strength of the simple plate and the midship

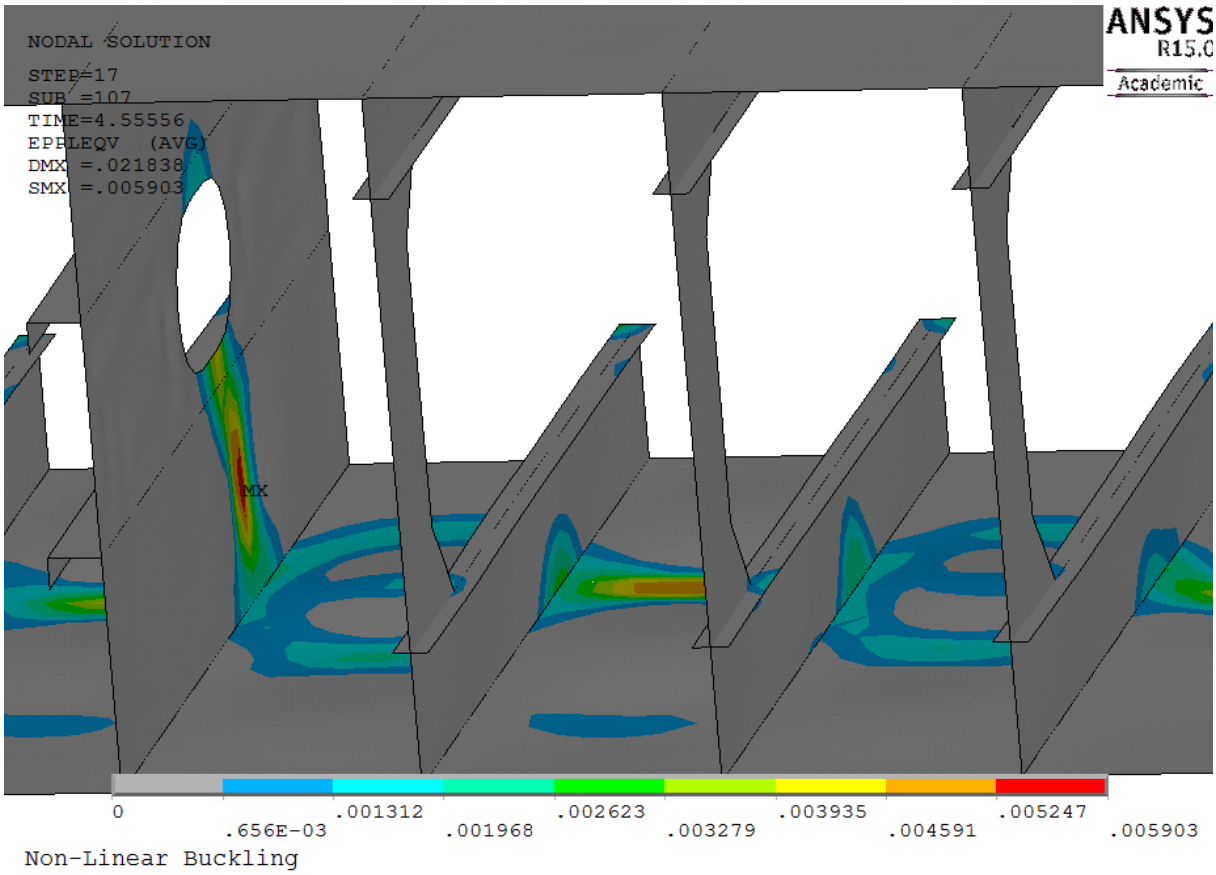

Figure 6.12.: Von Mises plastic strain in the "Crash Section" of the 3 Web Model between the longitudinal girders at 3*b and 9*b looking forward.

section. The ratio for the simple plate is $0.8555 \cdot \sigma_y$ and for the midship section $0.9087 \cdot \sigma_y$. A matter of interest is the point at which the structure starts failing and which components start yielding first. As already mentioned plasticity in the model occurs already at lower load levels. However the crucial area for the failure is the bottom region. The first yield appears in the bottom plate inwards of the longitudinal girder at 9*b at the maximal rule level. This proves the suspicion that local plate buckling between the stiffeners occurs first. The von Mises stress distribution can be seen in Figure 6.11. The stress in the bottom region (1) is already arranged in the typical four half wave buckling pattern. Three other locations are yielding in the figure. Especially the longitudinal girder at midship is exposed to large shear stress and shear strain (2). This is caused by the symmetry boundary and the corresponding reduced plate thickness. Additionally the cut-out in the longitudinal girders produces plastic strains (3). This might have several reasons. Singularities might reveal from the rel-

atively coarse mesh around the opening. Otherwise the neglected local reinforcements will reduce the local stresses as well. An other possible error can be the insufficient stiff design of the design, which should be further investigated. Also plasticity occurs at the boundaries of the model. In the webs of the stiffeners below the flanges occur plasticity at all bottom stiffeners (4). This is caused by the clamped boundary and the constrained rotation of the rigid body link and is negligible.

Loading the structure until ultimate capacity creates more plasticity. The status of failure is shown in Figure 6.12. The Crash Section is shown with all longitudinal components and the transverse parts are hidden. The plastic strain follows clearly the buckling pattern already seen for the first yield case. On top of that occurs large plastic strain below the cut-out in the longitudinal girder. This might indicate an insufficient thickness of the girder in combination with the cut out. The strain has reached the stiffener webs from the bottom plates and starts to deform the stiffeners upwards. This indicates a plate induced failure of the structure. Further occurs plasticity in the stiffener flange. On the one hand at the forward end of the flange at the transverse bulkhead and on the other hand at the end of the vertical stiffeners of the aft web frame. The global deflection at the ultimate capacity can be seen in the Appendix in Figure F.8. The buckling pattern shows clearly the four half sine waves with deflections up to 0.02 meter. The pattern spreads slowly through the width of the ship. Thus the buckling pattern is clearly anti-symmetric and does not follow the hungry horse mode. The pattern shows good correspondence with the panel calculated in PULS.

6.3.4. Post Collapse Behaviour of Midship Section

In this calculation the considered models are pushed further into the post collapse region. The idea is to get a grasp on how the structure will ultimately fail. The results in Figure 6.13 are the computational most time consuming results. The CPU time was 84 hours using one Node on VILJE. This is caused by the large non-linear deformations of the structure. The exact ultimate capacity can not be estimated using this calculation, because the used time steps are too coarse to capture the right value.

Even though the ultimate capacity is different for both models the paths are matching later

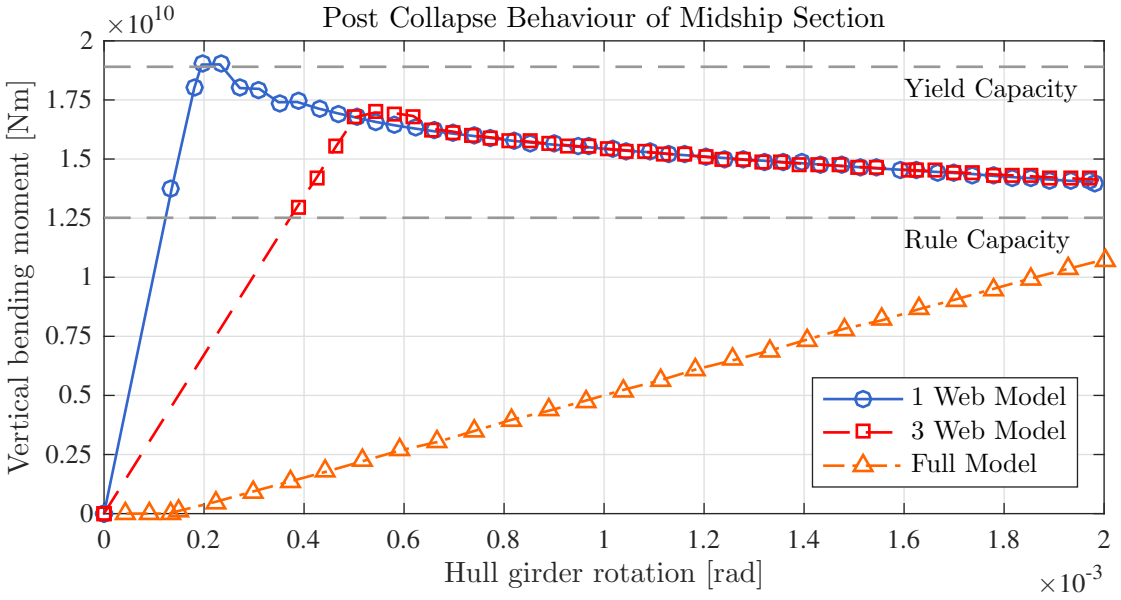

Figure 6.13.: Post Collapse path of the 1 Web Model, 3 Web model and Full Model.

on. This might lead to the assumption that the influence of the boundaries is reduced for the post collapse region compared to the collapse behaviour.

The post collapse deformation is shown in Figure 6.14. The buckling pattern is fully developed and the distortion reaches from midship until the height of the neutral axis over the whole shell. The inwards deflection of the bottom shells is up to 0.7 meter. The inner bottom has started to buckle as well. The pattern in Figure F.9 shows distortion in the crash section from the neutral axis downwards until the inner bottom is reached. The deformation at the inner bottom is spreading to the boundaries where distortions occur.

A closer look inside the crash box is given in Figure F.10. The stiffeners have started to buckle as well, which is caused by the excessive plate buckling. Additionally to the stiffeners have the longitudinal bulkheads started to display large deformations. Finally the whole structure has began to unload and shows large plastic deformations.

6.3.5. Ultimate Capacity of Floating Model

The next step is to validate the Floating Model with verified 3 Web Model. In Figure 6.15 the ultimate capacity curves are compared. The Floating Model follows the 3 Web Model relatively close. The undamped model shows high fluctuations above the true path. This is

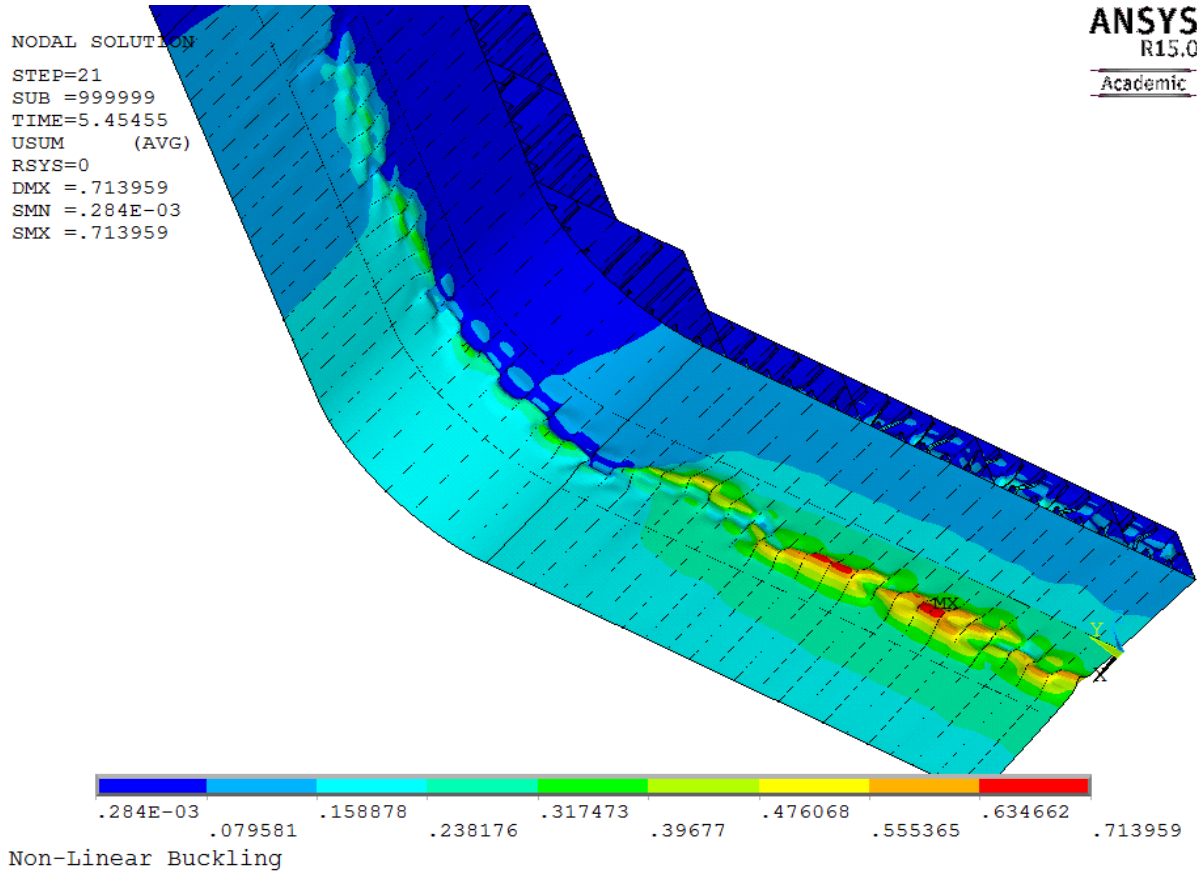

Figure 6.14.: Displacement vector sum of the 3 Web Model at the last time step, showing excessive distortion in the bottom region.

unacceptable, especially the ultimate capacity can not be estimated due to the high oscillations. The path varies between the buckling load and the yield level which is a difference of 9.1 %.

The variations can be diminished by the introduction of damping on the springs. In reality this corresponds with the heave damping of the ship. The applied 2 % damping of the critical damping smooths the path remarkably. The deviation is reduced to an oscillation of 2 %. The post collapse path is followed by all three graphs, thus no differences can be seen. The model with damping is suitable for calculations and the results are reasonable correct. Nonetheless care should be taken during the post processing due to the oscillations.

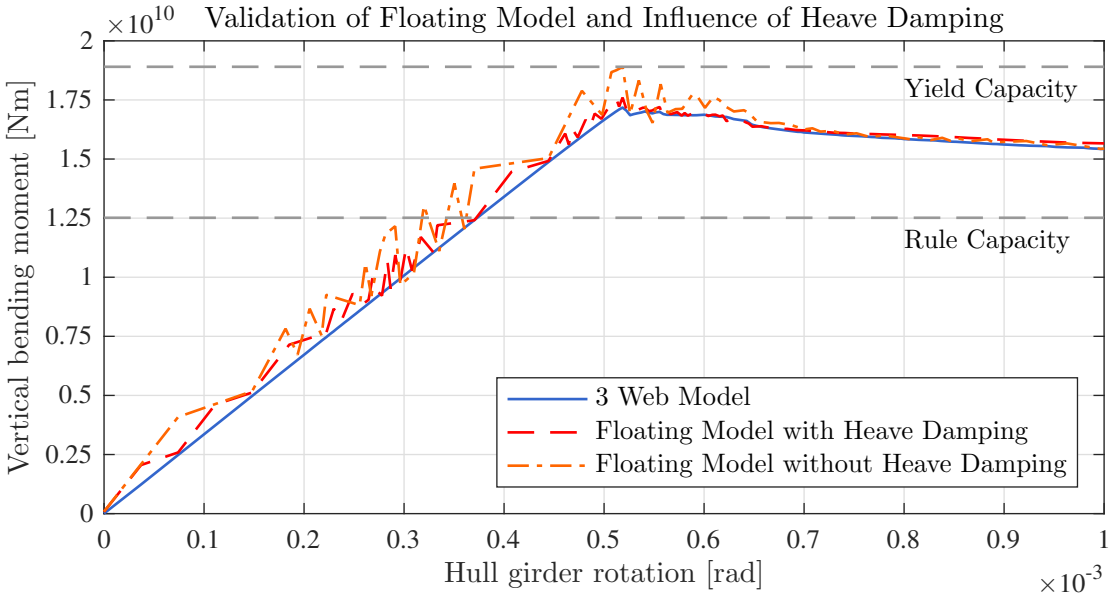

Figure 6.15.: Ultimate capacity of the static 3 Web Model and the Floating Model and the influence of 2 % critical heave damping of the structure.

6.3.6. Effect of Rigid Body Motion

The effect of rigid body motions is included and evaluated. In Figure shows 6.16 the post collapse path of the 3 Web Model, the 3 Web Rigid Model and the Floating Model.

The 3 Web Rigid Model shows large fluctuations in the pre- and post-buckling region. However the ultimate capacity and the post collapse are very stable. The capacity is of the same magnitude as of the the 3 Web Model. The post collapse path shows a higher capacity than the static model. This is the expected influence of the rigid body rotation.

The ultimate capacity for the floating model is not precise which is caused by the coarse time steps. The post collapse however is very similar. An area of higher instability can be seen around $1.6-1.8\cdot10^{-3}$ but the remaining part is very stable. It can be seen that from $1.2\cdot10^{-3}$ rad the floating model seems to have a higher remaining capacity, which can indicate that the rigid ends come in effect.

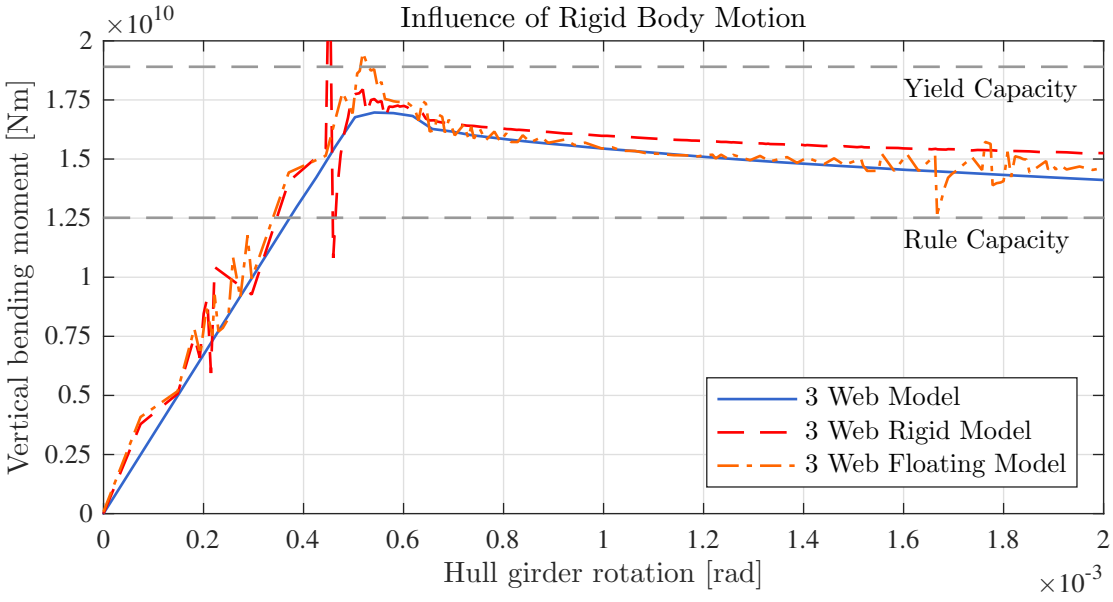

Figure 6.16.: Vertical bending moment-rotation curve evaluating the effect of rigid body motion for the 3 Web Model, the 3 Web Rigid Model and the Floating Model.

6.3.7. Application of Measured Strain Data

The validation of the ultimate capacity of the structure leads to the next step, the application of the measured strain data on the structure. The provided load set is already discussed in Section 2.3. For the investigation of the incremental collapse behaviour a single severe hogging wave is chosen. Figure 6.18 shows an extract of the half an hour time series shows in Figure 2.4. The considered wave is marked between second 356.3 - 359.75 of the original time series and between 356.5 - 361.25 for the Low-pass filtered time series. Reason for the different length is the zero crossing of the history. With a sampling frequency of 20 Hertz the time series results in 76 and 102 steps.

In the time series the still water bending is moment excluded. The vertical bending moment approach is shown in Figure 6.18. During the first three seconds the external and dynamic pressure is increased as well as the gravitational force until equilibrium is reached. From second 3 to 6 the still water bending moment is gradually increased. The loads are applied very slowly to avoid inertia forces and plasticity. Thereafter the transient vertical bending moment is applied according to the measured strain data. The magnitude is scaled until the desired bending moment is reached. When the wave load reaches the still water load again

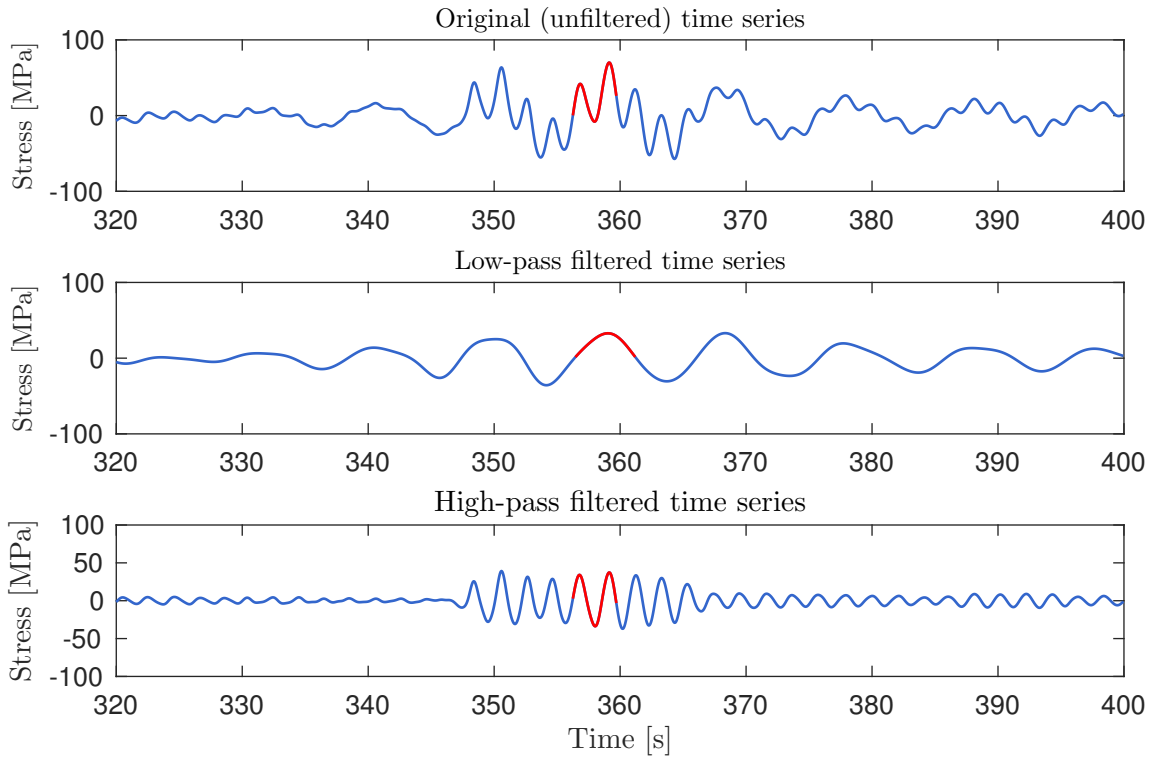

Figure 6.17.: Detailed plot of the filtered time series shown in Figure 2.4 with the positions used for the application on the structure. (Andersen and Jensen, 2014)

the load is smoothly reduced until zero.

6.3.8. Quasi-Static Wave Loads on the 3 Web Model

The quasi static wave load is applied on the 3 Web model and loaded until rule or ultimate capacity level. The moment-rotation curve is shown in Figure 6.19. The graph has a semi logarithmic scale for the x-axis. This enables to compare the results. The trend is similar with the plate test case in Figure 6.6. For the plate the loading follows the same path as the ultimate path for loading. When plasticity occurs the path to the base line is shifted in x-direction. For the plate the path is perfectly legible from the graph, however for the 3 Web Model not. The path follows parallel to the ultimate state, thus plasticity can be seen at the base line. Therefore the figure is given in a logarithmic scale.

The plasticity seen in the rotation is very small. The rotation occurs in the magnitude of 10^{-6} radiant. The plate loaded under axial thrust has a permanent deflection of 5 % of the

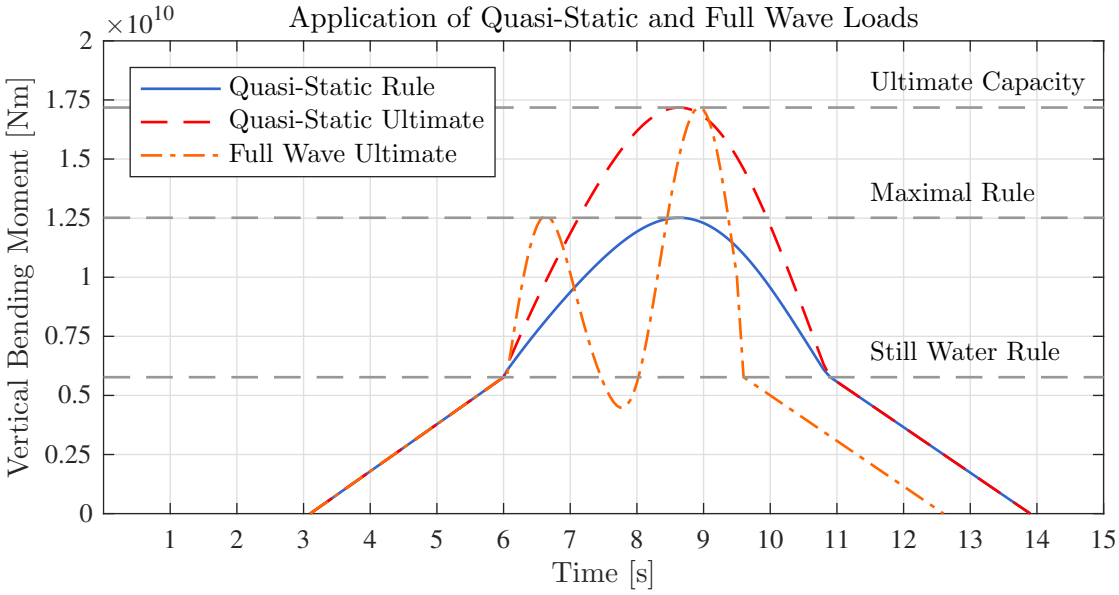

Figure 6.18.: Applied time series of the vertical bending moment on the structure. Quasi-static loads until the rule value and ultimate capacity of the structure. Additionally the full wave load data including dynamic effects until ultimate capacity.

ultimate deflection. The structure has a permanent deformation of 0.2 % in rotation. This makes the evaluation hard and this unusual way of illustration is chosen.

Considering the quasi-static path loaded until the rule value shows plasticity. This can have several factors. As shown in Figure 6.12 plasticity occurs at several positions caused by the boundaries. This will cause a permanent deflection as a by-product. Investigation shows small plasticity in the bottom area shown in Figure F.11. Thus the plasticity received is a superposition caused by the boundary and the collapse behaviour. The amount of plasticity is very limited and it would be interesting to see whether this plasticity grows with several cycles or not.

The model loaded until the ultimate capacity shows higher plasticity in the moment-rotation curve. The final stage of the model has a higher initial rotation than the initial stage. This is caused by higher plasticity in the bottom region shown in Figure F.12. The increase in permanent deformation is a combination of boundary interaction and bottom plasticity.

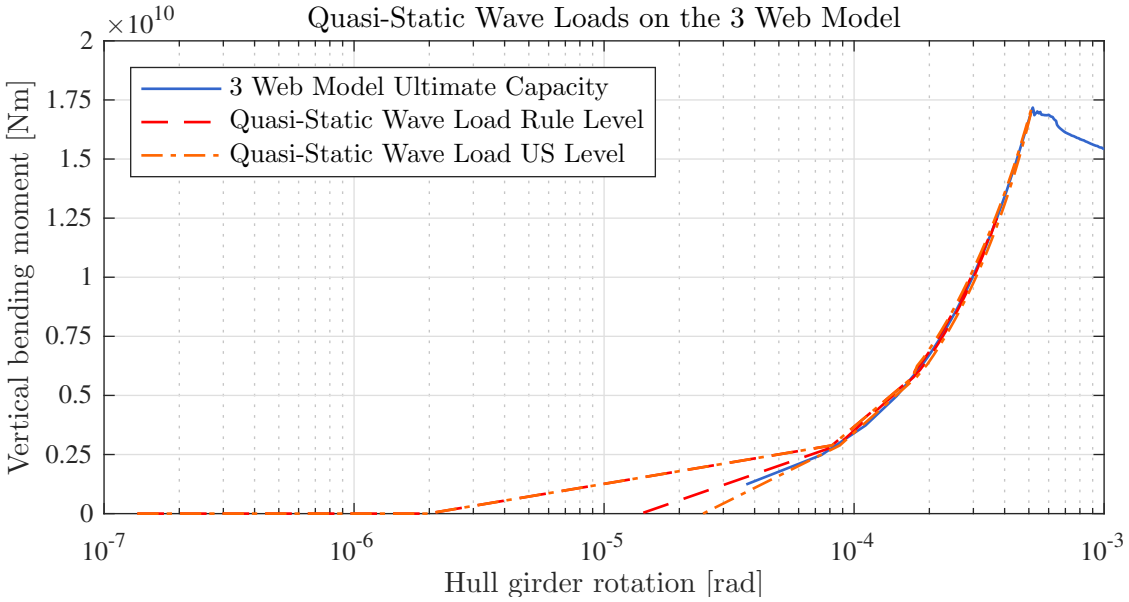

Figure 6.19.: Vertical bending moment-rotation curve for the 3 Web Model comparing the displacement controlled versus load controlled result.

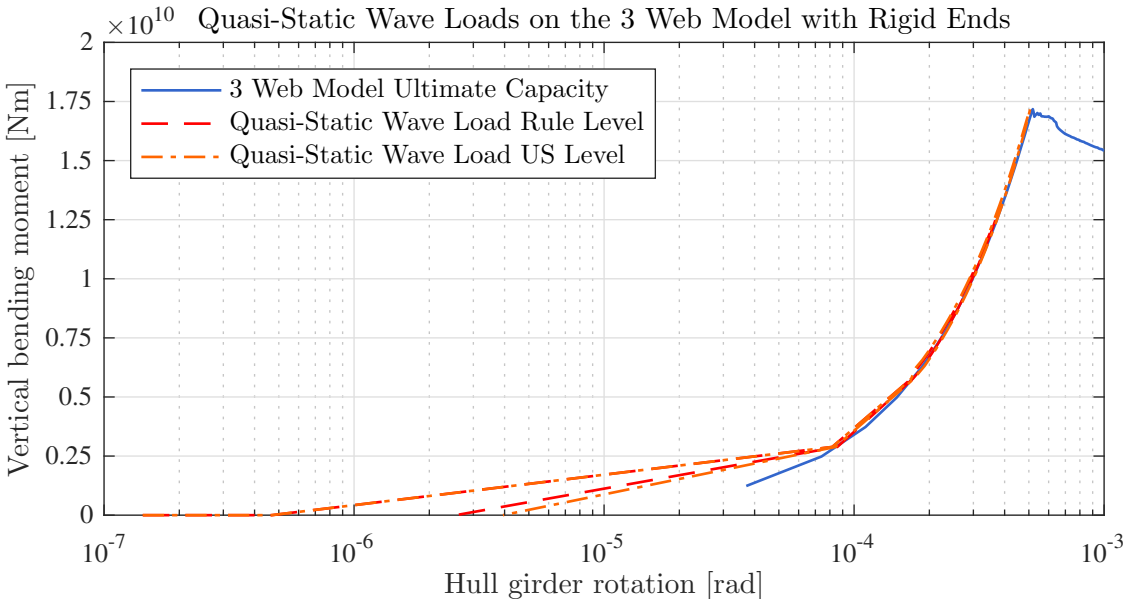

Figure 6.20.: Quasi-static wave loads applied on the 3 Web Rigid Model. The load level is scaled up to the rule level and the ultimate state.

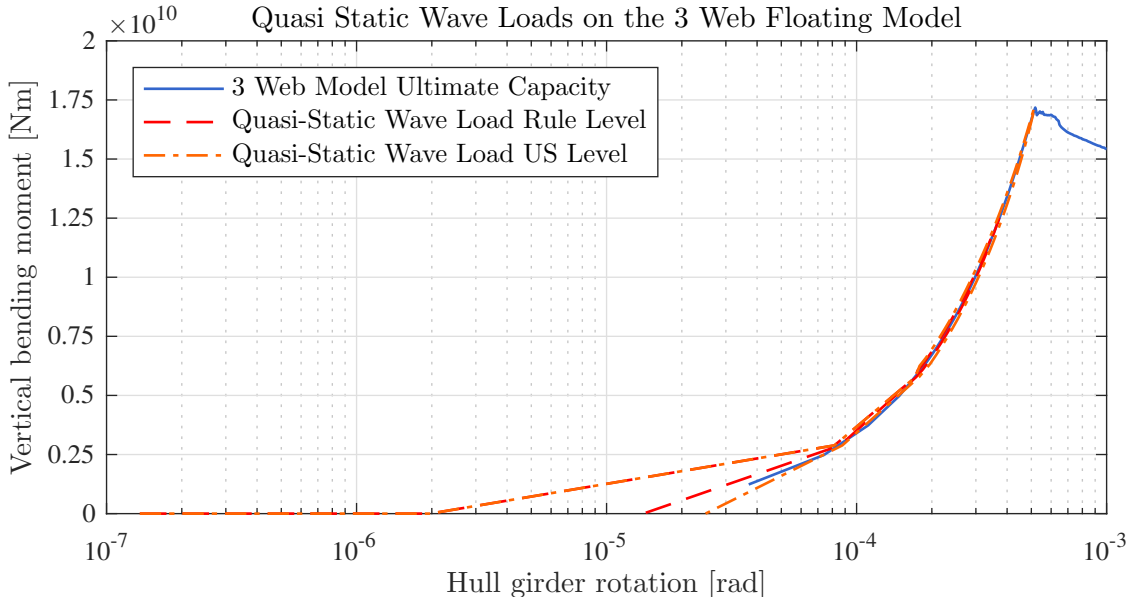

Figure 6.21.: Floating Model loaded with quasi-static wave loads scaled to rule and ultimate level compared with the static 3 Web Model case.

6.3.9. Quasi-Static Wave Loads on the 3 Web Rigid Model

The same load sets are applied on the 3 Web Rigid Model and the result is presented in Figure 6.20. The curve looks slightly different. The initial deflection starts at a lower value than for the 3 Web Model. The more important fact is, that the unloading path is closer to the initial value. Thus less plasticity is present in the current calculation. The difference between the rule and ultimate stage is approximately by the factor of ten smaller than for the previous model.

6.3.10. Quasi-Static Wave Loads on the Floating Model

The bending bending moment-rotation curve for the same load sets are shown in Figure 6.21. The results received for the Floating Model are nearly identical with the 3 Web Model. Comparing Figure 6.19 with Figure 6.21 gives a very good correspondence. Thus the quasi-static assumption of the loads is right, because no influence of inertias is given.

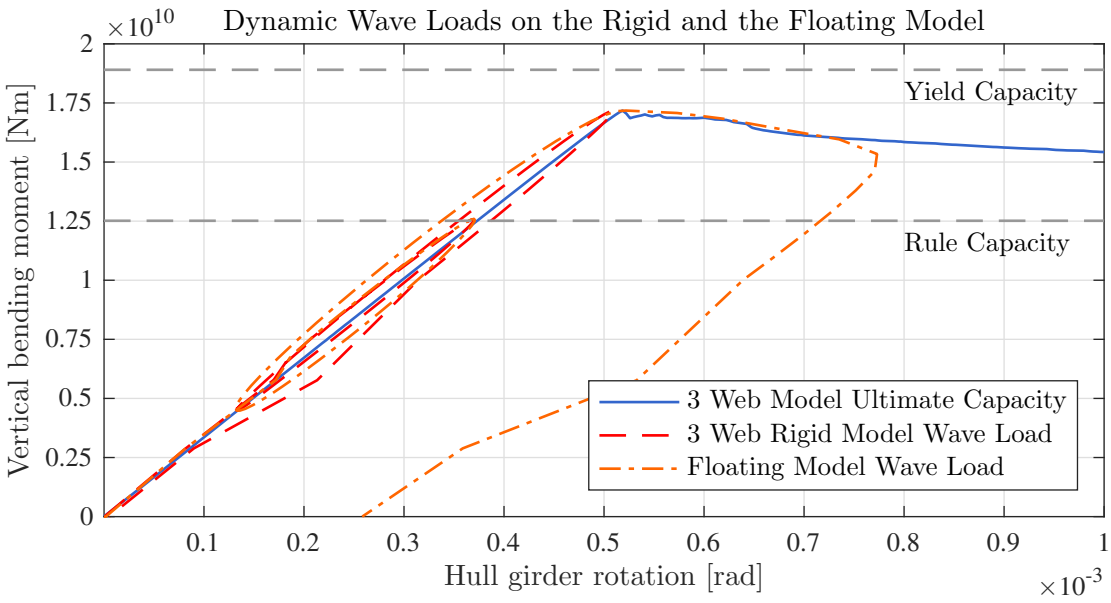

Figure 6.22.: Vertical bending moment-rotation curve for the full dynamic wave load set applied on the 3 Web Rigid Model and the Floating Model.

6.3.11. Dynamic Wave Loads on the 3 Web Models

In a last approach the full wave load set scaled until the ultimate capacity is applied on the 3 Web Rigid Model and the Floating Model. The moment-rotation curve is shown in Figure 6.22. The 3 Web Rigid Model goes up and down the pre-buckling path of the ultimate capacity curve and shows little plasticity afterwards.

The Floating Model follows the path in the beginning, but starts to collapse when the climax is reached. This behaviour is very unexpected, because of the low plasticity in the quasi-static case. The reason for this unexpected behaviour need to be discussed in depth later on.

6.3.12. Partial Safety Factors based on Rule Values

The introduced partial safety factors for whipping loads are calculated for the given ship. The bow flare angle for the TULCS ship is 45 degree (Andersen, 2014). The main dimensions of the ship are within the range for the calculations according to all rules. The results are presented in Table 6.2. The partial safety factor for waves γ_W is equal for all rules using this

Table 6.2.: Comparison of partial safety factors according to different classification societies.

Partial Safety Factor	DNV	DNVGL	BV	ClassNK	ABS	LR
Wave	1.2	1.2	0	1.2	(1.05)	-
Whipping	1.2771	1.1753	1.0	1.3	-	-
Whipping + Dynamic Collapse	1.2771	1.1578	1.0	1.3	-	-

concept. ClassNK has the most conservative value with a factor of 1.3 for whipping loads. That might be caused by the recent loss of the *MOL Comfort*. As discussed earlier the values of ABS and LR are not estimated in this thesis. An interesting fact is that the values developed by DNV are decreased for the new DNVGL rule set. Also does the introduction of the partial safety factor for the dynamic collapse γ_{dU} decrease the factor additionally. The lowest value is achieved by the rules of BV because the size of ship is too small for the consideration of whipping loads.

The calculated values are only representing the partial safety factors of the ultimate capacity. The rule design bending moments are not calculated for the ship according to the different rules. Classification societies with lower safety factors do not necessarily have less conservative rule values. For example BV uses an own prediction tool which includes whipping loads. As well have ABS and LR other ways of including these values.

7. Discussion

In this chapter is a brief discussion about the validity and applicability of the received results. The methods performed are critically examined and interpreted.

7.1. Evaluation of ANSYS on a simple Plate

A bunch of tests are performed on the simple plate with constrained edges. For the considered 20 millimetre thick plate the ultimate capacity is compared with several analytical approaches. Especially the most advanced methods, the method of effective width and the semi analytical program PULS show good correspondence with the ANSYS results.
The thickness of the plate is varied between zero and a plate thickness close to the yield limit. For plates between 15 - 35 mm the results are reasonable. For thinner plates the results of the method of effective width, PULS and ANSYS are very different. In this thesis, plate thicknesses of 15 mm and above are used, thus the deviations are ignored. For evaluating thinner plates, this phenomena should be investigated. Possible reasons might be the influence of the boundaries or a too coarse mesh size. Also other factors are not ruled out and should be investigated.
The mesh convergence study already shows good results for coarser meshes. A typical approach is to decrease the mesh size until the rate of change is below 5 %. In this case this is not reasonable since the deviation is already lower. Instead of using the global mesh size as the indicated value, the number of elements over the plate width is applied. The error has been analysed and an approved approach of a mesh size of 100 x 100 mm is chosen. The method has been used and acknowledged in several previously mentioned investigations.

The effect of different material models is examined. The material model has no influence on the ultimate capacity. Hardening affects the material behaviour in the post collapse region strongly while in the far post collapse region, the model is not of high importance. The direct collapse behaviour is drastically influenced by the material model used. DNV recommends the bilinear model which is compared with the Power law. Latter keeps the load longer in the ultimate region before the structure starts to unload. The model is recommended and tests have proven that it is the most realistic model (Storheim, 2016). The design stresses are taken to reveal conservative results.

7.2. Validation of midship model

Imperfections are included in the model to perform non-linear analysis. The deformations have been taken from the results of a linear buckling analysis. The first 2,500 eigenmodes are extracted of the Crash Section Model. The most suitable modes are selected and applied on the structure. ANSYS does not provide a function for applying a static load in the buckling analysis in addition to the buckling load like ABAQUS. An iterative process is necessary to include the external pressure loads. This effect is neglected in the linear buckling analysis. Also the application of several imperfection modes in a superposition is more troublesome than in ABAQUS. Specific deflection pattern can be applied on different parts of the model and stored separately. The different parts of the model can thereafter be reconsidered and merged. This enables the use of different imperfection eigenmodes on different parts of the structure.

A better controllable approach is the use of the introduced formula to induce a desired number of half waves over the length of the plate. This enables the use of different patterns, for example the hungry horse mode. The effect of both asymmetric and hungry horse mode should be investigated. The asymmetric mode is most likely to occur when overloading emerges, whereas the hungry horse mode is the likely existing imperfection. Troublesome with this method is the application of imperfections on the stiffeners. A second approach would be needed for the inclusion of stiffener imperfections. The introduction of residual stresses is neglected in this work. In the *MOL Comfort* case residual stresses are the trigger

of the plasticity starting point. This can play an important role in the first yield estimation of the structure. The static case of the full model shows an unsymmetrical deflection over the length of the ship. This is not included in the short model. The influence of it should be evaluated. Smaller singularities are present in the model. For this case the effect is minor and neglected. For a more realistic consideration the presented parts of the structure should be considered.

Estimating the ultimate strength of the midship section is problematic. Convergence difficulties are discussed and solution methods are proposed. Damping is a very important factor for the numerical stability and should be included in all calculations. The difficulties with the application of the bending moment through a rigid body link has been discussed and are solved for the use of ANSYS Distributed. Even though the use of a real MPC element would increase the accuracy of the calculation and decrease the computational expense.

A full four cargo hold model is designed with open and watertight web frames and open and closed bulkheads. Due to the time consuming calculations it has not been possible to solve this model. An optimisation for the working process would be to initially calculate a smaller model and slowly increase the model size. An idea might be to start with a simple plate, run a smaller panel, run a one web length model, run a three web length model and finally run a four cargo hold model. Also a more realistic time schedule should be set for the required calculation time. Problematic is the use of a HPC. The queuing time can be up to four days. For calculations running on one node, it might be more beneficial to run jobs on a strong personal computer with e.g. a 16 core processor. When a stable model is realized the use of a HPC might be considered.

Another opportunity of reducing the required calculation time is considering the explicit method instead of the implicit method. This would require very small time steps depending on the speed of sound through the material and the size of the smallest element. The explicit method is generally faster and used for crash simulations. If the higher amount of time steps still decreases the calculation might be estimated by test runs of a simple plate with a time history load set. A potential explicit solver might be the LS-DYNA code.

The ultimate strength of the system is analysed using a displacement controlled analysis. An alternative use of the arc-length method is impossible because of the used ANSYS Distrib-

uted. Thus a good guess of the ultimate capacity rotation is necessary to get results close to the ultimate strength. As a first try the value 10^{-3} radiant should be considered. The value is verified by the *MSC Napoli* BV estimations and in this thesis.

The model size is reduced to a 1 Web model according to the work of Xu et al. (2014). The reduced model reveals an ultimate capacity higher than the yield level. This is caused by the close clamped boundaries. A 3 Web model is used as a second option. The ultimate capacity shows good agreement with the applied incremental method by POSEIDON. A comparison with the full model would have been an opportunity to evaluate if a 3 Web model is large enough to consider the ultimate capacity correctly. This would be contrary to the recommendations given out by the classification societies suggesting a three cargo hold model.

The 3 Web model shows heavy distortion in the middle of the bottom area, whereas the inner bottom deforms largely at the boundaries. In most ultimate capacity models the number of non-linear compartments is limited to three and linear material is assumed in the rest of the ship. It is questionable if this distortion in the inner bottom occurs for the designed Full Model as well, but the use of more non-linear areas might be considered. The use of a non-linear material between stiffer parts of the structure, e.g. between two bulkheads might be a better method.

The Floating Model is validated against the regular 3 Web Model. The model fluctuates around the assumed path. This makes it impossible to read correct values of the graph. Spring damping is included for the spring elements. This corresponds with heave damping used in strip theory. The system is reasonable damped and the ultimate capacity can be estimated. The oscillation takes place above the ultimate capacity curve, thus an undamped system would be non-conservative.

The rigid ends seem to have no influence on the collapse process. An increase of the capacity can be seen further in the post collapse path. Thus the effect of rigid body motion can be neglected for the estimation of the ultimate capacity.

It should be noted that the combination of large variations in element sizes, element stiffness and material properties causes calculation instability. All calculations of the 3 Web Rigid Model or the Floating Model show oscillations of a certain level. Also combining values of different magnitudes inside the stiffness and mass matrix causes a larger solution time.

Further research might be necessary to stabilize the calculations.

7.3. Application of time history data

The provided measured strain data set is used. The most severe wave of the set is examined. A method to apply the loads on the structure is developed by loading the external loads gradually first. In a second step the bending moment is increased until the still water bending moment is reached. Thereafter the quasi static or full wave set respectively is loaded onto the structure. When the load reaches the still water bending moment again the load is reduced gradually in order to neglect inertia effects.

An initial angle of rotation occurs due to the external pressure on the structure. The loading of the structure follows the expected path. The ends of the path are compared in the result chapter. This reveals the plasticity and the permanent change in the initial angle. For the loading up to the rule level plasticity is already present. This has two reasons. Yielding occurs at the boundaries, due to the wrong clamped conditions and yielding occurs due to a slight overloading of the structure. The model loaded until the ultimate capacity level reveals more plasticity in the bottom area.

The effect of plasticity on the boundaries should be evaluated in depth. An interesting aspect is to see whether or not the plasticity of the boundaries vanish after several cycles. Furthermore a larger model might reduce this effect. The validation of a larger model would be of high interest.

The bending moment rotation curves show a good agreement for the 3 Web Model and the Floating Model in terms of initial and final condition for either the rule level as well as the ultimate level load case. Inertia does not change the results of the two cases. Thus a quasi-static assumption is correct. The 3 Web Rigid Model reveals lower rotations than both other models. This can be caused by an influence of the springs on the initial bending moment from the external pressure.

Running several cycles will increase the required calculation time. The time is highly depending on the number of substeps and iterations. Both numbers increase for non-linear deflections. With a computational time of 3 hours, the cases mentioned are very fast. An ul-

timate state calculation takes around 80 hours. The difference between both values is large and makes it hard to predict a reasonable wall clock time for these calculations. Hence, several cycles causing the collapse of the hull girder will increase the required computational time.

The models loaded with the full wave load deliver interesting results. The result for the 3 Web Rigid Model is similar to the static case. However the Floating Model collapses for the dynamic load case. This behaviour is unexpected and indicates a wrong model description. The collapse is caused by the accelerated masses at the rigid ends. Thus the method of applying bending moments on the developed model is not correct. The problem arises from the mixture of applying bending moments at midship and using a strip theory approach. Where as the quasi-static case shows normal results, in the dynamic case the masses do not follow the desired behaviour.

In a nutshell the loads should either be applied on the 3 Web Rigid Model even thought the inertia of the ship is not correct. It should be evaluated if a pure shell model is suitable to represent a bigger structure in case of withstanding dynamic loads. Also should the model size be carefully evaluated because size and masses of and on the model might play an important role. Another option is to use a pure strip theory approach in which the loads are generated by the accelerates masses caused by incoming waves. This would avoid the problem of the wrongly accelerated masses at the ends. Using a strip theory approach accounting for hydro-elasticity will include whipping loads as well.

8. Conclusion

The thesis gives an entrance into the subject of dynamic collapse. The finite element method used in ANSYS is proven to be valid in the applied range. Compliance between the analytical results, the semi analytical approach used in PULS and the numerical finite element method are shown. The ultimate capacity of the designed midship section is estimated and verified by the incremental method used in POSEIDON. A first set of time history data is applied and the results are compared.

The global design of the midship section using POSEIDON is valid. Local plasticity occurs when loading the structure. This can be neglected and has no influence on the ultimate capacity and is considered as valid.

Grand calculation times have led to large difficulties in meeting the estimated time frame. A better estimation of the required time should be done for future projects. The use of the explicit method instead of the implicit method might be considered. For future checks a comparable computer program study on a simple panel should be performed with a time series, calculating high and low deformation problems. It should be considered to avoid the use of ANSYS Distributed to get around the limitations for the arc length method and MPC elements. The use of a strong personal computer should be considered.

Applying a strip theory approach in the finite element method shows good agreement for the Floating Model in static conditions. This holds true for the static ultimate capacity curve as well as for the quasi-static wave load. The model fails when loaded with the full wave load set. This is caused by the acceleration of the masses at the end, which are predicting wrong bending moments. The combination of strip theory as load generator and a non-linear midship section should be considered.

The findings might be summed up as follows:

- The capacity of a single plate and panel loaded under axial thrust does not decrease severely when transverse pressure is applied
- Material hardening has only influence on post collapse path
- The used 1 Web model is too short for the estimation of the ultimate capacity and a larger model should be used
- The incremental method gives good correspondence with the finite element approach
- No influence of the rigid body parts is measured for the ultimate capacity
- Stabilization of the system in the form of damping is necessary to solve it
- A single wave with bending moment corresponding to the ultimate strength causes only a small angle of plasticity
- The result of the quasi static wave reveals no difference for the 3 Web and the Floating Model, thus the assumption of a quasi-static load is valid
- The combination of ship masses and applied bending moments is not valid and causes wrong inertia accelerations

9. Recommendation for further work

This thesis discuss the basic assumptions for the work performed and give first results on the influence of a static wave. Since the topic could not be brought to an end the work should be continued. This work proves, that the chosen method for the static case reveals valid results and is worth to investigate in.

The influence of imperfection on the initial structure is not discussed in this thesis. Especially the differences between the hungry horse mode and the asymmetrical buckling mode are of interest. Also the effect of residual stresses, which is considered to be of high importance for the loss of the *MOL Comfort* is not evaluated. Both are important factors influencing the capacity of the structure and should be considered in future work.

Additional uncertainties are present for the length of the non-linear part of the model. The inner bottom shows high deformations along the ends of the non-linear model. Thus an extension of the non-linear part until the bulkheads of a container ship might be considered.

Prior to future research it might be beneficial to estimate the time difference between the use of the implicit or explicit method, regarding the required calculation time. This might reduce the computation time and the calculations become easier to handle.

The used method has failed to predict the influence of dynamic loads on the hull girder. It should be evaluated if the application of bending moments on a pure shell model produces trustworthy results. An other option is to investigate the possibility of combining strip theory with the finite element model. The loads would than be generated by the accelerated masses of the strips and not by a measured strain history. This approach assures the right inertia of the global system.

Bibliography

Abaqus User Manual IV (2012). *Abaqus 12.6 Analysis User's Manual Volume IV: Elements*. Dassault Systèmes Simulia Corp.

ABS Guidance Notes (2014). *Guidance Notes on Whipping Assessment for Container Carriers*. ABS American Bureau o Shipping.

Amdahl, J. (2013). *TMR4205 Buckling and Ultimate Strength of Marine Structures, Chapter 3: Buckling of Stiffened Plates*.

Amlashi, H. K. K. (2008). *Ultimate Strength and Reliability-based Design of Ship Hulls with Emphasis on Combined Global and Local Loads*. PhD thesis, NTNU Norwegian University of Science and Technology Institute for Marine Technology.

Amlashi, H. K. K. and Moan, T. (2008). Ultimate strength analysis of a bulk carrier hull girder under alternate hold loading condition – A case study Part 1: Nonlinear finite element modelling and ultimate hull girder capacity. In *Marine Structures*, volume 21, pages 327–352. Elsevier Ltd.

Andersen, I. M. V. (2014). *Full Scale Measurements of the Hydro-Elastic Response of Large Container Ships for Decision Support*. PhD thesis, Kgs. Lyngby: Technical University of Denmark (DTU). (DCAMM Special Report; No. S166).

Andersen, I. M. V. and Jensen, J. J. (2012). On the Effect of Hull Girder Flexibility on the Vertical Wave Bending Moment for Ultra Large Container Vessels. In *Proceedings of the ASME 2012 31st International Conference on Ocean, Offshore and Arctic Engineering*, volume 31, pages 1–8, Rio de Janeiro, Brazil. ASME.

Andersen, I. M. V. and Jensen, J. J. (2014). Measurements in a container ship of wave-induced hull girder stresses in excess of design values. In *Marine Structures*, volume 37, pages 54–85. Elsevier Ltd.

ANSYS Element Reference (2009). *ANSYS Element Reference*. ANSYS Inc.

ANSYS LS-DYNA (2009). *ANSYS LS-DYNA User's Guide*. ANSYS Inc.

ANSYS Structural Analysis Guide (2009). *ANSYS Structural Analysis Guide*. ANSYS Inc.

Barhoumi, M. and Storhaug, G. (2014). Assessment of whipping and springing on a large container vessel. In *International Journal of Naval Architecture and Ocean Engineering*, 6, pages 442–458.

Brubak, L. (2016). Advanced Buckling & Panel Ultimate Limit State (PULS). Technical Seminar. DNVGL AS.

BV-NR-583 (2015). *Rule Note NR 583 DT R01 E Whipping and Springing Assessment*. Bureau Veritas.

ClassNK Rules (2015). *Rules for the Survey and Construction of Steel Ships, Guidance for the Survey and Construction of Steel Ships, Part C Hull Construction and Equipment, Amendment No.3*. ClassNK Nippon Kaiji Kyokai.

Cook, R. D. (1995). *Finite element modeling for stress analysis*, volume 1. John Wiley and Sons Inc.

Distributed ANSYS Guide (2009). *Distributed ANSYS Guide*. ANSYS Inc.

DNV-CN-No.30.12 (2013). *Class Notes No. 30.12 Fatigue Strength and Ultimate Capacity Check of Container Vessels Including the Effect of Springing and Whipping*. DNV Det Norske Vertitas AS.

DNV-OS-C401 (2013). *Offshore Standard DNV-OS-C401 Fabrication and Testing of Offshore Structures*. Det Norske Veritas.

DNV PULS (2006). *Nauticus Hull User Manual PULS*. DNV Det Norske Vertitas AS.

DNV-RC (2011). *Rule for Classification of Ships/ High Speed, Light Craft and Naval Surface Craft Part 6 Chapter 11 Hull Monitoring Systems.* DNV Det Norske Vertitas AS.

DNV-RP-C208 (2013). *Recommended Practice DNV-RP-C208 Determination of Structural Capacity by Non-linear FE analysis Methods.* DNV Det Norske Vertitas AS.

DNVGL-CG-0128 (2015). *Class Guideline DNVGL-CG-0128 Buckling.* DNVGL AS.

DNVGL-CG-0153 (2015). *Class Guideline DNVGL-CG-0153 Fatigue and ultimate strength assessment of container ships including whipping and springing.* DNVGL AS.

DNVGL Rules (2016). *Rules for Classification, Ships, Part 3 Hull, Chapter 4 Loads.* DNVGL AS.

DNVGL Rules Part 3 Chapter 7 (2016). *Rules for Classification, Ships, Part 3 Hull, Chapter 7 Finite element analysis.* DNVGL AS.

DNVGL Rules Part 3 Chapter 8 (2016). *Rules for Classification, Ships, Part 3 Hull, Chapter 8 Buckling.* DNVGL AS.

DNVGL Rules Part 6 Chapter 1 (2016). *Rules for Classification, Ships, Part 6 Additional class notations, Chapter 1 Sructural strength and integrity.* DNVGL AS.

Drummen, I. (2008). *Experimental and Numerical Investigation of Nonlinear Wave-Induced Load Effects in Containerships considering Hydroelasticity.* PhD thesis, NTNU Norwegian University of Science and Technology Institute for Marine Technology.

Faltinsen, O. M. (1990). *Sea loads on ships and offshore strucures.* Cambridge University Press. ISBN 0-521-45870-6.

Fricke, W. and Bronsart, R., editors (2012). *Commitee III.1 Ultimate Strength.* 18th International Ship and Offshore Structures Congress (ISSC 2012), Rostock, Germany, ISBN 978-3-87700-131-5,8.

Fujikubo, M. and Kaeding, P. (2002). New simplified approach to collapse analysis of stiffened plates. In *Marine Structures*, volume 15, pages 251–283.

GL Guidelines (2011). *Rules for Classification and Construction, V Analysis Techniques, 1 Hull Structural Design Analyses, 1 Guidelines for Global Strength Analysis of Container Ships*. Germanischer Lloyd SE.

GL Rules (2015). *Rules for Classification and Construction, I Ship Technology, 1 Seagoing Ships, 5 Structural Rules for Container Ships*. Germanischer Lloyd SE.

Heggelund, S. E., Storhaug, G., and Choi, B.-K. (2011). Full scale measurement of fatigue and extreme loading including whipping on an 8600 teu post panmax container vessel in the asia to europe trade. In *Proceedings of the ASME 2011 30th International Conference on Ocean, Offshore and Arctic Engineering*, volume 30, pages 1–10, Rotterdam, The Netherlands.

IACS UR-S (2016). *UR-S Requirements concerning Strength of Ships*. International Association of Classification Societies LTD.

IACS UR-W (2016). *UR-W Requirements concerning Material and Welding*. International Association of Classification Societies LTD.

Iijima, K. and Fujikubo, M. (2012). Post-ultimate strength behaviour of very large floating structures subjected to extreme wave loads. In *Proceedings of the ASME 2012 31st International Conference on Ocean, Offshore and Arctic Engineering*, 31, Rio de Janeiro, Brazil.

Iijima, K., Kimura, K., Xu, W., and Fujikubo, M. (2011). Hydroelasto-plasticity approach to predicting the post-ultimate strength behavior of a ship's hull girder in waves. *Journal of Marine Science and Technology*, 16(4):379–389.

Jensen, J. J. (2001). *Load and global response of ships*, volume 4 of *Ocean Engineering Book Series*. Elsevier, 1 edition.

Jensen, J. J. and Pedersen, P. T. (1978). Wave-induced Bending Moments in Ships - A Quadratic Theory. *Trans RINA*, 121:151–65.

Johansen, T. and Bratbak, F. (2015). Structural strength and modelling strategy. In *TMR 4305 Advanced Analysis of Marine Structures. NTNU Norwegian University of Science and Technology Institute for Marine Technology*.

Jones, N. (2012). *Structural Impact, 2nd Edition*. Cambridge University Press, New York, USA. ISBN 9781107010963.

Kahl, A., Fricke, W., Paetzold, H., and von Selle, H. (2014). Whipping Investigations Based on Large-Scale Measurements and Experimental Fatigue Testing. In *International Journal of Offshore and Polar Engineering*, volume 25, pages 247–254. The International Society of Offshore and Polar Engineering.

Khosravi, P. and Sedaghati, R. (2008). Local Buckling and Mode Switching in the Optimum Design of Stiffened Panels. *AIAA*, 46(6).

Langen, I. and Sigbjörnsson, R. (1979). *Dynamisk analyse av konstruksjoner. [Dynamic analysis of structures]*. Tapir.

Larsen, C. M. (2014). *TMR4182 Marine Dynamics. NTNU Norwegian University of Science and Technology Institute for Marine Technology*. Kompendieforlaget.

Leira, B. J. (2014). *TMR4170 Marine Structures Basic Course. NTNU Norwegian University of Science and Technology Institute for Marine Technology*. Kompendieforlaget.

LR Rules (2016). *Rules and Regulatons for the Classification of Ships*. LR Lloyd's Register.

Mao, W., Ringsberg, J. W., and Rychlik, I. (2010). The effect of whipping/springing on fatigue damage and extreme response of ship structure. In *Proceedings of the ASME 2010 29th International Conference on Ocean, Offshore and Arctic Engineering*, volume 29, pages 1–9, Shanghai, China.

Marine Accident Investigation Branch (2008). *Report on the investigation of the structural failure of MSC Napoli English Channel on 18 January 2007*. Marine Accident Investigation Branch.

Marine Accident Investigation Branch Annex A-D (2008). *Report on the investigation of the structural failure of MSC Napoli English Channel on 18 January 2007 Annex A-D*. Marine Accident Investigation Branch.

Marine Accident Investigation Branch Annex E-G (2008). *Report on the investigation of the structural failure of MSC Napoli English Channel on 18 January 2007 Annex E-G*. Marine Accident Investigation Branch.

Moa, W. (2010). *Fatigue Assessment and Exreme Response Prediction of Ship Structures*. PhD thesis, Chalmers University of Gothenburg.

Moan, T. (2003a). *Kompendium TMR4190 Finite Element Modelling and Analysis of Marine Structure*. Kompendieforlaget.

Moan, T. (2003b). *Kompendium TMR4190 Finite Element Modelling and Analysis of Marine Structure, Chapter 12 - Nonlinear Analysis*. Kompendieforlaget.

Moe, E., Holtsmark, G., and Storhaug, G. (2005). Full scale measurements of the wave induced hull girder virbrations of an ore carrier trading the north atlantic. In *Trans RINA, International Conference, Design and Operation of Bulk carriers*, pages 57–85, London, UK.

PADT (2012a). *Overcoming Convergence Difficulties in ANSYS Workbench Mechanical, Part I: Using Newton-Raphson Residual Information*. PADT Inc.

PADT (2012b). *Overcoming Convergence Difficulties in ANSYS Workbench Mechanical, Part II: Quick Usage of Mechanical APDL to Plot Distorted Elements*. PADT Inc.

POSEIDON User Manual (2016). *POSEIDON 16.0 User Manual - GL Rules Edition 2016*. DNVGL - Maritime.

Salvesen, N., Tuck, E. O., and Faltinsen, O. (1970). Ship Motions and Sea Loads. *Trans SNAME*, 78(6):250–87.

Schwebe, T. T. (2015). Dynamic Collapse of the hull girder in a container ship in waves. Project Thesis. NTNU Norwegian University of Science and Technology Institute for Marine Technology.

Seng, S., Andersen, I. M. V., and Jensen, J. J. (2012a). On the influence of hull girder flexibility on the wave. In *Proceedings of the 6th International Conference on Hydroelasticity in Marine Technology*, volume 6, pages 341–353, Tokyo, JAPAN. University of Tokyo Press.

Seng, S. and Jensen, J. J. (2012). Slamming Simulations in a conditional wave. In *Proceedings of the ASME 2012 31st International Conference on Ocean, Offshore and Arctic Engineering*, volume 31, Rio de Janeiro, Brazil. OMAE2012-83310.

Seng, S. and Jensen, J. J. (2013). An Application of a Free Surface CFD Method in the Short-Term Extreme Response Analysis of Ships. In *Proceedings of the PRADS2013*, volume 12, pages 747 – 754, Changwon City, Korea. CECO.

Seng, S., Jensen, J. J., and Pedersen, P. T. (2012b). Numerical prediction of slamming loads. In *Journal of Engineering for the Maritime Environment*, volume 226, pages 120–134. Institution of Mechanical Engineers.

Shu, Z. (2010). *Uncertainty Assessment of Wave Loads and Ultimate Strength of Tankers and Bulk Carriers in a Reliability Framework*. PhD thesis, NTNU Norwegian University of Science and Technology Institute for Marine Technology.

Shu, Z. and Moan, T. (2012). Ultimate hull girder strength of a bulk carrier under combined global and local loads in the hogging and alternate hold loading condition using nonlinear finite element analysis. *J. Mar. Sci. Technol.*, 17:94–113.

Storhaug, G. (2014). The measured contribution of whipping and springing on the fatigue and extreme loading of container vessels. In *International Journal of Naval Architecture and Ocean Engineering*, volume 6, pages 1096–1110.

Storhaug, G., Derbanne, Q., Choi, B.-K., Moan, T., and Hermundstad, O. A. (2011). Effect of whipping on fatigue and extreme loading of a 13000 teu container vessel in bow quatering sea based on model tests. In *Proceedings of the ASME 2011 30th International Conference on Ocean, Offshore and Arctic Engineering*, volume 30.

Storhaug, G., Malenica, S., Choi, B.-K., Zhu, S., and Hermundstad, O. A. (2010). Consequence of whipping and springing on fatigue and extreme loading for a 13000teu container vessel based on model tests. In *PRADS 11th triennial, Practical Design of Ships and Other Floating Structures*, pages 1200–1209, Rio de Janeiro, Brazil.

Storheim, M. (2016). *Structural Response in Ship-Platform and Ship-Ice Collisions*. PhD thesis, Norwegian University of Science and Technology.

Sumi, Y., Fujikubo, M., Kawagoe, Y., Kidogawa, M., Kobayashi, K., Nakajima, Y., Nakano, T., Sunouchi, M., Tamura, K., and Ueda, N. (2013). Interim report of committee on large container ship safety. Technical report, Committee on Large Container Ship Safety.

Sumi, Y., Fujikubo, M., Kawagoe, Y., Kidogawa, M., Kobayashi, K., Nakajima, Y., Nakano, T., Sunouchi, M., Tamura, K., and Ueda, N. (2014). Investigation report on structural safety of large container ships. Technical report, Committee on Large Container Ship Safety.

VanDerHorn, E. and Wang, G. (2011). A statistical study on the material properties of ship-building steel. *Sustainable Maritime Transportation and Exploitation of Sea Resources*, pages 371–378.

Xia, J., Wang, Z., and Jensen, J. J. (1998). Non-linear wave loads and ship responses by a time-domain strip theory. *Marine Structures*, 11(3):101–123.

Xu, W., Duan, W., and Han, D. (2014). Investigation into the dynamic collapse behaviour of a bulk carrier under extreme wave loads. In *Ocean Engineering*, volume 106, pages 115–127.

Xu, W., Iijima, K., and Fujikubo, M. (2011a). Hydro-elastoplasticity approach to ship's hull girder collapse behavior in waves. In *Guedes Soares & Fricke (eds.), Advances in Marine Structures*, pages 239–247, Hamburg, Germany. Taylor & Francis Group, London.

Xu, W., Iijima, K., and Fujikubo, M. (2011b). Investigation into post-ultimate strength behaviour of ship's hull girder in waves by analytical solution. In *Proceedings of the ASME 2011 30th International Conference on Ocean, Offshore and Arctic Engineering*, volume 30 of *30*, pages 455–462, Rotterdam, The Netherlands.

Xu, W., Iijima, K., and Fujikubo, M. (2012). Parametric dependencies of the post-ultimate strength behavior of a ship's hull girder in waves. *Journal of Marine Science and Technology (Japan)*, 17(2):203–215.

A. Theoretical Background

A.1. Elastic Buckling of Initially Perfect Plates

The following parts follows Amdahl (2013) and has been used in a similar way in Schwebe (2015). To derive the elastic buckling load of initially perfect plates one might start with the equilibrium equation for a simple plate under axial compression:

$$\nabla^4 w = \frac{1}{D_{plate}}\left(q + N_x\frac{\partial^2 w}{\partial x^2} + 2N_{xy}\frac{\partial^2 w}{\partial x \partial y} + N_y\frac{\partial^2 w}{\partial y^2}\right). \tag{A.1}$$

In there w is the interpolation polynomial. D_{plate} is the plate stiffness given by:

$$D_{plate} = \frac{Et^3}{12\left(1-\nu^2\right)}. \tag{A.2}$$

Following some manipulations of the nabla operator ∇ the results is:

$$\nabla^4 = \left(\nabla^2\right)^2 = \Delta^2 = \left(\frac{\partial^2}{\partial x^2} + \frac{\partial^2}{\partial y^2}\right)^2. \tag{A.3}$$

Where the membrane stress resultants are given by:

$$N_x = \sigma_x t \tag{A.4}$$

$$N_y = \sigma_y t \tag{A.5}$$

$$N_{xy} = \sigma_{xy} t \tag{A.6}$$

Considering a simple supported plate the in in-plane loading equation (A.1) can be reduced to:

$$\nabla^4 w = \frac{N_x}{D_{plate}} \frac{\partial^2 w}{\partial x^2} \tag{A.7}$$

A suggested solution which satisfies the equation is given by Amdahl (2013, Egn.: 3.6):

$$w = C_{mn} \sin\left(\frac{m\pi x}{a}\right) \sin\left(\frac{n\pi y}{b}\right). \tag{A.8}$$

In there are m and n integer of half waves in the x and y direction. Finally the solution can be written as given by (Amdahl, 2013, Eqn. (3.7)):

$$\sigma_E = \frac{\pi^2 E}{12\left(1-\nu^2\right)} \left(\frac{t}{b}\right)^2 \cdot k \tag{A.9}$$

A.2. Establish the Dynamic Equation of Motion

The dynamic equation of motion can be derived from the common FEM stiffness relation:

$$\underline{\underline{K}}\, \underline{r} = \underline{R} \tag{A.10}$$

With Newton's second law of motion:

$$F = ma \tag{A.11}$$

and using d'Alembert's principle one may get:

$$\underline{F}(t) = \underline{\underline{M}}\, \underline{\ddot{r}}(t). \tag{A.12}$$

Combining it with the static case and applying Newton's laws:

$$-\underline{\underline{M}}\,\underline{\ddot{r}}\,(t) = \underline{\underline{K}}\,\underline{r}\,(t) \tag{A.13}$$

$$0 = \underline{\underline{M}}\,\underline{\ddot{r}}\,(t) + \underline{\underline{K}}\,\underline{r}\,(t) \tag{A.14}$$

Finally introducing damping $\underline{\underline{C}}\,\underline{\dot{r}}\,(t)$ and an excitation force $\underline{R}\,(t)$ the equation becomes:

$$\underline{R}\,(t) = \underline{\underline{M}}\,\underline{\ddot{r}}\,(t) + \underline{\underline{C}}\,\underline{\dot{r}}\,(t) + \underline{\underline{K}}\,\underline{r}\,(t)\,. \tag{A.15}$$

A.3. Eigenvalue problem

Aim is to transfer the general eigenvalue problem in the special eigenvalue problem to solve it. The general eigenvalue problem is given by:

$$\left(\underline{\underline{K}} - \omega^2 \underline{\underline{M}}\right)\underline{\phi} = 0 \tag{A.16}$$

By using Cholesky decomposition for the mass matrix with:

$$\underline{\underline{M}} = \underline{\underline{L}}\,\underline{\underline{L}}^{\mathsf{T}} \tag{A.17}$$

Introducing it in the original equation gives:

$$\left(\underline{\underline{K}} - \omega^2 \underline{\underline{L}}\,\underline{\underline{L}}^{\mathsf{T}}\right)\underline{\phi} = 0 \tag{A.18}$$

By introducing a new eigenvector:

$$\underline{x} = \underline{\underline{L}}^{\mathsf{T}}\underline{\phi} \qquad \Rightarrow \qquad \underline{\phi} = \left(\underline{\underline{L}}^{\mathsf{T}}\right)^{-1}\underline{x} \tag{A.19}$$

The equation gets:

$$\left(\underline{\underline{K}}\left(\underline{\underline{L}}^{\mathsf{T}}\right)^{-1} - \omega^2 \underline{\underline{L}}\right)\underline{x} = 0 \tag{A.20}$$

Multiplying it with the term $\underline{\underline{L}}^{-1}$ reveals:

$$\left(\underline{\underline{L}}^{-1}\underline{\underline{K}}\left(\underline{\underline{L}}\right)^{-1} - \omega^2\underline{\underline{L}}\,\underline{\underline{L}}^{-1}\right)\underline{x} = 0 \tag{A.21}$$

Which can be written as:

$$\left(\underline{\underline{A}} - \omega^2\underline{\underline{I}}\right)\underline{x} = 0 \tag{A.22}$$

By substituting $\omega_i^2 = \lambda_i$ the final form is reached with:

$$\left(\underline{\underline{A}} - \lambda_i\underline{\underline{I}}\right)\underline{x} = 0 \tag{A.23}$$

B. Calculation of Rule Bending Moments

B.1. DNVGL Rules Still Water Bending Moment

DNVGL has developed a formula for a first estimation of the still water bending moment given for the hogging condition by DNVGL Rules (2016, P.4,C.4,S.4,2.2) by:

$$M_{SW-h-min} = f_{SW}\left(171 \cdot C_W L^2 B\,(C_B + 0.7)\,10^{-3} - M_{WV-h-mid}\right)$$

$$\underline{\underline{M_{SW-h-min} = 5.7707 \cdot 10^9 Nm}} \quad \text{(B.1)}$$

for the sagging condition:

$$M_{SW-s-min} = -0.85 f_{SW}\left(171 \cdot C_W L^2 B\,(C_B + 0.7)\,10^{-3} - M_{WV-s-mid}\right)$$

$$\underline{\underline{M_{SW-s-min} = -3.7849 \cdot 10^9 Nm}} \quad \text{(B.2)}$$

with:

$f_{SW} = 1$ for: $0.3L \leq x \leq 0.7L$

$C_W = 10.75$ for: $300 < L \leq 350$

To be able to estimate the still water bending moments, it is necessary to estimate the vertical wave bending moment in hogging according to the DNVGL rule set by DNVGL Rules (2016, P.4,C.4,S.4,3.1):

$$M_{WV-h} = 0.19 f_{nl-vh}\, f_m\, f_p\, C_W\, L^2\, B\, C_B \qquad \underline{\underline{M_{WV-h} = 6.7529 \cdot 10^9 Nm}} \tag{B.3}$$

and for sagging:

$$M_{WV-s} = 0.19 f_{nl-vs}\, f_m\, f_p\, C_W\, L^2\, B\, C_B \qquad \underline{\underline{M_{WV-h} = -8.0708 \cdot 10^9 Nm}} \tag{B.4}$$

with:

$f_{nl-vh} = 1$	for strength assessment
$f_{nl-vs} = f_{nl-s}$	
$f_{nl-s} = 0.58\left(\frac{C_B + 0.7}{C_B}\right)$	for strength assessment
$f_m = 1$	at midship
$f_p = f_{ps}$	for strength assessement
$f_{ps} = 1$	for extreme loading

B.2. GL Rules Wave Bending Moment

The maximum bending moment is calculated according to Rules 1, Part 1, Chapter 5, Section 5, D.1.1.3 (GL Rules, 2015, R. 1, P. 1, C. 5, S. 5, D.1.1.3) by:

- $M_T = M_{SW,max} + M_{WV,hog}$ for the maximum vertical bending moment, or
- $M_T = M_{SW,min} + M_{WV,sag}$ for the minimum vertical bending moment.

Where the total shear force is calculated by:

- $Q_T = \begin{bmatrix} Q_{SW,max} + Q_{WV,max} \\ |Q_{SW,min} + Q_{WV,min}| \end{bmatrix}$

The initial still water bending moment is calculated according to GL Rules (2015, R. 1, P. 1, C. 5, S. 5, D.1.2.1.1).

$$M_{SM} = n_1 \cdot c_0 \cdot L^2 \cdot B \cdot (0.123 - 0.015 \cdot C_B) \qquad \underline{\underline{M_{SM} = 7.2893 \cdot 10^9 Nm}} \tag{B.5}$$

with:

$n = 10,500$	max. number TEU of mass G
$n_1 = 1.07 \cdot \left[1 + 1.5\left(\frac{n}{10^5}\right)^2\right] \leq 1.2$	$n_1 = 1.2$
$c_{RW} = 1$	for unlimited service Range
$c_0 = \left[10.75 \cdot \left(\frac{300 - L}{100}\right)^{1.5}\right] \cdot c_{RW}$	$c_0 = 10.75 \quad \text{for} \quad L > 300\ m$

The static torsional moment is calculated according to GL Rules (2015, R. 1, P. 1, C. 5, S. 5, D.1.2.1.2).

$$M_{ST} = 0.568 \cdot M_{ST,max} \cdot (|c_{T1}| + c_{T2}) \qquad \underline{\underline{M_{ST} = \pm 173.35 \cdot 10^6\ Nm}} \tag{B.6}$$

with:

$M_{ST,max} = \pm 20 \cdot B \cdot \sqrt{CC}$	$M_{ST,max} = \pm 305.18 \cdot 10^6\ Nm$
$CC = n \cdot G$	maximal permissible cargo capacity
$n = 10,500$	max. number TEU of mass G
$G = 10.48\ t$	assumed deadweight 110,000 ton
$c_{T1} = \sin\left(2 \cdot \pi \cdot \frac{x}{L}\right)$	$c_{T1} = 5.6655 \cdot 10^{-16}$
$x = \frac{L}{2}$	For stresses at Midship section
$c_{T2} = \sin^2\left(\pi \cdot \frac{x}{L}\right)$	$c_{T2} = 1$

Dynamic loads are calculated starting by the vertical wave bending moment in hogging. (GL Rules, 2015, R. 1, P. 1, C. 5, S. 5, D.1.3.1)

$$M_{WV,hog} = L^2 \cdot B \cdot c_0 \cdot c_1 \cdot c_M \qquad \underline{\underline{M_{WV,hog} = 6.9576 \cdot 10^9 \; Nm}} \tag{B.7}$$

with:

$$c_0 = \left[10.75 \cdot \left(\frac{300 - L}{100}\right)^{1.5}\right] \cdot c_{RW} \qquad c_0 = 10.75 \quad \text{for} \quad L > 300 \; m$$

$$c_{1,hog} = 0.19 \cdot C_B \qquad c_{1,hog} = 0.1292$$

$$c_M = 1 \qquad \text{for midship section}$$

For the vertical bending moment in sagging occurs the following result. (GL Rules, 2015, R. 1, P. 1, C. 5, S. 5, D.1.3.1)

$$M_{WV,sag} = L^2 \cdot B \cdot c_0 \cdot c_1 \cdot c_M \qquad \underline{\underline{M_{WV,sag} = 8.1746 \cdot 10^9 \; Nm}} \tag{B.8}$$

with:

$$c_{1,sag} = -0.11 \cdot (C_B + 0.7) \qquad c_{1,sag} = -0.1518$$

C. Calculation of external Pressure

The total external pressure is calculated according to the rules of DNVGL Rules (2016, R. 1, P. 3, C. 4, S. 5, 1) by:

$$P_{ex} = P_S + P_W \tag{C.1}$$

Thus the chapter is divided into the statical and dynamic external Pressure.

C.1. Static External Pressure

The hydrostatic pressure is given, below the water line by (DNVGL Rules, 2016, R. 1, P. 3, C. 4, S. 5, 1.2):

$$P_S = \rho g\,(T_{LC} - z) \tag{C.2}$$

C.2. Dynamic External Pressure

The hydrodynamic pressure is calculated for the different vertical locations by using (DNVGL Rules, 2016, R. 1, P. 3, C. 4, S. 5, 1.3):

$$P_W = P_{HS} \qquad \text{for:} \quad z \leq T_{LC} \tag{C.3}$$

$$P_W = P_{W,WL} - \rho q\,(z - T_{LC}) \qquad \text{for:} \quad z < T_{LC} \leq h_W + T_{LC} \tag{C.4}$$

$$P_W = 0 \qquad \text{for:} \quad z > h_W + T_{LC} \tag{C.5}$$

Where the hydrostatic pressure is given by:

$$P_{HS} = C_{f_T}\ f_{ps}\ f_{nl}\ f_h\ k_a\ k_p\ f_{yz}\ C_W \sqrt{\frac{L_0 + \lambda - 125}{L}} \tag{C.6}$$

with:

$$C_{f_T} = f_T + 0.5 - \left(0.7 \cdot f_T - 0.2\right) C_B \tag{C.7}$$

$$f_T = 1$$

$$f_{nl} = 0.9$$

$$f_h = 3 \cdot \left(1.21 - 0.66 \cdot f_T\right)$$

$$k_a = 1 \qquad \text{for:} \quad 0.15 \leq f_{xL} \leq 0.7$$

$$k_p = 1 \qquad \text{for:} \quad 0.8 - 0.2 f_T$$

$$f_{yz} = C_x \cdot \frac{z}{T_{LC}} + (2 - C_x)\, f_{yB} + 1$$

$$C_x = 1.5 - \frac{|x - 0.5L|}{L}$$

$$f_{yB} = \frac{|2y|}{B_x}$$

$$C_W = 10.75 \qquad \text{for:} \quad 300 < L \leq 350$$

$$\lambda = 340$$

$$L_0 = 340$$

Resulting in

$$P_{HS} = 23.86248 \cdot \left(\left(1.5 \cdot \frac{z}{T}\right) + \left(0.5 \cdot \frac{y}{B/2}\right) + 1\right) \tag{C.8}$$

D. Beam Model Extensions

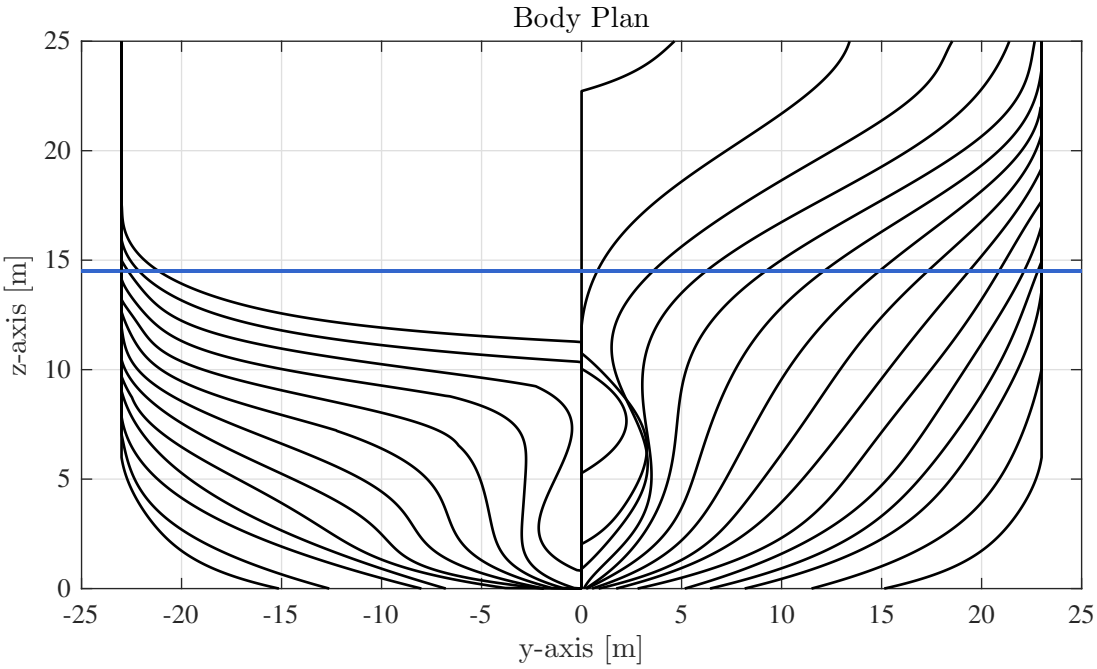

Figure D.1.: Hull geometry of the considered ship with the considered scantling water line at 14.5 meter. (Andersen and Jensen, 2014)

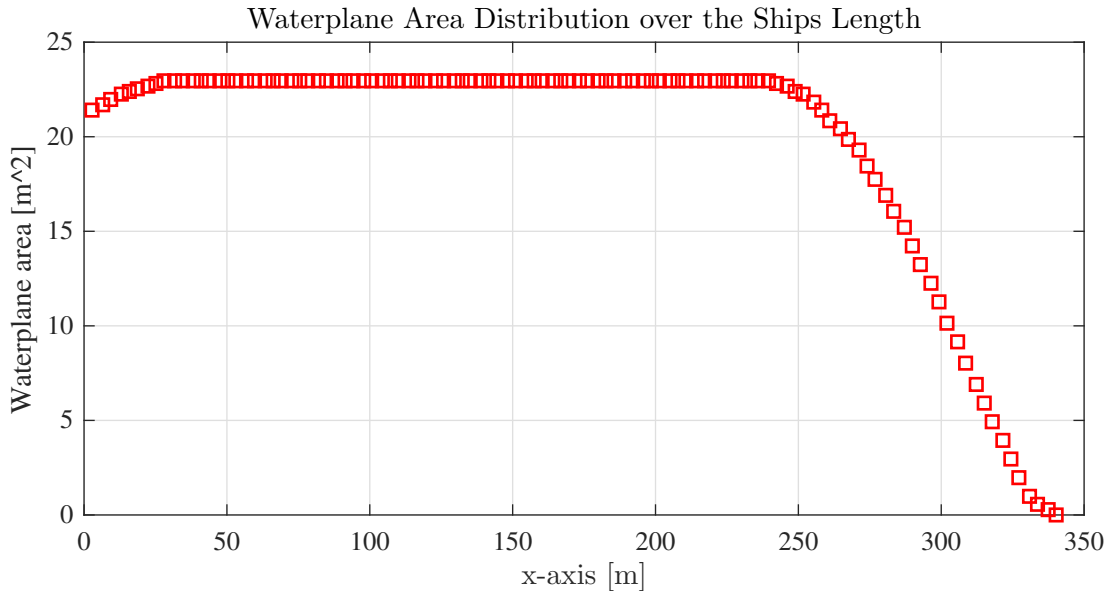

Figure D.2.: Waterplane area distribution over the ship length at a draft of 14.5 meter. The area is the value of a strip of 4*a = 3.15 meter length.

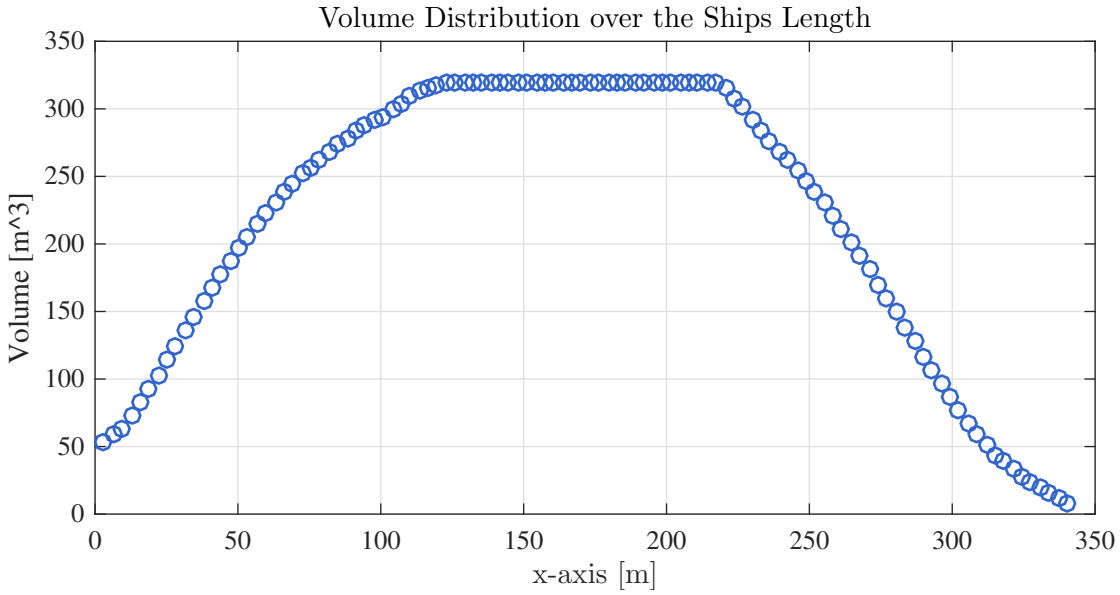

Figure D.3.: Volume distribution over the ship length at a draft of 14.5 meter. The volume is the value of a strip of 4*a = 3.15 meter length.

E. PULS Figures

In this chapter the deformation pattern of the DNV program PULS are shown.

E.1. Simple Plate Results

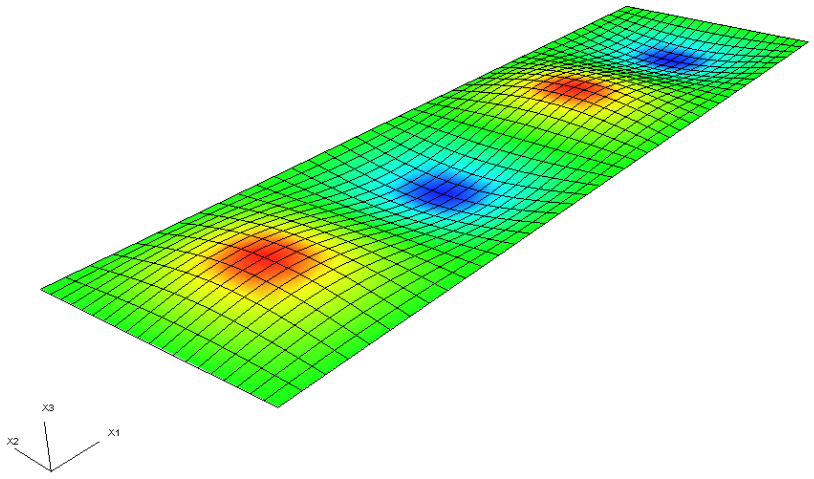

Figure E.1.: Simple plate with length of 3.15 meter and width 0.833 meter. The boundaries are pinned. Shown is the vertical deflection for the in the ultimate capacity state of the plate.

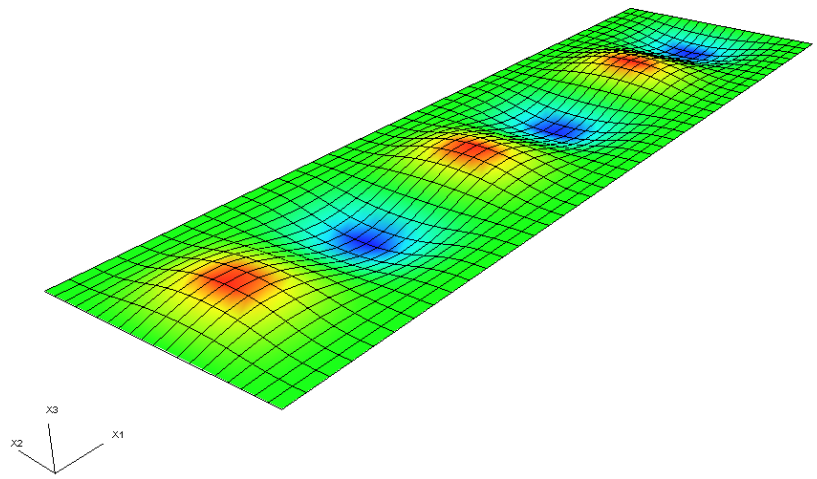

Figure E.2.: Simple plate with length of 3.15 meter and width 0.833 meter. The boundaries at the sides are clamped, the boundaries at the short ends are pinned . Shown is the vertical deflection for the ultimate capacity of the plate.

E.2. Panel Results

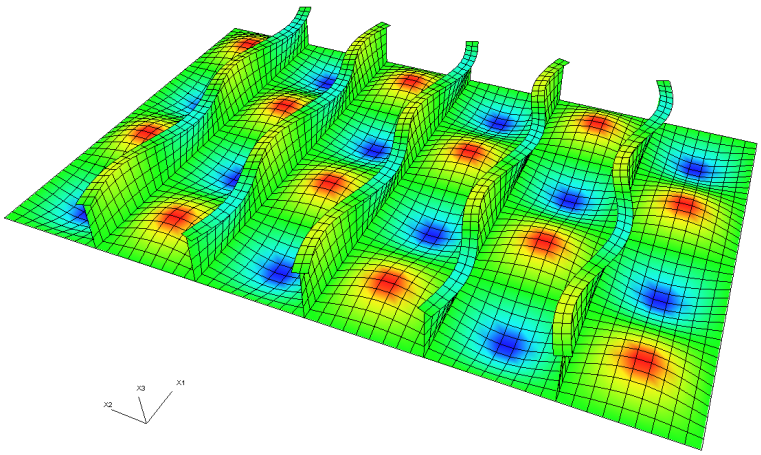

Figure E.3.: Model of the double bottom panel between the longitudinal bulkheads and webs. The length of the panel is 3.15 meter and the width is 6 x 0.833 meter. Five tee-bar stiffeners with the dimensions of 450x15+100x20 mm are mounted. The boundaries represent the plate in a continuous hull girder. Shown is the local imperfection.

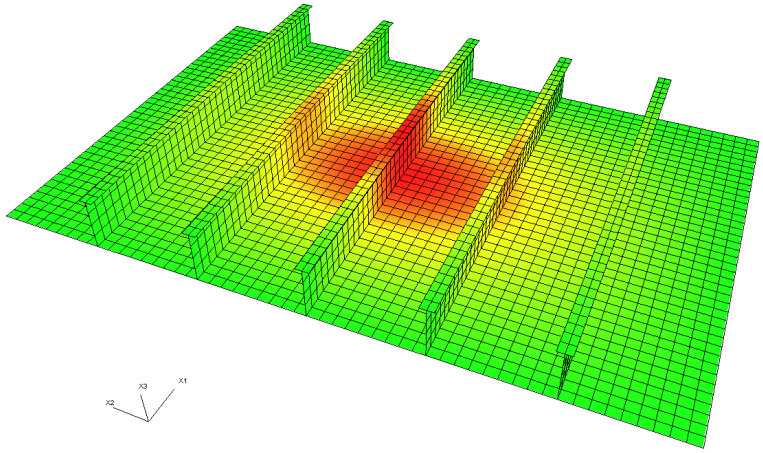

Figure E.4.: Model of the double bottom between the longitudinal bulkheads and webs. The length of the panel is 3.15 meter and the width is 6 x 0.833 meter. Five tee-bar stiffeners with the dimensions of 450x15+100x20 mm are mounted. The boundaries represent the plate in a continuous hull girder. Shown is the global imperfection.

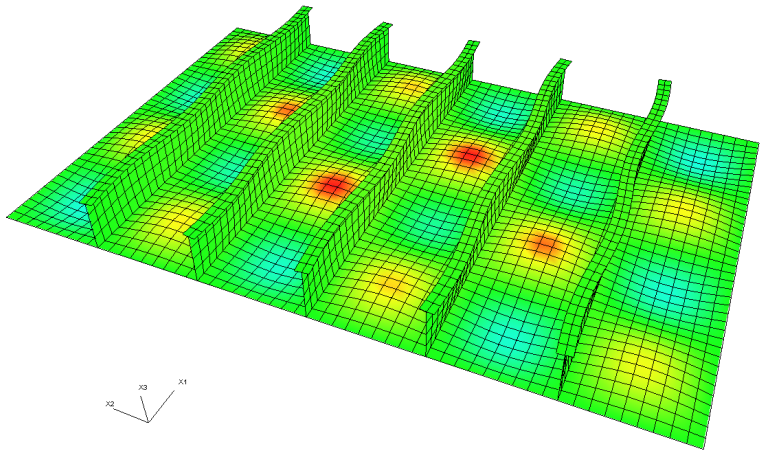

Figure E.5.: Model of the double bottom between the longitudinal bulkheads and webs. The length of the panel is 3.15 meter and the width is 6 x 0.833 meter. Five tee-bar stiffeners with the dimensions of 450x15+100x20 mm are mounted. The boundaries represent the plate in a continuous hull girder. Shown is the state of the ultimate capacity.

F. ANSYS Figures

In the following chapter are figures of the finite element model shows in various conditions. The figures should give a better understanding of the deformations of the model.

F.1. Results for the simple Plate

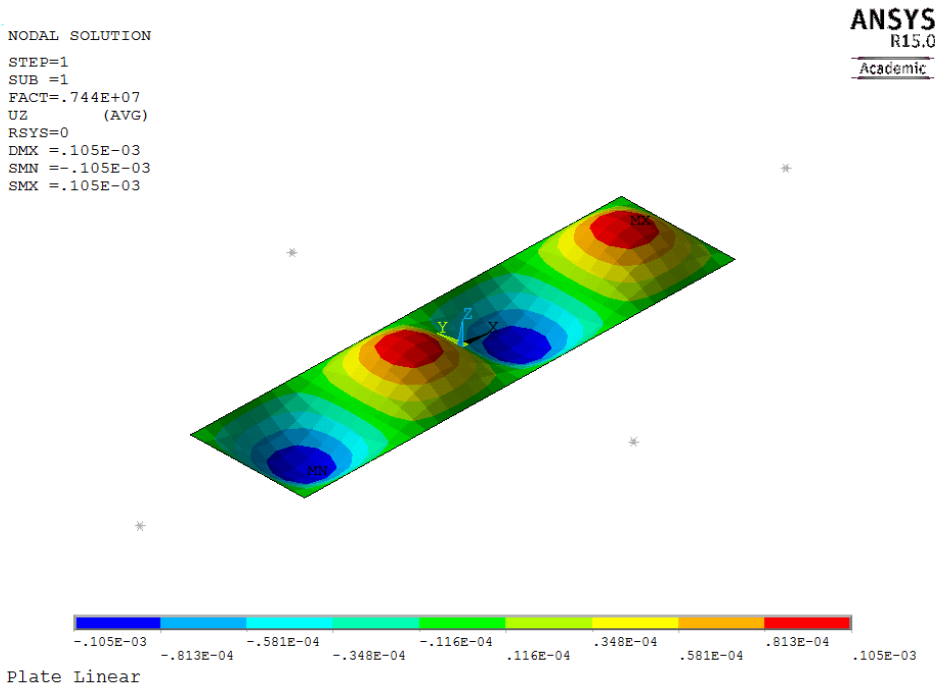

Figure F.1.: First eigenmode of the simple plate 3.15 meter long and 0.833 meter width with constrained edges consisting of 4 sine half waves under axial thrust.

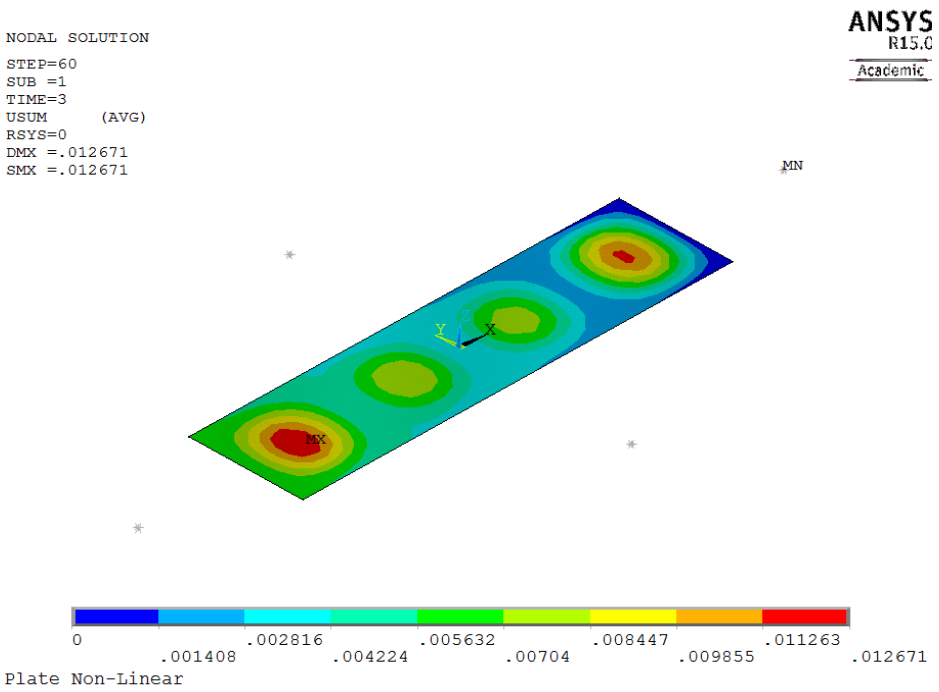

Figure F.2.: Deflection of the simple plate 3.15 meter long and 0.833 meter width with constrained edges. Displacement vector sum at the ultimate capacity.

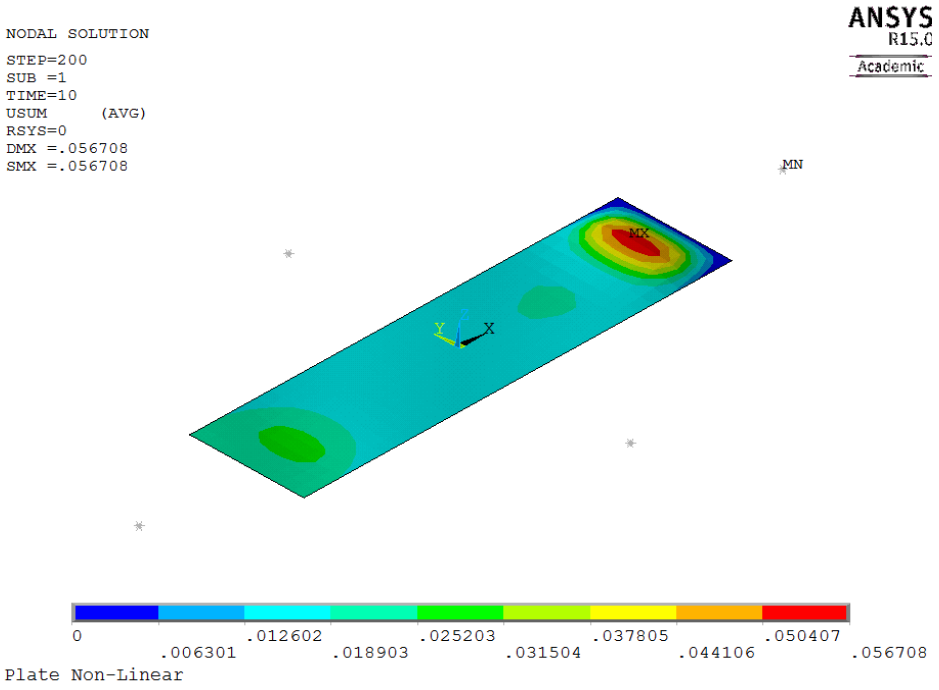

Figure F.3.: Deflection of the simple plate 3.15 meter long and 0.833 meter width with constrained edges. Displacement vector sum at the post buckling path.

F.2. Used Finite Element Midship Models

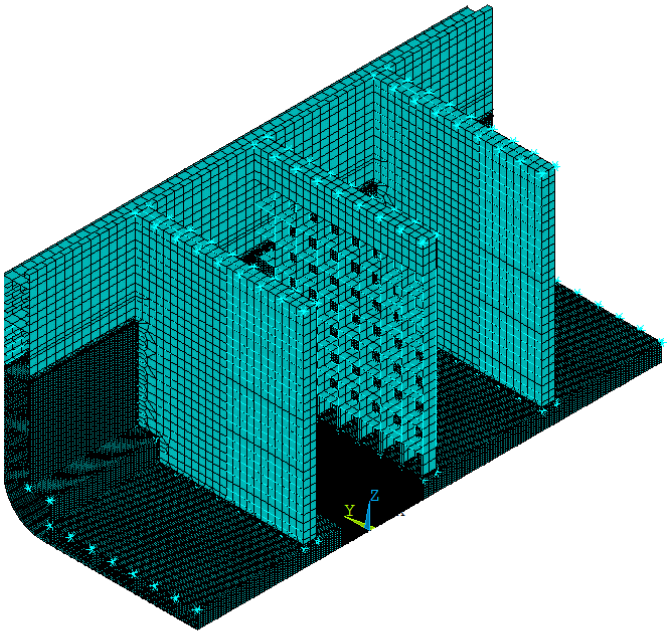

Figure F.4.: Full Model

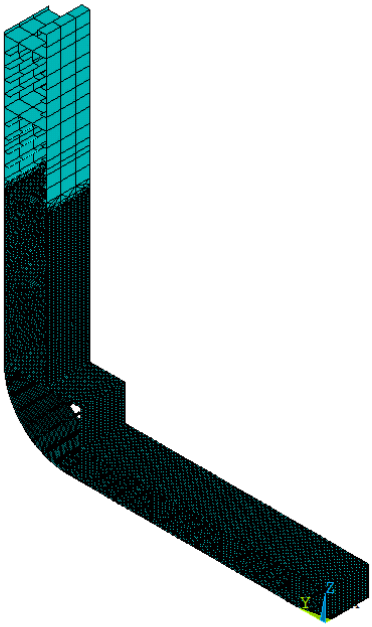

Figure F.5.: 1 Web Model

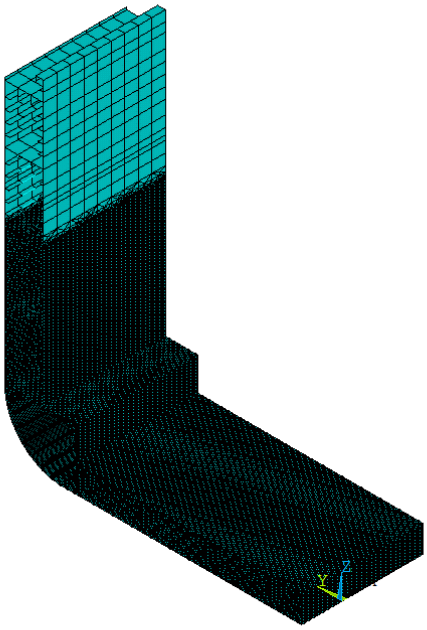

Figure F.6.: 3 Web Model

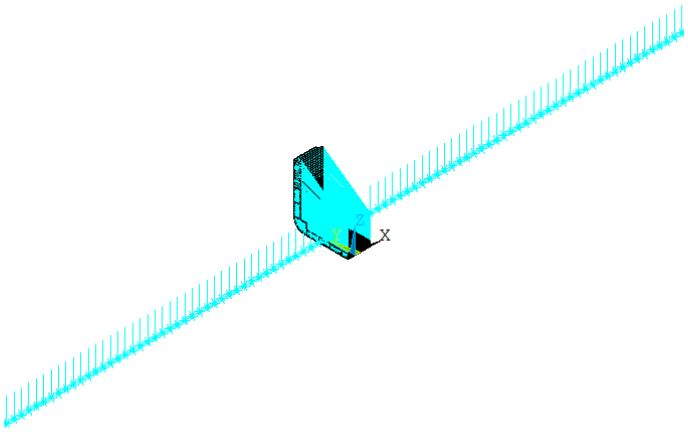

Figure F.7.: 3 Web Rigid Model & Floating Model

F.3. Ultimate Limit State of 3 Web Model

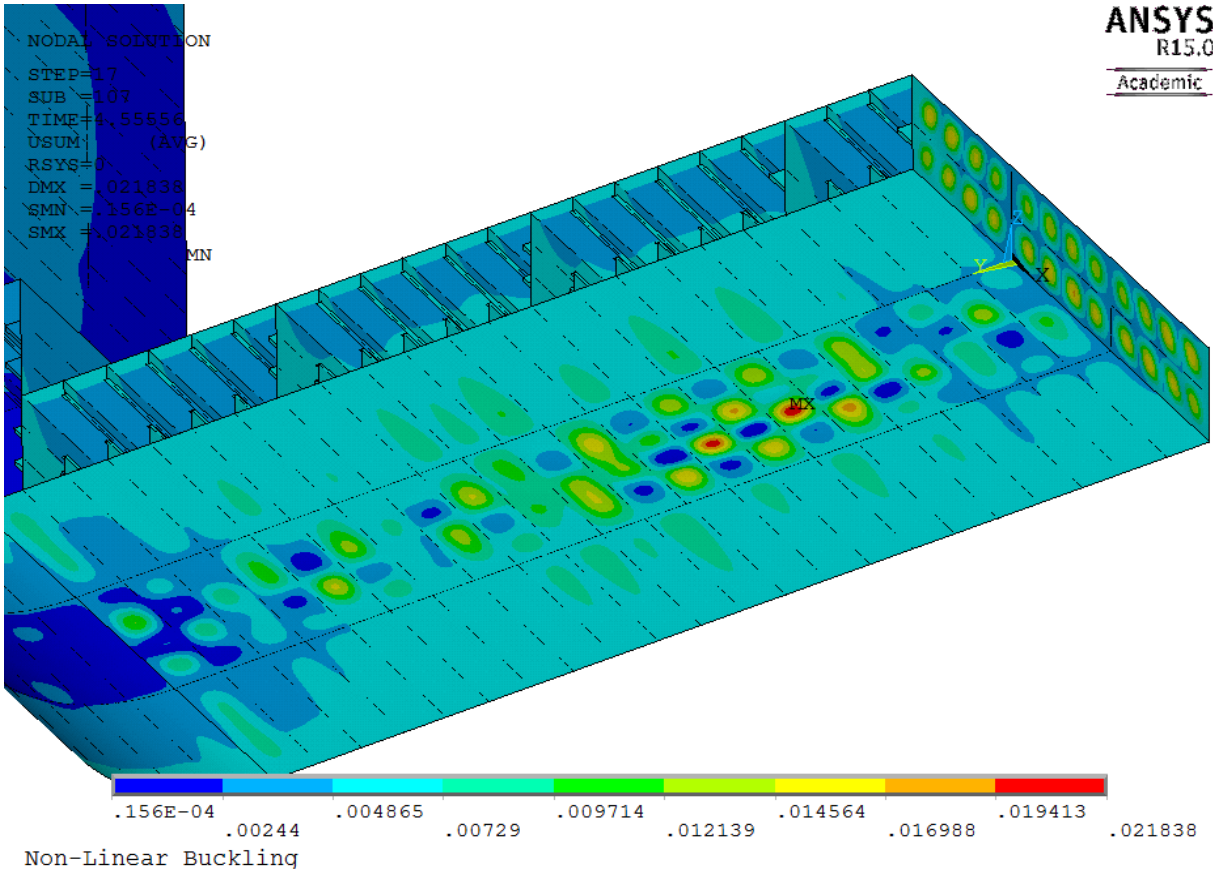

Figure F.8.: 3 Web model loaded until ultimate capacity and showing clearly the assumed four half waves buckling pattern in the bottom region.

F.4. Post Collapse of 3 Web Model

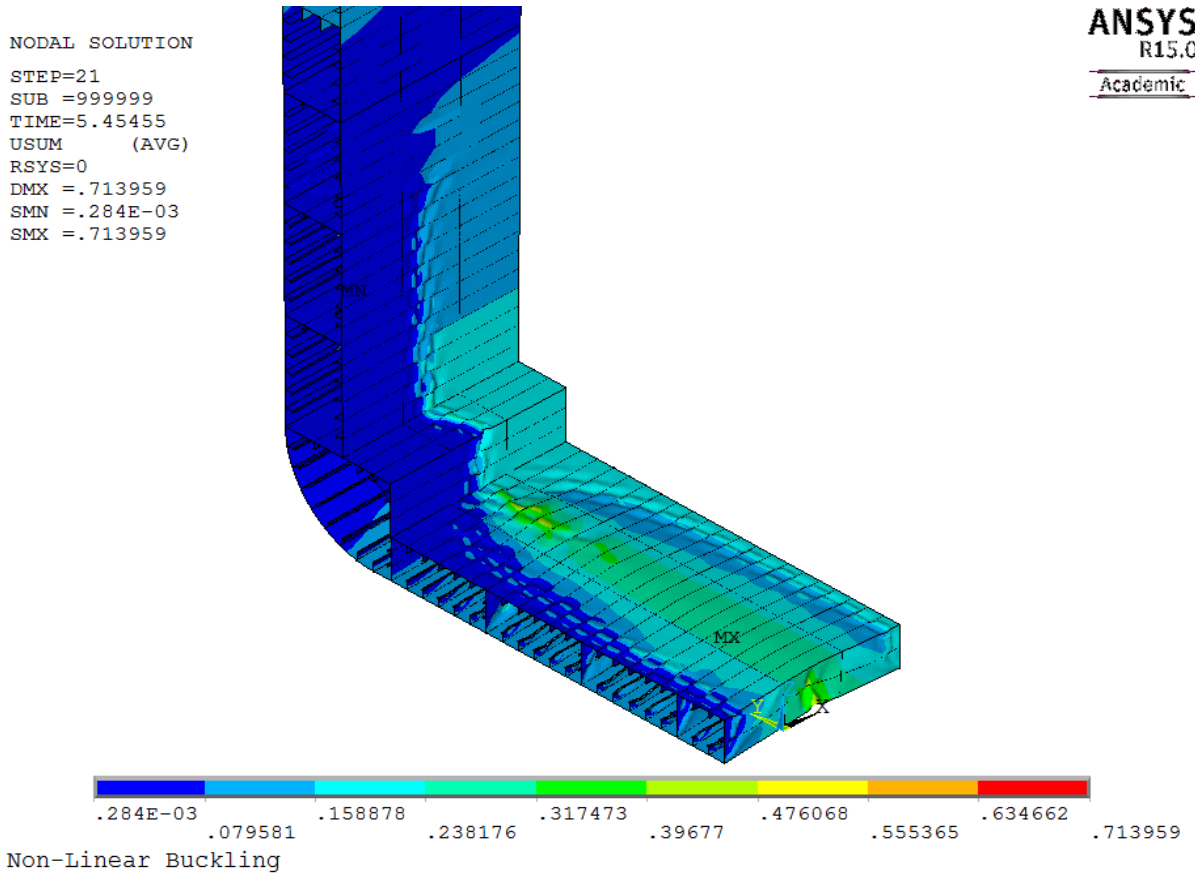

Figure F.9.: 3 Web Model loaded until ultimate capacity. Shown is the displacement vector sum. Clearly visible is the deformation close to the boundaries.

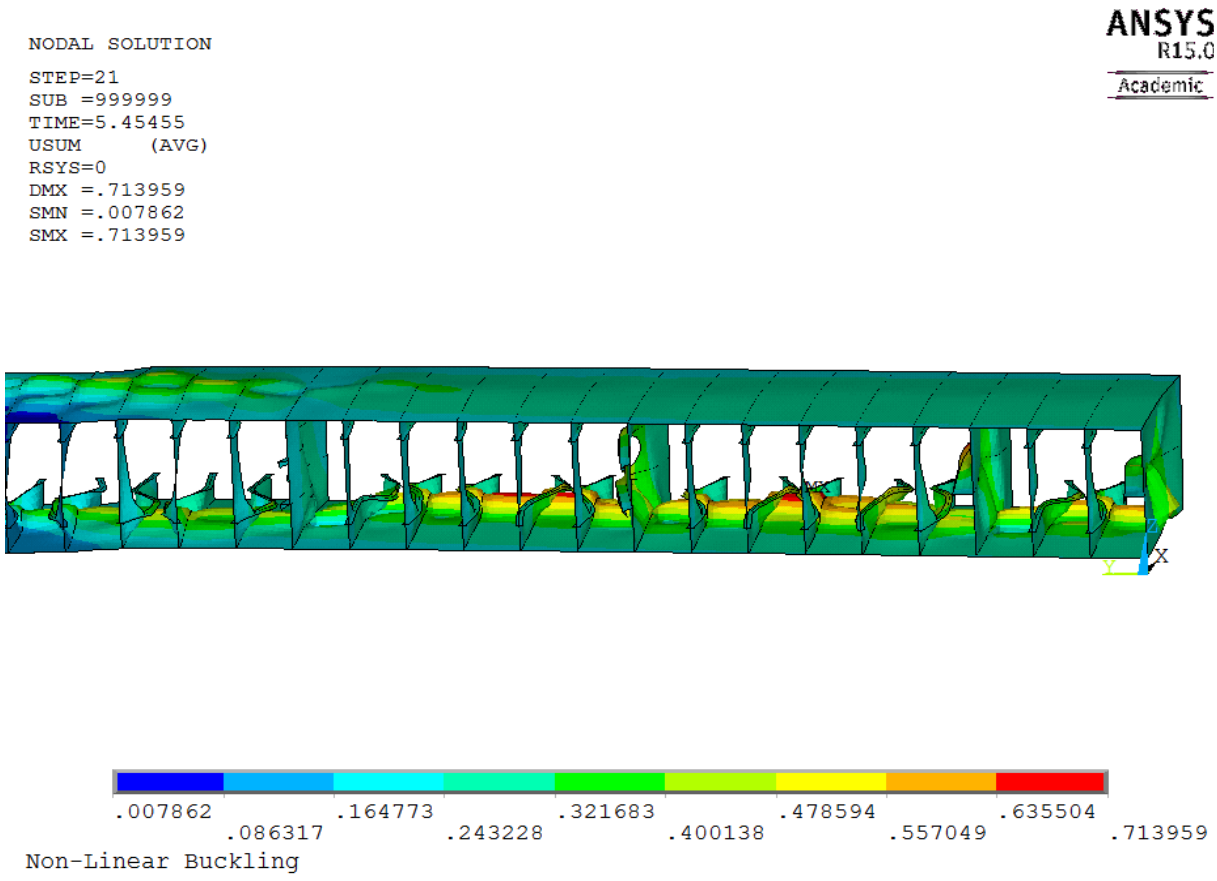

Figure F.10.: Detail of the Crash Section far in the post collapse range. Shown is the displacement vector sum. All members have started to deform.

F.5. Quasi-Static Wave Load on the 3 Web Model

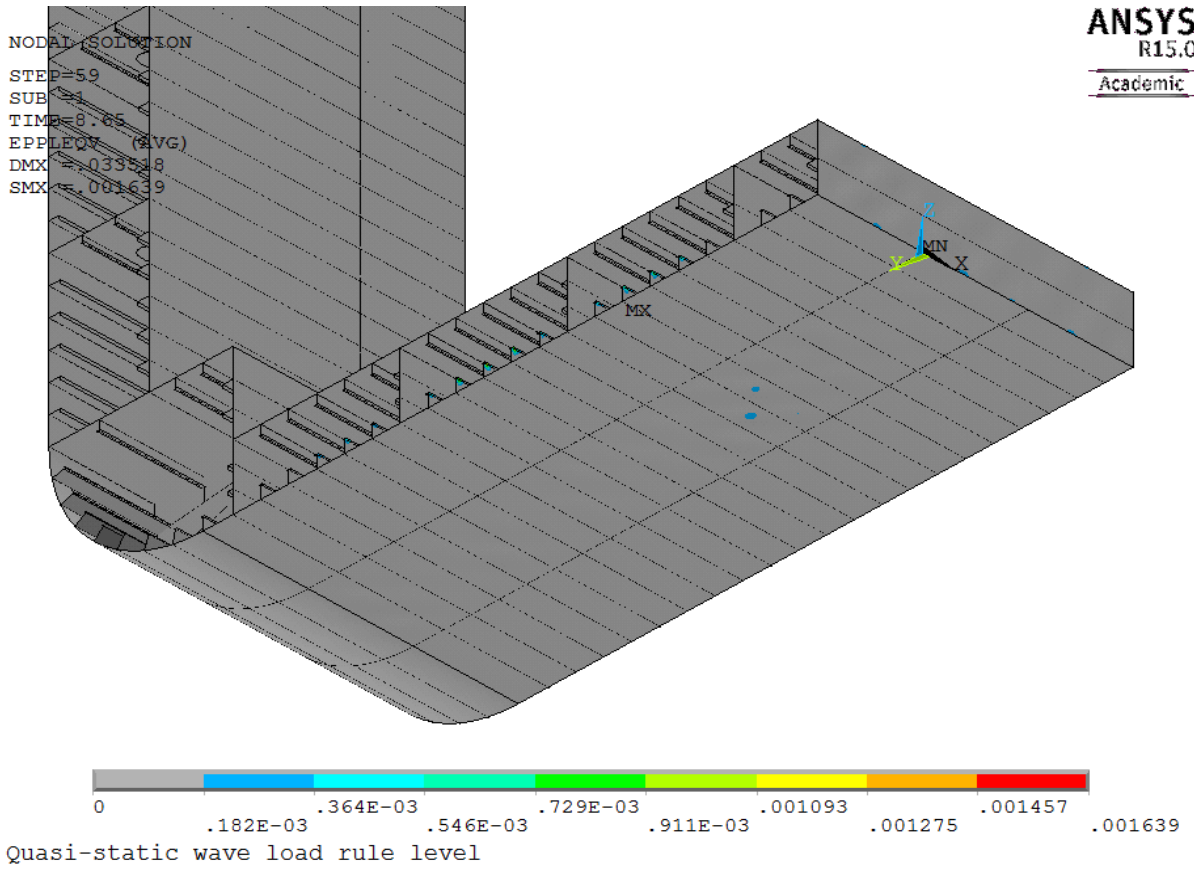

Figure F.11.: 3 Web Model loaded with the quasi-static wave loads up to the rule level. Shown is the von Mises plastic strain at the load peak.

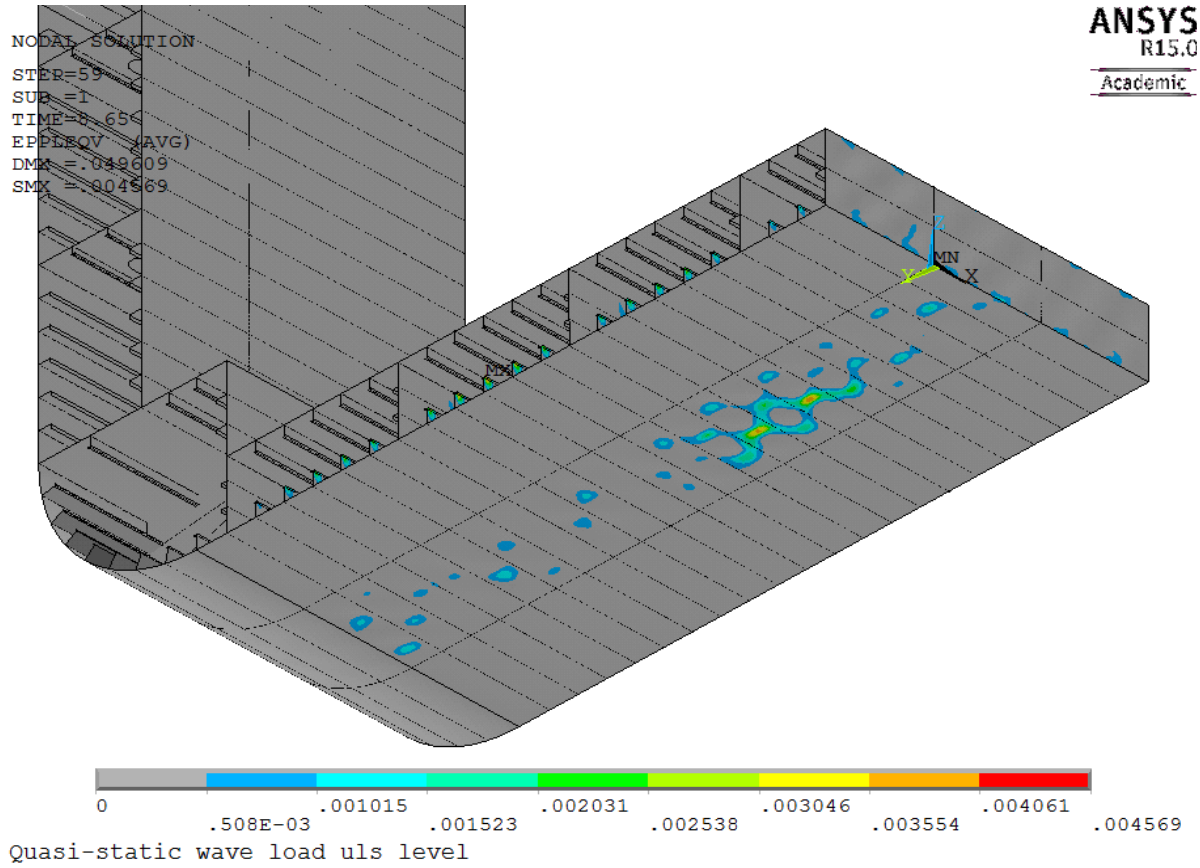

Figure F.12.: 3 Web Model loaded with the quasi-static wave load until the ultimate capacity level. Shown is the von Mises plastic strain at the load peak.

G. APDL Listings

G.1. Eigenvalue Solver

Listing G.1: ANSYS APDL solver for the eigenvalue analysis

```
1  !=====================================================================!

2  ! Solver: Modal Solution
      !
3  !=====================================================================!

4  FINISH                                ! Close PREP7
5  /SOLU                                 ! Begin Solution
6  ANTYPE,2                              ! Modal analysis
7  MODOPT,SUBSP,5                        ! Subspace, 5 modes
8  EQSLV,FRONT                           ! Frontal solver
9  MXPAND,5                              ! Expand 5 modes
10 LUMPM,1
11 SOLVE                                 ! Solve system
```

G.2. Static Solver

Listing G.2: ANSYS APDL solver for the static analysis

```
1  !=====================================================================!

2  ! Solver: Static Calculation
      !
```

```
3  !=====================================================================!

4  FINISH                                ! Close PREP7
5  /SOLU                                 ! Begin Solution
6  ANTYPE,0                              ! Analysis Type Static
7  PSTRES,1                              ! Prestress effects on
8  SOLVE                                 ! Solve system
```

G.3. Linear Buckling Solver

Listing G.3: ANSYS APDL solver for the linear buckling analysis

```
1  !=====================================================================!

2  ! Solver: Static Calculation
      !
3  !=====================================================================!

4  FINISH                                ! Close PREP7
5  /SOLU                                 ! Begin Solution
6  ANTYPE,0                              ! Analysis Type Static
7  PSTRES,1                              ! Prestress effects on
8  SOLVE                                 ! Solve system
9  FINISH
10 !
11 !=====================================================================!

12 ! Solver: Buckling linear
      !
13 !=====================================================================!

14 /SOLU
15 ANTYPE,1                              ! Analysis Type Linear Buckling
16 BUCOPT,LANB,2500,0,0,CENTER           ! BUCOPT,Method,
17 SOLVE                                 ! Solve system
```

G.4. Non-linear Buckling Solver

Listing G.4: ANSYS APDL solver for the non linear transient analysis

```
1  !=====================================================================!

2  ! Solver: Non-Linear Transient
     !
3  !=====================================================================!

4  FINISH                                ! Close PREP7
5  /SOLU                                 ! Begin Solution
6  ANTYPE, TRAN                          ! Transient analysis
7  TRNOPT,FULL,                          ! (Default) Full solution method
8  LUMPM,0                               ! (Default) No lumped loads
9  NROPT,FULL, ,OFF                      ! Full Newton-Raphson (Recom.)
10 TIMINT,ON,ALL                         ! (Default) Transient effects
11 !
12 ! Solution Control Options
13 AUTOTS,ON                             ! Automatic Time Stepping (Default)
14 SOLCONTROL,ON                         ! Solution Control on
15 NSUBST,1,1000,1                       ! Number of substeps
16 LNSRCH,AUTO                           ! Line Search auto (Recom.)
17 !
18 ! Non-linear options
19 NLGEOM,ON                             ! Non-linear geometries activated
20 PSTRES,ON                             ! First Load Step stresses included
21 SSTIF,ON                              ! Stress Stiffening
22 !
23 ! Structural Damping
24 ALPHAD,0.0127                         ! Mass Damping
25 BETAD,0.0276                          ! Stiffness Damping
26 !
27 ! Convergence Options
28 NEQIT,35                              ! 35 instead of 25 iterations
29 NCNV,0                                ! Do not stop for convergence error
```

```
30  !
31  ! Define Output Options
32  OUTRES,ERASE                          ! Erase previous results
33  OUTRES,ALL,NONE                       ! Store Nothing
34  OUTRES,NSOL,-10                       ! NSOL for 10 substeps
35  OUTRES,RSOL,-10                       ! RSOL for 10 substeps
36  OUTRES,STRS,LAST                      ! Element Nodal Stresses each step
37  OUTRES,EPPL,LAST                      ! Element Plastic Strain each step
38  OUTRES,NLOAD,LAST                     ! Nodal Loads each step
39  !
40  ! Define Initial Timestep
41  TIME,0                                ! Initial Time Step
42  LSWRITE                               ! Write First Load Step (Boundaries
        )
```

H. VILJE Input Listings

Listing H.1: VILJE input bash script for the job Ship_nl with a wall clock time of 95 hours.

```
#!/bin/bash
#####################################################
#
#  Ansys Mechanical Job
#
#####################################################
#
#PBS -N Ship_nl
#PBS -A ntnu252
#PBS -l select=1:ncpus=32:mpiprocs=16
#PBS -l walltime=95:00:00
#

# Load ANSYS
module load ansys/15.0

# Define the case variable
case=$PBS_JOBNAME

# Go to Jobname directory
cd $PBS_O_WORKDIR

# Create (if necessary) the working directory
w=/work/$PBS_O_LOGNAME/ansys/$case
if [ ! -d $w ]; then mkdir -p $w; fi

```

```
27 # Copy inputfiles and move to working directory
28 cp $case.db $w
29 cp $case.inp $w
30 cd $w
31
32 machines=`uniq -c ${PBS_NODEFILE} | awk '{print $2 ":" $1}' | paste -s
       -d ':'`
33
34 export MPI_WORKDIR=$w
35
36 ansys150 -j $case -b -dis -usessh -machines $machines -i $case.inp -o
      $case.out
37
38 # Copying the results back to the own directory
39 cp $case.out /home/ntnu/tjarkts/$case/
40 cp Ship_nl0.err /home/ntnu/tjarkts/$case/
41 cp $case.db /home/ntnu/tjarkts/$case/
42 cp $case.rst /home/ntnu/tjarkts/$case/
```